



Powerful Radio Sources in the Southern Sky. I. Optical Identifications

F. Massaro^{1,2,3,4} , S. V. White⁵ , A. García-Pérez^{1,6} , A. Jimenez-Gallardo^{1,2,7} , A. Capetti² , C. C. Cheung⁸ ,
W. R. Forman⁹ , C. Mazzucchelli^{10,11} , A. Paggi^{12,13,14} , N. P. H. Nesvadba¹⁵ , J. P. Madrid¹⁶ , I. Andruchow¹⁷ ,
S. Cellone^{18,19} , H. A. Peña-Herazo²⁰ , R. Grossová^{21,22} , B. Balmaverde¹³ , E. Sani¹⁰ , V. Chavushyan^{6,9} ,
R. P. Kraft⁹ , V. Reynaldi^{18,23} , and C. Leto²⁴

¹ Dipartimento di Fisica, Università degli Studi di Torino, via Pietro Giuria 1, I-10125 Torino, Italy; f.massaro@unito.it

² Istituto Nazionale di Astrofisica (INAF)—Osservatorio Astrofisico di Torino, via Osservatorio 20, I-10025 Pino Torinese, Italy

³ Istituto Nazionale di Fisica Nucleare (INFN)—Sezione di Torino, via Pietro Giuria 1, I-10125 Torino, Italy

⁴ Consorzio Interuniversitario per la Fisica Spaziale, via Pietro Giuria 1, I-10125 Torino, Italy

⁵ Department of Physics and Electronics, Rhodes University, PO Box 94, Grahamstown, 6140, South Africa

⁶ Instituto Nacional de Astrofísica, Óptica y Electrónica, Luis Enrique Erro 1, Tonantzintla, Puebla 72840, México

⁷ Dipartimento di Fisica e Astronomia, Università di Bologna, via P. Gobetti 93/2, I-40129 Bologna, Italy

⁸ Space Science Division, Naval Research Laboratory, Washington, DC 20375, USA

⁹ Center for Astrophysics | Harvard & Smithsonian, 60 Garden Street, Cambridge, MA 02138, USA

¹⁰ European Southern Observatory, Alonso de Córdova 3107, Vitacura, Región Metropolitana, Chile

¹¹ Instituto de Estudios Astrofísicos, Facultad de Ingeniería y Ciencias, Universidad Diego Portales, Avenida Ejército Libertador 441, Santiago, Chile

¹² Dipartimento di Fisica, Università degli Studi di Torino (UniTO), via Pietro Giuria 1, I-10125 Torino, Italy

¹³ Istituto Nazionale di Astrofisica—Osservatorio Astrofisico di Torino, via Osservatorio 20, I-10025 Pino Torinese, Italy

¹⁴ Istituto Nazionale di Fisica Nucleare—Sezione di Torino, via Pietro Giuria 1, I-10125 Torino, Italy

¹⁵ Université de la Côte d’Azur, Observatoire de la Côte d’Azur, CNRS, Laboratoire Lagrange, Bd de l’Observatoire, CS 34229, F-06304 Nice cedex 4, France

¹⁶ Department of Physics and Astronomy, The University of Texas Rio Grande Valley, Brownsville, TX 78520, USA

¹⁷ Instituto Argentino de Radioastronomía, CONICET-CICPBA-UNLP, CC5 (1897) Villa Elisa, Prov. de Buenos Aires, Argentina

¹⁸ Facultad de Ciencias Astronómicas y Geofísicas, Universidad Nacional de La Plata, Paseo del Bosque, B1900FWA La Plata, Argentina

¹⁹ Complejo Astronómico El Leoncito (CASLEO), CONICET-UNLP-UNC-UNSJ, Av. España 1512 (sur), J5402DSP San Juan, Argentina

²⁰ East Asian Observatory, 660 N. A’ohōkū Place, Hilo, HI 96720, USA

²¹ Department of Theoretical Physics and Astrophysics, Faculty of Science, Masaryk University, Kotlářská 2, Brno, CZ-611 37, Czech Republic

²² Astronomical Institute of the Czech Academy of Sciences, Bocni II 1401, 141 00, Prague, Czech Republic

²³ Instituto de Astrofísica de La Plata (CCT La Plata-CONICET-UNLP), La Plata, Argentina

²⁴ ASI—Agenzia Spaziale Italiana, Via del Politecnico snc, I-00133 Roma, Italy

Received 2022 August 29; revised 2022 December 10; accepted 2022 December 12; published 2023 March 15

Abstract

Since the early sixties, our view of radio galaxies and quasars has been drastically shaped by discoveries made thanks to observations of radio sources listed in the Third Cambridge Catalog and its revised version (3CR). However, the largest fraction of data collected to date on 3CR sources was performed with relatively old instruments, rarely repeated and/or updated. Importantly, the 3CR contains only objects located in the Northern Hemisphere, thus having limited access to new and innovative astronomical facilities. To mitigate these limitations, we present a new catalog of powerful radio sources visible from the Southern Hemisphere, extracted from the GLEAM 4 Jy (G4Jy) catalog and based on equivalent selection criteria as the 3CR. This new catalog, named G4Jy-3CRE, where the E stands for “equivalent,” lists a total of 264 sources at decl. below -5° and with 9 Jy limiting sensitivity at ~ 178 MHz. We explored archival radio maps obtained with different surveys and compared them with optical images available in the Pan-STARRS, DES, and DSS databases to search for optical counterparts of their radio cores. We compared mid-infrared counterparts, originally associated in the G4Jy, with the optical ones identified here, and we present results of a vast literature search carried out to collect redshift estimates for all G4Jy-3CRE sources resulting in a total of 145 reliable z measurements.

Unified Astronomy Thesaurus concepts: [Extragalactic radio sources \(508\)](#)

Supporting material: figure set, machine-readable tables

1. Introduction

Since the early sixties, the Third Cambridge Catalog of Radio Sources (3C; Edge et al. 1959), together with all its revised editions (3CR and 3CRR; Bennett 1962; Laing et al. 1983, respectively), has been considered a long-standing fundamental sample to understand the nature and evolution of powerful radio galaxies and quasars (Begelman et al. 1984; Urry 1995; Harvanek et al. 2001; O’Dea et al. 2009;

Tremblay et al. 2009; Massaro et al. 2011), and the relationships with their environments (i.e., feedback processes), at all scales and across cosmic time (Boehringer et al. 1993; Churazov et al. 2000, 2001; McNamara & Nulsen 2007, 2012; Alexander & Hickox 2012; Fabian 2012; Morganti 2017). The classical classification scheme for radio galaxies, distinguishing between edge-darkened (i.e., FR I) and edge-brightened (i.e., FR II) sources, was developed on the basis of the 3C observations (Fanaroff & Riley 1974; Leahy 1993).

The first revised version of the Third Cambridge Catalog of Radio Sources (3CR; Spinrad et al. 1985) lists the most powerful radio sources detected in the Northern Hemisphere at 178 MHz above a 9 Jy flux density threshold listing 298 extragalactic



Original content from this work may be used under the terms of the [Creative Commons Attribution 4.0 licence](#). Any further distribution of this work must maintain attribution to the author(s) and the title of the work, journal citation and DOI.

sources, with only a small fraction (i.e., less than $\sim 8\%$) still unidentified.

In the past decades a vast suite of multifrequency campaigns were dedicated to the 3CR radio sources and carried out at radio (see, e.g., Clarke 1964; Wills & Parker 1966; Law-Green et al. 1995; Hardcastle & Worrall 2000; Giovannini et al. 2005), infrared (see, e.g., Simpson et al. 1999; Madrid et al. 2006; Baldi et al. 2010; Werner et al. 2012; Dicken et al. 2014), optical (see, e.g., Wyndham 1966; Sandage 1967; Longair & Lilly 1984; Saunders et al. 1989; Longair et al. 1995; McCarthy et al. 1995; de Koff et al. 1996; McCarthy et al. 1996, 1997; Martel et al. 1999; Lehnert et al. 1999; Chiaberge et al. 2000), and X-ray frequencies (see, e.g., Prieto 1996; Evans et al. 2006; Hardcastle et al. 2006; Balmaverde et al. 2012; Wilkes et al. 2013; Kuraszkiewicz et al. 2021). Initial studies of the 3CR catalog were performed to estimate source redshifts and obtain optical classifications (see, e.g., Smith et al. 1976; Kristian et al. 1978; Djorgovski et al. 1988; Hiltner & Roeser 1991; Martel et al. 1998; Buttiglione et al. 2009, 2010, 2011; Capetti et al. 2011; Baldi et al. 2013). Later work was carried out to dig deeper into the physical properties of active galactic nuclei (AGNs), their large-scale environments, and the intracluster medium (ICM) when harbored in galaxy clusters (see, e.g., Baum et al. 1988; Blanton et al. 2011; Kotyla et al. 2016; Balmaverde et al. 2018).

The legacy value of 3CR follow-up surveys can also be highlighted by results achieved thanks to (i) the Hubble Space Telescope (HST) Snapshot Survey of 3CR Radio Source Counterparts²⁵ (Privon et al. 2008; Chiaberge et al. 2015; Hilbert et al. 2016), (ii) the 3CR Chandra Snapshot Survey (Massaro et al. 2010, 2012b, 2013b, 2018; Stuardi et al. 2018; Jimenez-Gallardo et al. 2020), and (iii) the Muse Radio Loud Emission line Snapshot survey (Balmaverde et al. 2018, 2019, 2021, 2022; Speranza et al. 2021). The former campaign allowed us to obtain a full overview of optical properties of these powerful radio sources at $\sim 90\%$ level of completeness (even if not uniform in terms of instruments and filters adopted), while the latter one (i.e., the MURALES campaign), still ongoing, can be performed only on 3CR sources at $z < 0.8$ and at decl. $< 20^\circ$, being visible from the Very Large Telescope (VLT) in Chile. In 2008 the 3CR Chandra Snapshot survey also began aiming to (i) detect new jets, hot spots, and lobes emitting in the X-ray band; (ii) investigate nuclear emission of powerful radio sources; and (iii) discover new galaxy clusters (see also Hardcastle et al. 2010, 2012; Dasadia et al. 2016; Madrid et al. 2018; Ricci et al. 2018; Jimenez-Gallardo et al. 2021, 2022; Missaglia et al. 2023), covering all 3CR sources lacking X-ray observations. Despite a small number of 3CR sources that are still unidentified and unobserved in the X-rays (Maselli et al. 2016; Missaglia et al. 2021), more than 95% of the 3CR catalog has high-energy data already available in the Chandra archive (see, e.g., Massaro et al. 2015a).

However, the 3CR has, unfortunately, the following drawbacks and limitations. It was created more than six decades ago, and the largest fraction of 3CR radio, infrared, and optical data collected to date was obtained with relatively old instruments, only rarely repeated and/or updated. It lists radio sources lying in the Northern Hemisphere, with limited access to observations that can be performed with state-of-the-art and upcoming astronomical facilities, such as the Multi Unit Spectroscopic

Explorer (MUSE; Bacon et al. 2010) mounted at the Very Large Telescope (VLT), the Atacama Large Millimeter/submillimeter Array (ALMA), and in the near future the world's most powerful radio telescopes: the Square Kilometre Array²⁶ (SKA; McMullin et al. 2020), the Large Synoptic Survey Telescope (LSST; Ivezić et al. 2019), and the Extremely Large Telescope²⁷ (ELT).

In the eighties the Molonglo Reference Catalog of Radio Sources (MRC; Large et al. 1981), containing nearly 12,000 discrete sources with flux densities greater than 0.7 Jy at 408 MHz in the decl. range between $+18.5^\circ$ and -85° and excluding regions within 3° of the Galactic equator, was created. Several multifrequency campaigns were then dedicated to augment the information of MRC sources, eventually restricted to bright samples (see, e.g., McCarthy et al. 1996; Kapahi et al. 1998).

A first attempt to create a complete sample similar to the 3CR, but selected at 408 MHz, was performed by Best et al. (1999) using the MRC. They selected a sample listing 178 radio sources with flux density S_{408} above 5 Jy, in the range of decl. between -30° and 10° and having Galactic latitudes $|b| \geq 10^\circ$. The equatorial location of all sources listed therein allowed them to achieve high spectroscopic completeness, and its footprint certainly mitigated one of the previously mentioned limitations of the 3CR: visibility from Southern Hemisphere telescopes.

An additional attempt to build a catalog equivalent to the 3CRR was carried out by Burgess & Hunstead in 2006, starting from the Molonglo Southern 4 Jy sample (MS4; see also Burgess & Hunstead 2006b). The MS4 is a complete sample of 228 southern radio sources detected at 408 MHz with integrated flux densities above 4.0 Jy, Galactic latitude $|b| > 10^\circ$, and decl. in the range between -85° and $+30^\circ$, all imaged at 843 MHz with the Molonglo Observatory Synthesis Telescope to obtain positions with an accuracy of $\sim 1''$. Then, radio spectra for the MS4 sources were compiled from the literature to estimate flux densities at 178 MHz, and the subset of SMS4 with $S_{178} > 9$ Jy was extracted. Some sources listed in the SMS4 were also recently observed in the soft X-rays (Maselli et al. 2022).

The recent Galactic and Extragalactic All-sky Murchison Widefield Array (MWA) survey (GLEAM; Wayth et al. 2015; Hurley-Walker et al. 2017) offers today a unique opportunity to create a southern sample of powerful radio sources matching the selection criterion of the 3CR catalog. Thanks to the MWA observations available for the whole southern sky at declinations $\delta < 30^\circ$ in the frequency range between 72 and 231 MHz, White et al. (2018, 2020a, 2020b) built a complete sample of radio sources with flux density above 4 Jy at 151 MHz, namely the GLEAM 4 Jy sample (hereinafter labeled as G4Jy). The majority of radio sources included therein are extragalactic, mainly AGNs with extended structures detected at low radio frequencies (i.e., at hundreds of megahertz). This sets the basis for extracting, from the G4Jy catalog, a new sample of radio sources equivalent to the 3CR (hereinafter G4Jy-3CRE) but including only those located in the Southern Hemisphere.

Here we introduce the G4Jy-3CRE catalog, listing the 264 very brightest radio sources, selected from the larger parent G4Jy catalog, above a flux density threshold of 9 Jy at ~ 178

²⁵ <https://archive.stsci.edu/prepds/3cr/>

²⁶ <https://www.skao.int>

²⁷ <https://elt.eso.org>

MHz, as the nominal value of the 3C, at declinations below -5° . There are several differences with respect to the previous analysis carried out on the G4Jy catalog as listed below. In the present work we restricted our investigation to a small fraction of sources, 264 with respect to ~ 1900 listed in the G4Jy catalog, with the potential advantage of performing deeper analyses with more astronomical facilities and instruments, but with the disadvantage of a limited number of high- z sources, implying less robust claims from a statistical perspective. On the other hand, radio sources listed in the G4Jy-3CRE sample are potentially primary targets for SKA, being the brightest ones and preparing the sample before its advent allows us to start collecting multifrequency observations that will be crucial to investigate their nature and that of their environments.

This first paper is mainly devoted to the comparison between radio images, at higher resolution than that achievable with previously available radio maps, with mid-infrared (mid-IR) and optical archival observations to confirm counterparts previously assigned to each radio source and/or determine potential incorrect associations. The analysis presented here is based on archival radio maps with higher angular resolution than those used for the G4Jy associations, such as those retrieved from the Very Large Array (VLA) Sky Survey (VLASS; Lacy et al. 2020) and the National Radio Astronomy Observatory (NRAO) VLA Archive Survey (NVAS)²⁸ databases, available for at least 60% of the G4Jy-3CRE catalog. This counterpart search is crucial to identify targets for future spectroscopic campaigns that are necessary to obtain source redshifts and their optical classification. We also present results of an extensive literature search carried out to obtain redshift estimates for G4Jy-3CRE sources.

The paper is structured as follows. In Section 2 we present the criteria underlying the G4Jy-3CRE sample selection. In Section 3 we present the results of our search for optical counterparts and a comparison with the mid-IR sources associated with the G4Jy catalog, while Section 4 is dedicated to a brief description of a literature search for redshift estimates. Summary, conclusions, and future perspectives are given in Section 5. Appendix A is dedicated to a brief description of individual sources, while Appendix B is devoted to the cross-identifications obtained comparing the G4Jy-3CRE sample with other radio catalogs based on observations carried out in the Southern Hemisphere. Finally, Appendix C is dedicated to a statistical test for the radio and mid-IR crossmatches carried out to search for counterparts of G4Jy sources, in comparison with the optical analysis presented here.

We adopt cgs units for numerical results, and we assume a flat cosmology with $H_0 = 69.6 \text{ km s}^{-1} \text{ Mpc}^{-1}$, $\Omega_M = 0.286$, and $\Omega_\Lambda = 0.714$ (Bennett et al. 2014). For optical photometric data we used the catalog obtained from the Panoramic Survey Telescope and Rapid Response System (Pan-STARRS; Flewelling et al. 2020) survey, where magnitudes are reported in the AB system (Oke 1974; Oke & Gunn 1983). The same applies for the Dark Energy Survey (DES; Abbott et al. 2018), for which observations are performed in optical filters similar to those of Pan-STARRS and the Sloan Digital Sky Survey (SDSS; Ahn et al. 2012). Limiting sensitivity for both the Pan-STARRS and DES optical survey reaches ~ 23 mag in the r band. For optical magnitudes we did not apply the correction for Galactic extinction, but we report the total extinction A_V ,

extracted from the Galactic Dust Reddening and Extinction database²⁹ (Schlegel et al. 1998; Schlafly & Finkbeiner 2011). Spectral indices, α , are defined by flux density, $S_\nu \propto \nu^{-\alpha}$. Finally, given the large number of acronyms used in the paper, these are summarized in Table 1.

2. Sample Selection

The MWA, operating since 2013 and being the SKA precursor at low radio frequencies (Tingay et al. 2013), performed the GLEAM survey³⁰ (Wayth et al. 2015). The extragalactic GLEAM catalog (Hurley-Walker et al. 2017) covers $\sim 25,000 \text{ deg}^2$, at declinations south of $+30^\circ$ and Galactic latitudes $|b| > 10^\circ$, and excluding some regions such as the Magellanic Clouds. It lists $\sim 3 \times 10^5$ radio sources with 20 separate flux density measurements across the frequency range 72–231 MHz, selected from a time- and frequency-integrated image centered at 200 MHz, with an angular resolution of $\sim 2'$. Based on the GLEAM survey and selecting all radio sources with S_{151} above 4 Jy, White et al. (2020a, 2020b) built the G4Jy catalog (see also Wayth et al. 2015), a flux-limited sample listing nearly 2000 sources over an area of $\sim 25,000 \text{ deg}^2$. The selection criterion on the Galactic latitudes (i.e., Galactic latitudes $|b| > 10^\circ$) was used to lower the contamination of Galactic sources and focus on the extragalactic sky. This sets the basis to extract a southern catalog of extragalactic radio sources: the G4Jy-3CRE, fully equivalent, in terms of radio flux density selection, to the northern 3CR extragalactic sample, which lists powerful radio sources at declinations above -5° and having a flux density higher than 9 Jy at 178 MHz (Bennett 1962; Spinrad et al. 1985). We remark that the brightest sources at declinations below $+30^\circ$ and Galactic latitudes $|b| > 10^\circ$, including the Orion Nebula, were all masked in the GLEAM extragalactic catalog and thus are not listed in the G4Jy sample (see White et al. 2020a and references therein for a list of them and additional details).

Sources listed in the G4Jy-3CRE are selected to have (i) decl. $< -5^\circ$ and (ii) flux densities at 174 and 181 MHz, integrated over the GLEAM bands, above the following thresholds: $S_{174} > 8.13 \text{ Jy}$ and $S_{181} > 7.85 \text{ Jy}$, respectively.³¹ The flux density thresholds adopted here correspond to the 9 Jy limiting sensitivity at $\sim 178 \text{ MHz}$, the nominal value adopted to prepare the 3CR. Sources close to the Galactic plane (i.e., at Galactic latitudes $|b| < 10^\circ$) are excluded since they were not originally listed in the G4Jy catalog (White et al. 2020a). All sources listed in the G4Jy-3CRE catalog are visible from the Southern Hemisphere and lie in a footprint not covered by the 3CR catalog, whereas the handful of targets in common were removed. The final G4Jy-3CRE catalog lists 264 radio sources. At declinations below $+20^\circ$ there are 106 out of 298 3CR objects; thus, the new G4Jy-3CRE sample includes about three times the number of powerful radio sources visible with southern telescopes.

After the release of the 3CR, several radio analyses (see, e.g., Roger et al. 1973) were carried out to refine the sample; some of them led to the 3CRR release (Laing et al. 1983). The flux density threshold adopted to create the G4Jy-3CRE, even if

²⁸ <http://www.vla.nrao.edu/astro/nvas/>

²⁹ <https://irsa.ipac.caltech.edu/applications/DUST/>

³⁰ <https://www.mwatelescope.org/gleam>

³¹ These thresholds are computed assuming a power-law description for the radio spectrum of the G4Jy sources and adopting the spectral index reported in the G4Jy catalog.

Table 1
Table of Acronyms Used across the Paper

Acronym	Meaning
Generic	
AGN	Active galactic nucleus
BCG	Brightest cluster galaxy
BLRG	Broad-line radio galaxy
CSS	Compact steep-spectrum radio source
FSRQ	Flat-spectrum radio quasar
GPS	Gigahertz-peaked spectrum
HyMoR	Hybrid morphology radio source
ICM	Intracluster medium
HERG	High-excitation radio galaxy
LERG	Low-excitation radio galaxy
NLRG	Narrow-line radio galaxy
QSO	Quasi stellar object
USS	Ultra-steep-spectrum radio source
WAT	Wide-angle tail radio galaxy
Institutes	
NRAO	National Radio Astronomy Observatory
TIFR	Tata Institute of Fundamental Research
Telescopes and Instruments	
ALMA	Atacama Large Millimeter/submillimeter Array
ATCA	Australia Telescope Compact Array
CASLEO	Complejo Astronómico El Leoncito
ELT	Extremely Large Telescope
GMRT	Giant Metrewave Radio Telescope
HST	Hubble Space Telescope
LSST	Large Synoptic Survey Telescope
MUSE	Multi Unit Spectroscopic Explorer
MWA	Murchison Widefield Array
SKA	Square Kilometre Array
VLT	Very Large Telescope
WISE	Wide Infrared Survey Explorer
Catalogs and Surveys	
2 Jy	Bright extragalactic radio sources at 2.7 GHz
3C	Third Cambridge Catalog
3CR	Third Cambridge Catalog Revised
6dFGS	Six-degree Field Galaxy Survey
AT20G	Australia Telescope 20 GHz Survey Catalog
CRATES	Combined Radio All-Sky Targeted Eight GHz Survey
DES	Dark Energy Survey
DSS	Digital Sky Survey
GLEAM	Galactic and Extragalactic All-sky MWA
G4Jy	GLEAM 4 Jy sample
MRC	Molonglo Reference Catalog of Radio Sources
MS4	Molonglo Southern 4 Jy sample
MURALES	MUse RADio Loud Emission line Snapshot
NED	NASA Extragalactic Database
NVAS	NRAO VLA Archive Survey
NVSS	NRAO VLA Sky Survey
Pan-STARRS	Panoramic Survey Telescope & Rapid Response System
PMN	Parkes-MIT-NRAO Surveys
PKSCAT90	Parkes radio catalog
SIMBAD	Set of Identifications, Measurements, and Bibliography for Astronomical Data
SDSS	Sloan Digital Sky Survey
SUMSS	Sydney University Molonglo Sky Survey
TGSS	TIFR GMRT Sky Survey
TXS	Texas Survey of Radio Sources at 365 MHz
VLA	Very Large Array
VLAAS	VLA Sky Survey
VLSSr	VLA Low-Frequency Sky Survey Redux

similar to the nominal value of the 3CR, allowed us to create a comparable statistical sample for radio sources mainly visible from the Southern Hemisphere, with access to the state-of-the-art observing facilities there. For reference, the 3CR lists 298 radio sources, while the 9 Jy cut used for the G4Jy-3CRE results in a list of 264 objects. However, to make a more precise comparison with the 3CR, we added a flag to all 181 radio sources out of 264 filtered for having radio flux densities above 9.8 Jy^{32} at 178 MHz; this threshold has been computed to account for calibration differences with respect to original 3C observations (see, e.g., Roger et al. 1973, and references therein).

The analysis of White et al. (2020a, 2020b) revealed that in the G4Jy catalog 86% of the radio sources appear to be associated with a mid-IR counterpart, detected in the all-sky survey performed with the Wide-field Infrared Survey Explorer (WISE; Wright et al. 2010). In the present analysis we only report WISE images at $3.4 \mu\text{m}$, but we refer to mid-IR counterparts of G4Jy sources considering those listed in the allWISE data release and thus based on the detection in all filters (Cutri et al. 2012, 2013). In our selected sample, 225 G4Jy-3CRE sources (i.e., $\sim 85\%$) are associated with a mid-IR counterpart detected in the WISE all-sky survey (White et al. 2020b).

Radio positions reported in the G4Jy were then computed using the NRAO VLA Sky Survey (NVSS; Condon et al. 1998) and/or Sydney University Molonglo Sky Survey (SUMSS; Mauch et al. 2003) images, while data available from the Tata Institute of Fundamental Research (TIFR) Giant Metrewave Radio Telescope (GMRT) Sky Survey (TGSS; Intema et al. 2017) were inspected to obtain a better overview of the radio structure. Thus, for sources at declinations above -39.5° , the position reported in the NVSS catalog was used, while for the remaining ones the one reported in the SUMSS catalog was adopted. Thus, given their relatively low angular resolution, there are sources, having an unusual radio morphology and/or being asymmetric, for which the location of the radio core, and consequently that of their host galaxy, was not clearly identified. For these reasons, as we described below, we expended considerable effort to investigate higher-resolution radio observations.

In Figure 1 we show the sky distribution, plotted adopting the Hammer–Aitoff projection, of the 3CR sources in the Northern Hemisphere alongside their equivalent sample of southern celestial objects, G4Jy-3CRE, to highlight their complementary footprints. Sources at Galactic latitudes $|b| < 10^\circ$ are excluded since they were not originally listed in the G4Jy catalog (White et al. 2020a).

3. Searching for Optical Counterparts

3.1. Identification Flags

We identified optical counterparts of radio nuclei overlaying radio contours on optical images. The same comparison with mid-IR images of the WISE all-sky survey³³ was then crucial to verify both (i) the presence of a mid-IR counterpart and (ii) the robustness of all associations reported in the original G4Jy

³² This flux density threshold was computed at 178 MHz extrapolating that between 174 and 181 MHz reported in the G4Jy catalog using the radio spectral index between these two frequencies. It corresponds to that used to create the original 3C catalog taking into account refined intercalibrations.

³³ <https://wise2.ipac.caltech.edu/docs/release/allwise/>

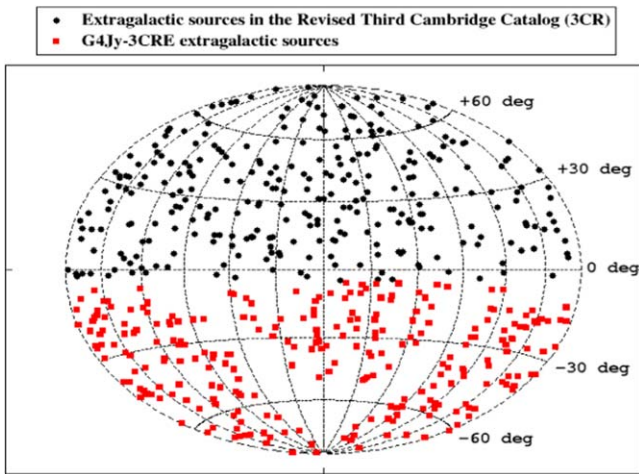


Figure 1. The sky distribution, shown in the Hammer–Aitoff projection, of the 3CR sources located in the Northern Hemisphere (black circles) in comparison with those belonging to the G4Jy-3CRE catalog (red squares), equivalent to the 3CR but located in the Southern Hemisphere. It is clear how footprints of both surveys are complementary, and the region of the Galactic plane was excluded to select the G4Jy-3CRE catalog.

catalog. As previously stated, we only report in our analysis a comparison between radio maps and mid-IR images at $3.4\ \mu\text{m}$ and the mid-IR associated counterpart as in the G4Jy based on detections of the AllWISE survey (Cutri et al. 2012).

We initially explored several radio databases to search for radio images of sources listed in the G4Jy-3CRE sample to identify the correct position of their radio cores. At radio frequencies we compared GLEAM images with those available in the databases of the VLA Low-Frequency Sky Survey Redux³⁴ (VLSSr; Cohen et al. 2007), TGSS,³⁵ NVSS,³⁶ and VLASS³⁷ (Lacy et al. 2020) for sources visible from the Northern Hemisphere, while we used mainly the SUMSS³⁸ for those lying outside of footprints of previous surveys. High-resolution radio surveys, such as the VLASS, allowed us to obtain a precise measurement of the radio core location.

To achieve our goals, we additionally checked the NVAS radio archive, mainly searching for radio images at 1.4, 5, and 8 GHz; however, these were useful only for a handful of sources, allowing us to clearly detect the position of their radio cores. NVAS radio maps, with angular resolution in the range between $0''.5$ and $\sim 10''$, are available for 124 out of 264 sources listed in the G4Jy-3CRE. Here, host galaxy search and identification are partially biased, being more efficient, toward sources located above declinations of $\sim -40^\circ$, where JVLA data are available.

For optical images, we retrieved optical images for 178 G4Jy-3CRE sources from the Pan-STARRS³⁹ and the DES⁴⁰ -databases, while for the remaining 86 objects, lying outside the footprints of these surveys, we inspected observations/images provided in the red filter of the Digital Sky Survey⁴¹ (DSS).

³⁴ <http://cade.irap.omp.eu/dokuwiki/doku.php?id=vlssr>

³⁵ <https://tgssadr.strw.leidenuniv.nl/doku.php>

³⁶ <https://www.cv.nrao.edu/nvss/>

³⁷ <https://public.nrao.edu/vlass/>

³⁸ <http://www.astrop.physics.usyd.edu.au/sumss/>

³⁹ <https://panstarrs.stsci.edu>

⁴⁰ <https://www.darkenergysurvey.org>

⁴¹ <https://archive.eso.org/dss/dss>

We adopted the following identification flags (IDFs) with a summary of all criteria described below. Association results based on these IDFs are all summarized in Table 2, together with several examples. In Table 3 we report all IDFs assigned to each source listed in the G4Jy-3CRE, together with other parameters. For the IDFs we distinguished the following cases:

1. $IDF = 1.0$: sources for which the position of the radio core is coincident with the mid-IR source associated in the original G4Jy catalog, and it also corresponds to a unique optical source detected in the r band of the Pan-STARRS/DES catalogs or in the red filter image obtained with the DSS, as shown for G4Jy 312 in Figure 2.
2. $IDF = 2.0$: sources having an optical counterpart of their radio core. However, on the basis of the mid-IR counterpart, we distinguished the following:
 - (a) $IDF = 2.1$: those sources having the radio core associated with a unique optical counterpart, different from the mid-IR one listed in the original G4Jy catalog ($IDF = 2.1$, as reported for G4Jy 524 in Figure 3).
 - (b) $IDF = 2.2$: those cases for which there is an optical counterpart but lacking an associated mid-IR source (i.e., $IDF = 2.2$, as shown for G4Jy 593 in Figure 3). According to the analysis performed by White et al. (2020a, 2020b), the latter ones are cases for which the identification of the host galaxy was partially or completely limited by the mid-IR data, either being undetected in the AllWISE survey or having its emission affected by a relatively bright nearby object.
3. $IDF = 3.0$: sources for which the low angular resolution of radio observations did not allow us to uniquely identify the optical counterpart ($IDF = 3.0$, as reported for G4Jy 934 in Figure 4), despite the presence of an associated mid-IR source. These are simply “confused” cases.
4. $IDF = 4.0$: sources for which there is no optical counterpart, being undetected at the sensitivity limit of the survey data we used to search for it. We also distinguished here several subcategories:
 - (a) $IDF = 4.1$: those lacking an optical counterpart but with an assigned mid-IR counterpart in the original G4Jy catalog ($IDF = 4.1$, as shown for G4Jy 1846 in Figure 5).
 - (b) $IDF = 4.2$: those for which there is no optical counterpart but the radio map used allowed us to verify that the previously assigned mid-IR one is incorrect ($IDF = 4.2$, as shown for G4Jy 1057 in Figure 5).
 - (c) $IDF = 4.3$: those lacking counterparts at both mid-IR and optical frequencies ($IDF = 4.3$, as reported for G4Jy 1587 in Figure 5).

Here we assume that a source is detected only if it is reported in the catalog corresponding to each survey used in the current analysis, thus having a detection threshold equal to the level of confidence of the survey itself. No associations between radio and mid-IR/optical counterparts were considered reliable if the angular separation between their positions is greater than $5''.4$. This is also supported by the seeing of optical surveys being $\sim 2''$ and by the statistical analysis reported in Section 3.

Table 2
Details on the Identification Flags (IDF) Adopted in Our Analysis and List of Examples

IDF	Criteria	Example	Cases
1.0	optical counterpart \equiv mid-IR counterpart	G4Jy 312	184 (70%)
2.1	optical counterpart \neq mid-IR counterpart	G4Jy 524	5 (2%)
2.2	optical counterpart but no mid-IR counterpart	G4Jy 593	21 (8%)
3.0	confused (not possible to assign either an optical and/or a mid-IR counterpart)	G4Jy 934	14 (5%)
4.1	no optical counterpart but mid-IR counterpart	G4Jy 1846	19 (7%)
4.2	no optical counterpart and incorrect mid-IR counterpart	G4Jy 1057	4 (2%)
4.3	no optical counterpart and no mid-IR counterpart	G4Jy 1587	17 (6%)

In Figures 2, 3, 4, and 5, we show WISE images collected at $3.4 \mu\text{m}$ with radio contours overlaid. The frequency of the radio map from which radio contours were drawn is reported in the figure, together with the intensity of the first level. All radio contours increase in level by a binning factor also reported in the figure. Radio maps obtained through the VLASS, NVSS, and SUMSS archives correspond to a nominal frequency of 3, 1.4, and 843 MHz, respectively. We also show optical images collected from one of the surveys used in our analysis. If the optical image has a label “red filter,” it was obtained from the DSS archive, while “*r* band” marks those retrieved from Pan-STARRS or DES archives. Radio contours are also overlaid on optical images. The red cross, if present, marks the position of the associated mid-IR counterpart according to the G4Jy catalog, while the cyan cross corresponds to the position of brightness-weighted radio centroids reported in the G4Jy (White et al. 2020a, 2020b). The blue dashed circle, whenever present, indicates the position of the optical counterpart identified in our analysis. We remark that the scales of the mid-IR and optical images are different on purpose. The underlying reasons are as follows: (i) the angular resolution is different, and (ii) mid-IR images, reported with a larger field of view, allow us to highlight the large-scale radio structure, while optical images were mainly used to identify counterparts as finding charts.

Sources having IDF = 1.0 (namely, those for which the resolution of radio maps allows us to firmly establish the position of the radio core) include also cases for which we do not clearly detect the radio nucleus but the brightness-weighted radio centroid of all radio maps used is coincident with a unique optical counterpart with no nearby companions, within an angular separation of $5''$ – $10''$. An example is shown in Figure 6, where we report the case of G4Jy 122, a classical FR II radio galaxy at $z = 0.4$, for which the radio morphology and the lack of optical sources within an angular separation of $10''$ from the potential optical counterpart allowed us to assign it an IDF = 1.0. We emphasize that for several sources we also used archival radio maps, collected from the NVAS database, that allowed us to unequivocally assign an optical counterpart (i.e., IDF = 1.0 rather than 3.0).

Once we identified the optical counterpart, we also searched the latest releases of both the Pan-STARRS and DES catalogs to obtain an estimate of its *r*-band magnitude. In Table 3 we summarize our main results, indicating (i) the G4Jy name, (ii) the name of the mid-IR counterpart associated in the G4Jy catalog using WISE images, both (iii) radio and (iv) optical positions, (v) the counterpart IDF, and (vi) the *r* magnitude of the optical counterpart, as previously mentioned, together with the optical magnitude and the Galactic extinction. Then, we added to the table the estimate of the Galactic extinction⁴² A_V

(Schlegel et al. 1998; Schlafly & Finkbeiner 2011). The entire Table 3 is reported in the online version of the journal, while only the first 10 lines are shown here for guidance regarding its form and content. Optical positions are reported from the Pan-STARRS and/or DES catalogs, when available, having all uncertainties lower than $\sim 0''.5$. We did not measure DSS magnitudes and positional uncertainties since we are already carrying out a photometric survey, mainly using telescopes at Complejo Astronómico El Leoncito (CASLEO), to estimate them for those sources lying outside of the Pan-STARRS and DES footprints.

We also inspected other optical images available in the Pan-STARRS/DES searching in the *g*, *i*, *z*, and *y* bands to detect the host galaxy of sources lacking an optical counterpart of their radio core but having an associated mid-IR object. This analysis confirmed previous results with the unique exception of G4Jy 818, for which we identified a marginal detection of an optical counterpart in the *y* band only.

3.2. Optical Identifications

We found that for 184 out of a total of 264 sources listed in the G4Jy-3CRE catalog (i.e., 70%) their optical counterpart is spatially coincident with the mid-IR match reported in the G4Jy catalog (White et al. 2020a, 2020b), thus confirming previous results. These are all marked with an IDF = 1.0 in our Table 3. In Figure 7 we report the distribution of the angular separation θ_{ow} between the optical and the mid-IR counterparts.

Only 5 out of 264 sources (i.e., $\sim 2\%$) show an incorrect association between the optical source we assigned and the mid-IR counterpart reported in the G4Jy catalog: G4Jy 4, G4Jy 524, G4Jy 1197, G4Jy 1302, and G4Jy 1854. For these five cases an IDF = 2.1 was assigned. Then, we identified new optical counterparts for 21 sources out of 264 (i.e., $\sim 8\%$, corresponding to IDF = 2.2) that did not have a mid-IR counterpart assigned in the original G4Jy catalog. This was mainly possible thanks to the use of high-resolution radio maps such as those retrieved from the VLASS and the NVAS archives. In particular, we found that four sources with IDF = 2.2, namely G4Jy 162, G4Jy 730, G4Jy 1301, and G4Jy 1330, have no mid-IR counterparts since they lie close to bright WISE sources and their detection could be contaminated by artifacts. In the case of G4Jy 593, again with IDF = 2.2, the detection of its mid-IR counterpart is indeed compromised by the poor angular resolution of WISE images. An additional 12 radio sources (out of 21) with IDF = 2.2, marked with a “u” host flag in the G4Jy catalog owing to possible ambiguities related to the complexity of their radio structure and/or the spatial distribution of nearby mid-IR sources (see White et al. 2020a, 2020b, for more details), have mid-IR counterparts, identified thanks to the refined optical

⁴² <https://irsa.ipac.caltech.edu/applications/DUST/>

Table 3
Full List of the G4Jy-3CRE Catalog

G4Jy Name	WISE Name	R.A. ^(r) (J2000)	Decl. ^(r) (J2000)	R.A. ^(o) (J2000)	Decl. ^(o) (J2000)	IDF	z	r (mag)	A_V (mag)	Sub.
4	J000322.14–172714.1	00:03:22.001	–17:27:11.412	00:03:21.9430	–17:27:11.663	2.1	1.465(?)	19.24	0.079	
9	J000557.94–562831.0	00:05:57.650	–56:28:31.512	00:05:57.8611	–56:28:30.930	1.0	0.2912	17.05	0.034	
12	J000616.50–830608.0	00:06:11.989	–83:05:56.911	00:06:16.5559	–83:06:07.280	1.0	...		0.578	✓
20	J001030.14–442257.1	00:10:30.550	–44:22:57.000	3.0	...		0.03	✓
26	J001524.35–380438.6	00:15:24.283	–38:04:35.375	3.0	...		0.045	
27	J001602.93–631003.8	00:16:02.681	–63:10:07.212	00:16:02.8827	–63:10:04.436	1.0	...	22.8	0.053	✓
33	J001851.42–124233.7	00:18:51.379	–12:42:33.516	00:18:51.3821	–12:42:34.041	1.0	1.589	22.96	0.11	✓
43	J002308.86–250229.6	00:23:09.341	–25:02:35.362	00:23:08.8739	–25:02:29.183	1.0	0.35	20.41	0.043	
45	J002430.15–292854.3	00:24:30.120	–29:28:48.900	00:24:30.1273	–29:28:54.426	1.0	0.40645	17.5	0.073	✓
48	J002549.22–260212.3	00:25:49.169	–26:02:12.804	00:25:49.1681	–26:02:12.786	1.0	0.32188	19.85	0.049	✓

Note. Column (1): the name reported in the G4Jy catalog. Column (2): the name of the assigned mid-IR counterpart, detected in WISE, as in the G4Jy catalog. Columns (3) and (4): R.A. and decl., in J2000 equinox, of the brightness-weighted radio centroid (r) collected from the G4Jy catalog. Columns (5) and (6): same as the previous two columns, but measured from the centroid of the optical counterpart (o) in the Pan-STARRS, DES, and DSS images. Column (7): identification flag adopted in our analysis (see Section 3 for all details). Column (8): the redshift value reported in the literature, where question marks highlight those with uncertain estimates. Column (9): r -band magnitude from the Pan-STARRS and DES counterparts. Column (10): Galactic extinction. Column (11): the check mark indicates whether the source belongs to the subsample selected with radio flux density above 9.8 Jy at ~ 178 MHz (see Section 2 for more details).

(This table is available in its entirety in machine-readable form.)

analysis presented here. These radio sources are G4Jy 113, G4Jy 350, G4Jy 530, G4Jy 611, G4Jy 672, G4Jy 680, G4Jy 939, G4Jy 1262, G4Jy 1365, G4Jy 1401, G4Jy 1518, and G4Jy 1740, and all their mid-IR associated counterparts are now reported in Table 3. In addition, for the two cases of G4Jy 837 and G4Jy 1590, both having $IDF = 2.2$ and both previously labeled with an “m” host flag in the G4Jy catalog (i.e., identification of their host galaxy limited by the mid-IR data; White et al. 2020b), the optical analysis presented here allowed us to recognize their mid-IR counterpart. In Table 4 we report the WISE name of these 14 mid-IR counterparts identified by refined optical analysis performed here. These are also included in Table 3. We marked the location of these 14 newly associated mid-IR counterparts using a red circle on the WISE image at $3.4 \mu\text{m}$ in the finding charts to distinguish them from those associated in the G4Jy catalog labeled with a red cross. The only two remaining sources, G4Jy 1498 and G4Jy 1532, are those clearly lacking a mid-IR counterpart, being undetected in the WISE images. In Figure 7 we also report the distribution of the angular separation θ_{ow} between the optical and the mid-IR counterparts, including those with $IDF = 2.2$ that have been assigned thanks to the optical analysis presented here.

We found that 14 out of the 264 sources (i.e., $\sim 6\%$) visually inspected are flagged as “confused,” since we were not able to identify a unique optical counterpart, and thus require a deeper investigation and eventually additional follow-up observations. If these sources are high-excitation radio galaxies (HERGs; Hine & Longair 1979) or quasars, due to their relatively low source density (i.e., number of sources per square degree in the sky), X-ray or optical spectroscopic observations could reveal the position of their counterpart and thus identify their host galaxies. However, the precise location of their radio core, necessary to identify the host galaxy position, can be only achieved using higher-resolution radio maps, in particular when they are hosted in elliptical galaxies with weak optical emission lines, as often occurs in low-excitation radio galaxies (LERGs; Hine & Longair 1979). For all of them the value of $IDF = 3.0$ is reported in Table 3.

There are 19 out of 264 sources that lack an optical counterpart of the radio core but have at least a mid-IR source associated with it (i.e., $\sim 7\%$ of the whole G4Jy-3CRE catalog), thus being marked with $IDF = 4.1$, as for G4Jy 1846 shown in Figure 5. For 4 more objects out of 264 (i.e., $\sim 2\%$), the associated mid-IR source does not appear to be correct, thus having $IDF = 4.2$ (see G4Jy 1057 in Figure 5, as well as G4Jy 183, G4Jy 1551, and G4Jy 1782). Lastly, 17 remaining sources ($\sim 6\%$ of the total) have no optical and no mid-IR counterpart associated with their radio core and are indicated with $IDF = 4.3$. Two of those radio sources labeled with $IDF = 4.3$ are G4Jy 77 and G4Jy 1605; the former is a radio phoenix of the galaxy cluster A85 (see, e.g., Bagchi et al. 1998; Kempner et al. 2004; Ichinohe et al. 2015), while the latter is the radio relic of A3667 (see, e.g., Johnston-Hollitt et al. 2008; Owers et al. 2009), as also discussed, in more detail, in Appendix A.

All sources with $IDF = 4.1$ or $IDF = 4.2$ or $IDF = 4.3$ have no detection of their radio cores in radio maps owing to their poor angular resolution, with the only exceptions of four objects: G4Jy 854, G4Jy 1010, G4Jy 1136, and G4Jy 1830. In these four cases the detection of the mid-IR counterpart could be contaminated by artifacts, due to the presence of bright WISE sources, for G4Jy 854 and G4Jy 1136, while for G4Jy 1010 and G4Jy 1830 no clear mid-IR emission is reported in the WISE all-sky catalog.

All numbers reported in this section are also summarized in Table 2.

Finally, there are 203 out of 264 sources listed in the G4Jy-3CRE sample (i.e., $\sim 77\%$) (i) having the optical counterpart coincident with the mid-IR one (i.e., $IDF = 1.0$) or (ii) lacking the optical counterpart of their radio core but having a mid-IR counterpart (i.e., $IDF = 4.1$). Thus, in Appendix C we computed the probability of spurious associations between mid-IR sources listed in the WISE all-sky survey and the full G4Jy radio catalog, as originally performed to assign mid-IR counterparts, and we found a good agreement with the refined analysis presented here.

4. Literature Results

Once we identified optical counterparts of radio sources, we performed a literature search to investigate the availability of

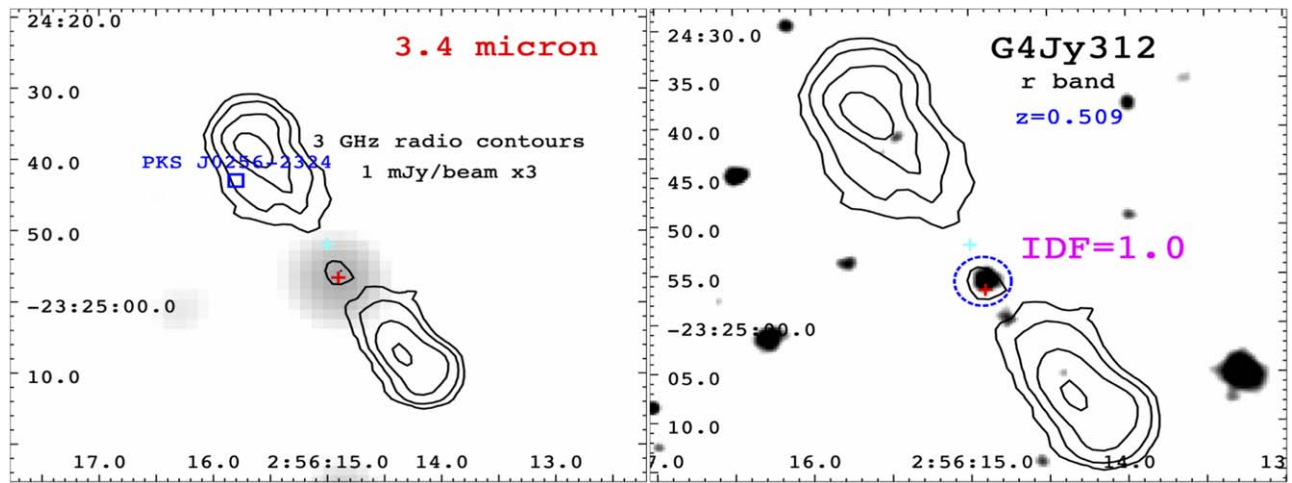


Figure 2. Left panel: the $3.4\ \mu\text{m}$ image available thanks to the WISE all-sky survey, with radio contours overlaid in black. The frequency of the radio map from which the radio contours were drawn is reported in the figure, together with the intensity of the first level and the binning factor. The symbol $\times 3$, reported in the image, indicates that radio contours, starting at $1\ \text{mJy beam}^{-1}$ level, increase by a factor of three. Radio maps from VLASS, NVSS, and SUMSS archives correspond to a nominal frequency of 3, 1.4, and 843 MHz, respectively. Right panel: the optical image collected from one of the optical surveys used in our analysis. If, below the source name, the label “red filter” is reported, then the optical image is collected from the DSS archive, while when it is written “r band,” as in this case, optical images were retrieved from Pan-STARRS or DES databases. Radio contours are also overlaid on the optical image. The red cross, if present, marks the position of the mid-IR counterpart associated in the G4Jy catalog, while the cyan cross corresponds to the position of the brightness-weighted radio centroid of the G4Jy catalog (White et al. 2020a, 2020b). The blue dashed circle, if present, indicates the position of the optical counterpart identified from our analysis. Both these images are an example of a source, i.e., G4Jy 312, having an $\text{IDF} = 1.0$, for which our analysis revealed that the mid-IR counterpart associated in the G4Jy catalog corresponds to the optical source lying at the same position of the radio nucleus in the high angular resolution radio map used here. The blue open square or the blue plus sign, if present in the left panel, marks the location of the closest radio source belonging to the Parkes radio catalog (PKSCAT90; Bolton et al. 1979) or to the MRC (Large et al. 1981), respectively (see also Appendix C for additional details about radio cross-identifications). The complete figure set, showing finding charts for all sources in the G4Jy catalog, is available in the online journal.

(The complete figure set (264 images) is available.)

redshifts. Results of this literature search, including uncertain z estimates, are also reported in each figure when available and in the finding charts. We also compared our final catalog with the several radio catalogs obtained from radio surveys (see Appendix B for a brief overview of all radio catalogs used here). All these identifications derived from these radio crossmatches are reported in Appendix B to simplify searches in astronomical databases such as the NASA Extragalactic Database (NED)⁴³ and the Set of Identifications, Measurements, and Bibliography for Astronomical Data (SIMBAD) Astronomical Database.⁴⁴

We found that for a total of 157 sources out of 264 (i.e., 59% of the whole sample) there is a spectroscopic redshift measurement already available in the literature, with 12 of them considered uncertain and thus labeled with a question mark, for a total of 145 radio sources with firm z estimates. Our search was carried out also using NED and SIMBAD. According to previous analyses carried out during past follow-up spectroscopic campaigns (Massaro et al. 2016; Peña-Herazo et al. 2020, 2022; Kosiba et al. 2022), we adopted the same conservative criteria, and we only considered confident redshift measurements reported in the literature those for which (i) we could verify a published image of the optical spectrum or (ii) there is a description of it with emission and/or absorption lines clearly reported in a table or in the manuscript. In this way, we marked redshifts z we could not verify with a question mark for 12 sources out of 157.

Moreover, we did not consider photometric redshifts since we are currently carrying out optical spectroscopic

observations, based on the analysis presented here, and more redshifts will be presented in a forthcoming paper (A. García-Pérez et al. 2023, in preparation). In some cases, and only for sources belonging to the MS4 (Burgess & Hunstead 2006a, 2006b), we reported values of photometric redshift estimates in Appendix A.

A large fraction of the spectra we found are available in Data Release 3 of the Six-degree Field Galaxy Survey (6dFGS) Database⁴⁵ (Jones et al. 2004, 2009) in addition to the spectroscopic observations of the equatorial sample of powerful radio galaxies (Best et al. 1999). In a few cases we also used other databases such as the Online Inventory of Extragalactic X-ray Jets⁴⁶ (XJET; Massaro et al. 2011) and references reported therein.

According to our literature search, we found that 131 sources out of 157 having $\text{IDF} = 1.0$ already have an available redshift measurement. For all these cases, with only two exceptions (G4Jy 1158 and G4Jy 1225), we found these estimates reliable (i.e., no question mark reported). The underlying choice of considering these estimates, at a first look correct, is also based on the relatively low sky density (i.e., number of sources per square degree) of radio galaxies and QSOs; thus, the probability of having more than a single radio-loud AGN close to the radio position within a circle with a radius of a few arcseconds is extremely low. This also proves the importance of collecting spectroscopic information that could confirm optical counterparts associated in the present analysis (see, e.g., results of spectroscopic campaigns carried out on radio-loud AGNs lying within the positional uncertainty regions of

⁴³ <http://ned.ipac.caltech.edu>

⁴⁴ <http://simbad.u-strasbg.fr/simbad/>

⁴⁵ <http://www-wfau.roe.ac.uk/6dFGS/index.html>

⁴⁶ <https://hea-www.harvard.edu/XJET/>

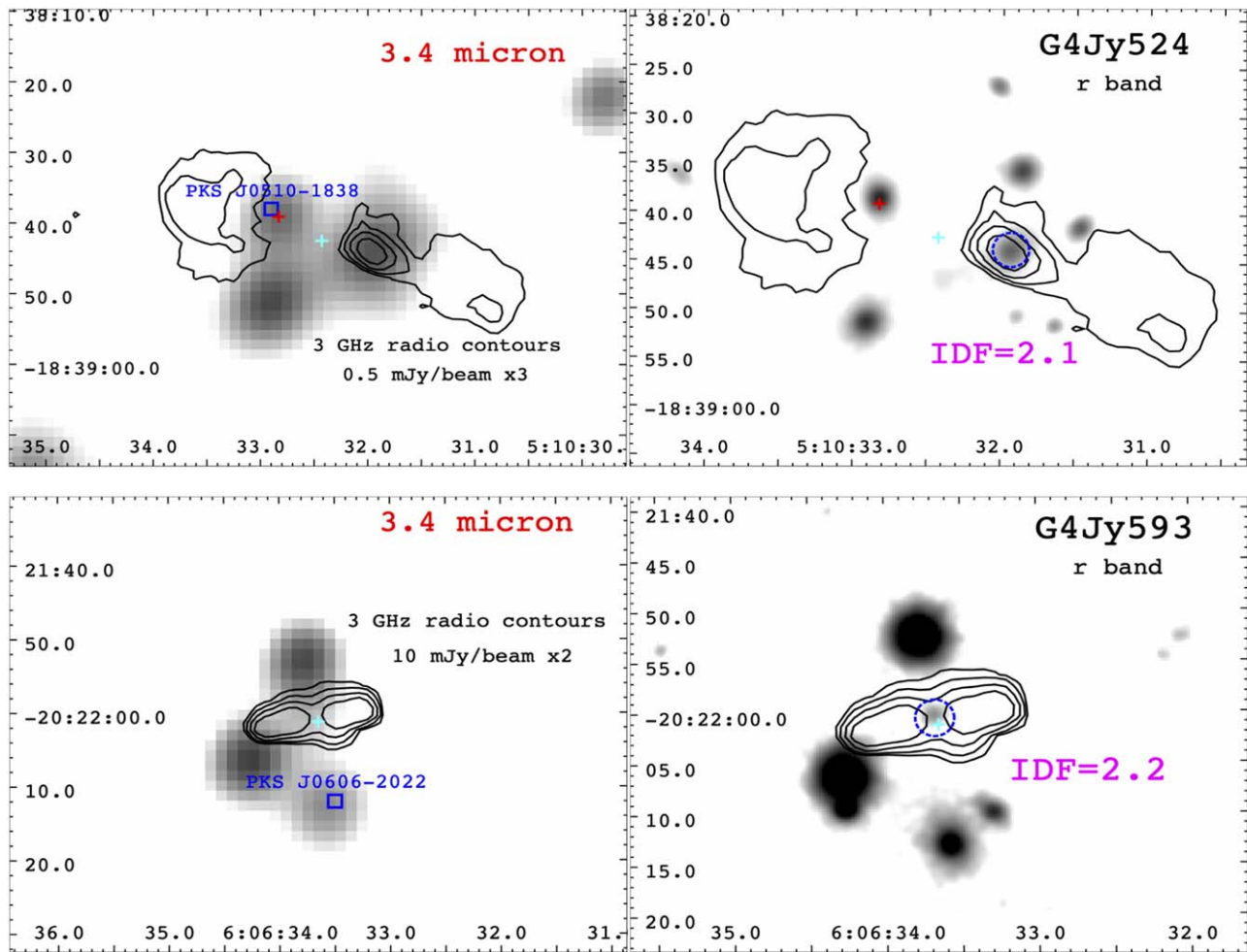


Figure 3. Top panels: same as Figure 2, but for the case of G4Jy 524, a radio source for which the mid-IR counterpart identified in the G4Jy catalog is different from the optical one that corresponds to the position of the radio core detected in the VLASS radio map at 3 GHz. Sources showing the same behavior were marked with an IDF = 2.1 in our analysis. Bottom panels: same as Figure 2, but for G4Jy 593. This radio source, having IDF = 2.2, is an example of those cases for which there is a clear optical counterpart but they lack an assigned mid-IR source in the G4Jy catalog.

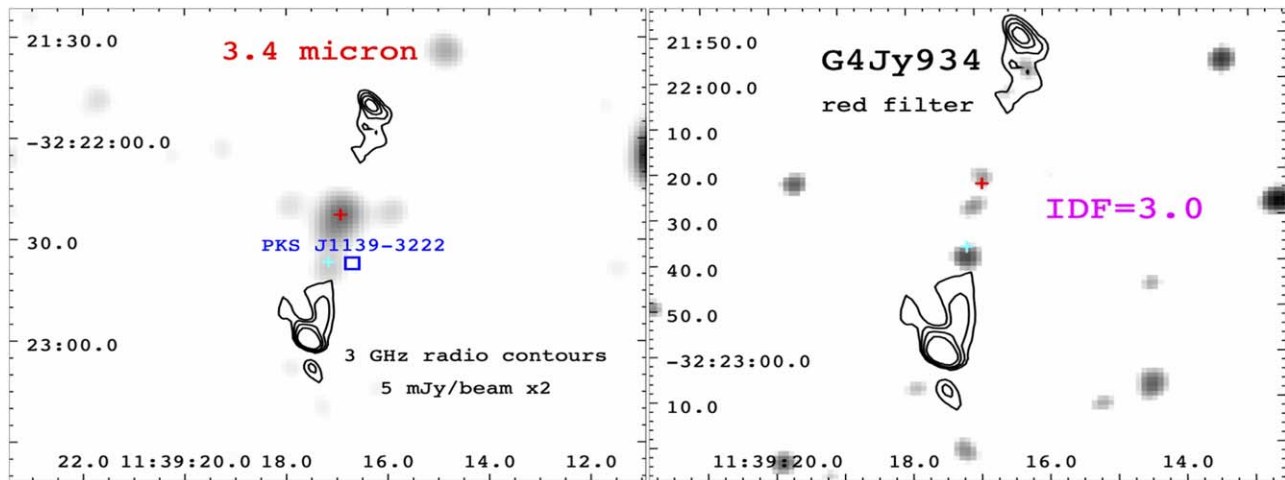


Figure 4. Same as Figure 2, but for G4Jy 934. The lack of a high angular resolution radio map (in this case the one from which radio contours are computed was collected from the SUMSS archive) prevented us from clearly identifying the host galaxy of the radio source. These cases are flagged as “confused” in our analysis and have IDF = 3.0.

gamma-ray sources; Landoni et al. 2015; Massaro et al. 2015b; Ricci et al. 2015; Álvarez Crespo et al. 2016). In Figure 8 we show the comparison between the redshift distribution for 157

radio sources, out of 264 listed in the G4Jy-3CRE catalog, having a z estimate and that excluding those 12 with uncertain z .

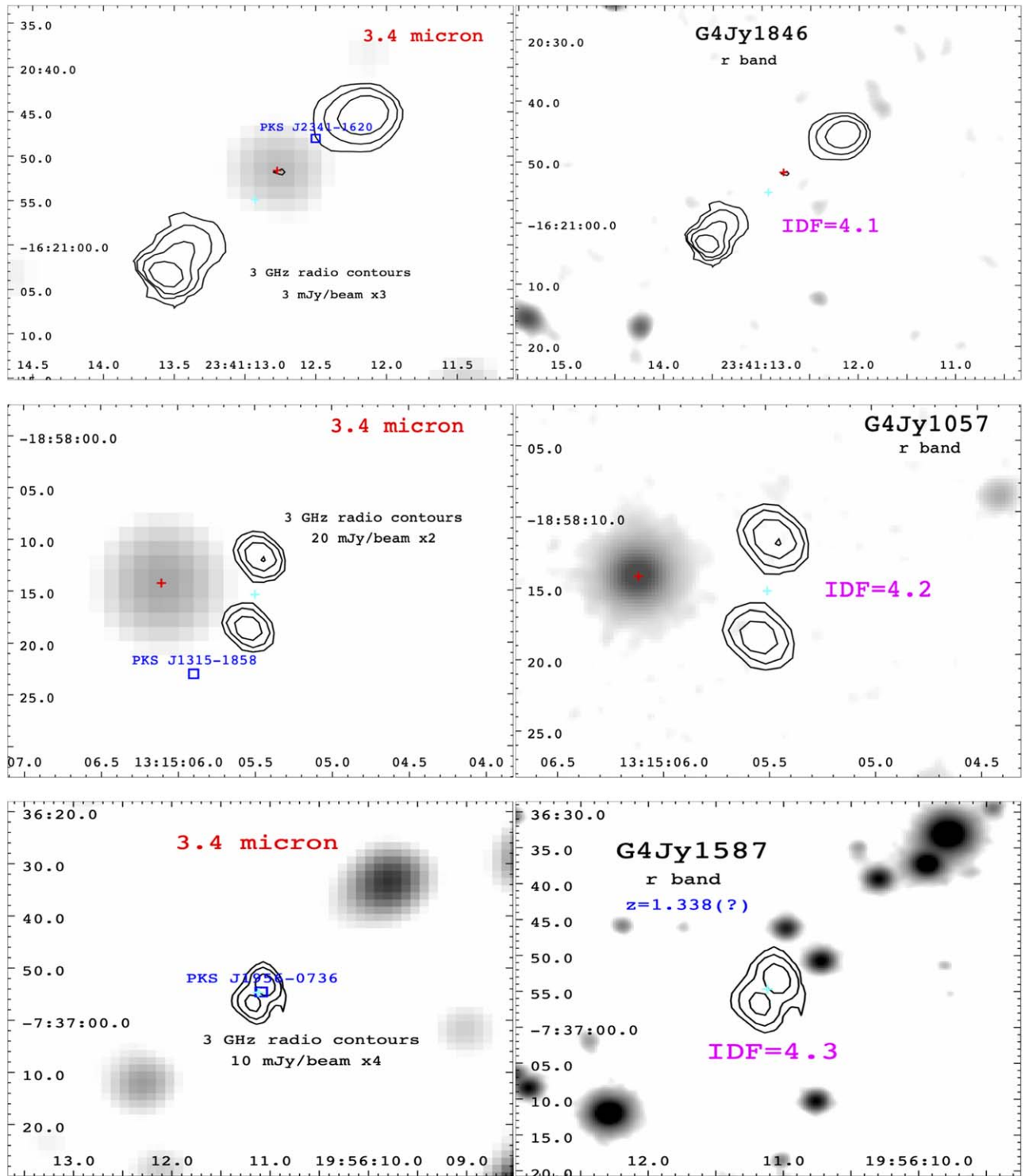


Figure 5. Top panels: same as Figure 3, but for G4Jy 1846. As shown in the right panel, the optical counterpart of the radio nucleus is too faint to be detected in the images available from the Pan-STARRS, DES, and DSS databases; however, it is clear from the left panel that the radio source has an infrared counterpart. These cases are indicated with $IDF = 4.1$. Middle panels: same images for G4Jy 1057, but in this case, despite the lack of a plausible optical counterpart, the radio map available indicates that the assigned mid-IR counterpart appears to be incorrect, thus marked in our analysis with $IDF = 4.2$. Bottom panels: same as the middle panels, but for sources such as G4Jy 1587 that lack both a mid-IR and an optical counterpart of its radio core. G4Jy 1587 has $IDF = 4.3$. These are radio sources for which we also visually inspected other optical images available in the Pan-STARRS and in the DES databases in the g , i , z , and y bands searching for signatures of their host galaxies.

For those sources with $IDF = 2.1$ or $IDF = 2.2$ we found a redshift estimate for 17 cases out of 26, namely 3 objects with $IDF = 2.1$ and 14 with $IDF = 2.2$. In two out of the three cases with $IDF = 2.1$, we report z estimates in Table 3, adding the question mark to indicate that these measurements are uncertain

given the lack of positional data about the target, while this situation does not occur for all radio sources with $IDF = 2.2$.

For only one case out of the “confused” sources (i.e., those labeled with $IDF = 3.0$), namely G4Jy 1626, that could potentially reside in galaxy-rich large-scale environments

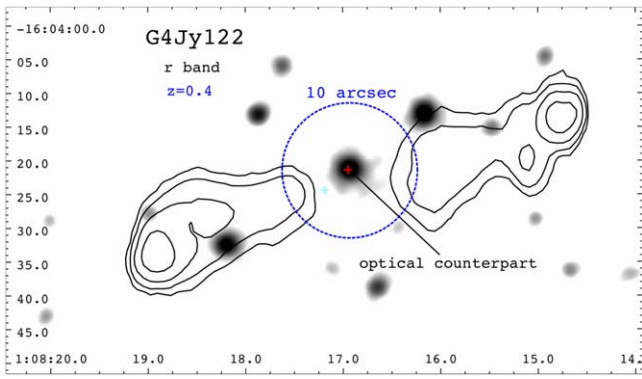


Figure 6. Same as the right panel of Figure 3, but for G4Jy 122. The dashed blue circle, having $10''$ radius, is centered on the location of the potential optical counterpart identified here since (i) it lies between the two radio lobes of G4Jy 122 showing a classical FR II radio morphology and (ii) there are no other optical sources within this area.

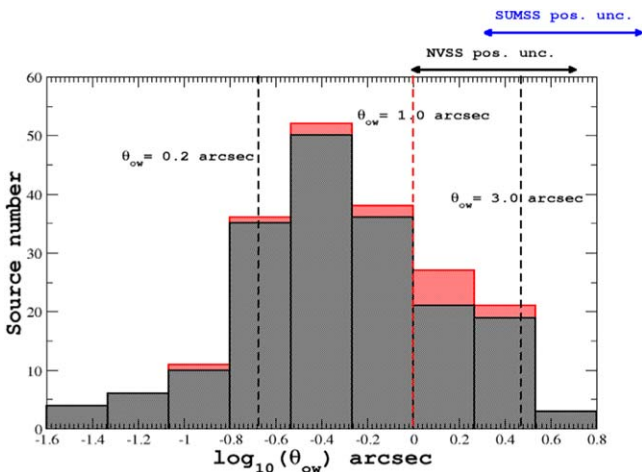


Figure 7. The black histogram shows the distribution of the angular separation θ_{ow} between the mid-IR counterpart, assigned in the G4Jy catalog, and the optical one for all those G4Jy-3CRE radio sources having $IDF = 1.0$, which, according to our analysis, implies that both counterparts are coincident. Two dashed black lines mark the location for θ_{ow} equal to $0''.2$, and $3''$, respectively, while the red one corresponds to $1''$. The red histogram includes also those radio sources with $IDF = 2.2$ for which our optical analysis helped to identify the mid-IR counterpart (see Section 3.2 for more details). As a comparison, we also report here the typical range of positional uncertainties of the NVSS and the SUMSS catalogs (Vollmer et al. 2005), mainly used in the G4Jy catalog to compute brightness-weighted radio centroids.

(i.e., groups or cluster of galaxies), we also report a z estimate with a question mark, while the remaining 13 sources all lack a z measurement.

Finally, we found that for 6 sources (out of 19) marked with $IDF = 4.1$, for which we were not able to identify the optical counterpart in the archival images, there is a z estimate in the literature, but since we could not verify which sources were targeted, they are all flagged as uncertain, with the only exception being G4Jy 417, for which we found the finding chart in the literature since it belongs to the 2 Jy sample (Wall & Peacock 1985; Morganti et al. 1997), even if we could not detect it in the DSS archival images used here. Then, all four radio sources with $IDF = 4.2$ have no z measurement, and the same occurs for 15 out of 17 of those labeled with $IDF = 4.3$. Both remaining radio sources with $IDF = 4.3$ have the z estimate marked with a question mark and are thus considered uncertain.

Current redshift distribution of the G4Jy-3CRE

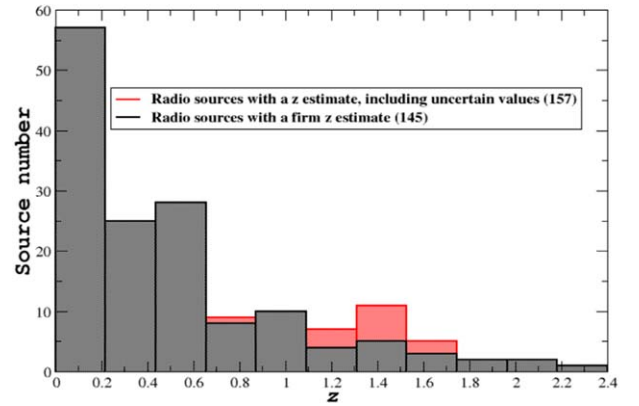


Figure 8. The redshift distribution obtained from our literature search for those 157 radio sources listed in the G4Jy-3CRE catalog with a z estimate. The red histogram includes also 12 radio sources with uncertain values, in comparison with that of radio sources with firm z measurements shown in gray.

Table 4
Newly Assigned Mid-IR Counterparts of Sources with $IDF = 2.2$

G4Jy Name	WISE Name	θ_{ow} (arcseconds)
113	J010241.76–215254.2	2.65
350	J032314.09–881605.2	1.84
530	J051247.41–482416.5	0.63
611	J062620.46–534135.1	1.31
672	J074331.61–672625.5	1.78
680	J080236.28–095739.9	0.38
837	J102003.93–425130.0	1.48
939	J114134.22–285048.0	0.32
1262	J153014.29–423151.7	1.9
1365	J164604.85–222804.6	1.05
1401	J172011.01–070132.2	0.14
1518	J191548.68–265257.4	0.28
1590	J195816.66–550934.9	0.59
1740	J215407.02–515012.8	1.18

Note. Column (1): the name reported in the G4Jy catalog. Column (2): the name of the mid-IR counterpart, detected in WISE, assigned thanks to the optical analysis presented here. Column (3): the angular separation θ_{ow} between the position of the optical and mid-IR counterpart, assigned thanks to the analysis performed here.

5. Summary, Conclusions, and Future Perspectives

We present the G4Jy-3CRE catalog extracted from the G4Jy catalog (White et al. 2020a, 2020b) and based on the low radio frequency observations of the MWA as part of the GLEAM survey. The G4Jy-3CRE catalog lists 264 sources with 9 Jy limiting sensitivity at ~ 178 MHz, which is the same as the nominal threshold for the 3CR, but including only targets at decl. $< -5^\circ$, having Galactic latitudes $|b| > 10^\circ$, all lying in the footprint not covered by the 3CR.

Thanks to a huge amount of effort carried out on the G4Jy catalog, a large fraction of radio sources listed therein (i.e., $\sim 85\%$) are associated with a mid-IR counterpart (being their host galaxy; White et al. 2020b) detected in the WISE all-sky survey (Wright et al. 2010). Here we present a refined analysis, restricted only to the G4Jy-3CRE sample, aimed at locating optical counterparts of their host galaxies. Thanks to recent high angular resolution radio observations, such as those

available in the VLASS, we can obtain a precise estimate of the position of their radio cores, for a significant fraction of the G4Jy-3CRE sources (i.e., 207 out of 264, nearly 78%). This allowed us to (i) improve the localization of the host galaxy in the optical images of Pan-STARRS, DES, and DSS archives and then (ii) search the literature for sources for which a redshift estimate is already available.

Results achieved by our inspection of archival radio, infrared, and optical images can be summarized as follows:

1. We found that for 184 out of 264 G4Jy-3CRE sources the optical counterpart associated in the present analysis is coincident with the mid-IR counterpart reported in the G4Jy catalog, confirming the robustness of the previous analysis (White et al. 2020a, 2020b).
2. There are 26 G4Jy-3CRE sources for which the optical counterpart we identified is different from the (previously assigned) mid-IR one. In particular, for 21 of them there is not a mid-IR source assigned/associated in the G4Jy catalog. For 14 out of these 21 radio sources we have been able to assign a mid-IR counterpart on the basis of our optical analysis.
3. For 14 sources the poor angular resolution of radio maps available and the presence of several optical sources around the position of their radio cores did not allow us to confirm their host galaxies.
4. There are an additional 40 sources with no optical counterpart of their radio core. For 4 cases the mid-IR counterpart associated in the G4Jy catalog does not appear to be correct ($IDF = 4.2$), while for 17 sources there is no mid-IR counterpart detected at the location of the radio cores, as reported in the G4Jy catalog (i.e., $IDF = 4.3$). The remaining 19 sources are only detected in the mid-IR images ($IDF = 4.1$).

According to our analysis, radio sources having the identification flags $IDF = 1.0$ or $IDF = 4.1$ are $\sim 77\%$ (i.e., 203 out of 264) of the whole G4Jy-3CRE sample and correspond to the more reliable mid-IR associations. This is in agreement with the statistical test we used to compute the expected number of spurious associations when matching the G4Jy with the AllWISE catalog.

Given the identified location of the host galaxies for a large fraction of the G4Jy-3CRE sources, we also checked the literature to search for possible redshift estimates. Adopting a conservative criterion, we found a total of 157 spectra, and 145 of them appear to provide a firm z estimate. Moreover, 129 are reliable since their optical counterpart coincides with that associated at mid-IR frequencies and are not labeled as possible sources having an uncertain z measurement.

Finally, we conclude by highlighting future perspectives on the potential use of the G4Jy-3CRE sample. Several proposals were already submitted to collect optical spectroscopic information for all sources listed in the G4Jy-3CRE catalog, and in a forthcoming paper of this series, part of these observations, already acquired, will be presented (A. García-Pérez et al. 2023, in preparation). A dedicated paper presenting the X-ray analysis, based on Swift data collected for ~ 80 G4Jy-3CRE sources, is also in preparation, highlighting the potential use of X-ray snapshot observations to refine the search for optical counterparts and host galaxies (F. Massaro et al. 2023, in preparation).

We thank the anonymous referee for useful and valuable comments that led to improvements in the paper. We wish to dedicate this paper to D. E. Harris and R. W. Hunstead. Their insight, passion, and contributions to radio astronomy are an inspiration.

A.J. acknowledges the financial support (MASF_CONTR_-FIN_18_01) from the Italian National Institute of Astrophysics under the agreement with the Instituto de Astrofísica de Canarias for the “Becas Internacionales para Licenciados y/o Graduados Convocatoria de 2017.” S.V.W. acknowledges financial assistance of the South African Radio Astronomy Observatory (SARAO).⁴⁷ W.F. and R.K. acknowledge support from the Smithsonian Institution and the Chandra High Resolution Camera Project through NASA contract NAS8-03060. W.F. also acknowledges support from NASA grants 80NSSC19K0116, GO1-22132X, and GO9-20109X. This investigation is supported by the National Aeronautics and Space Administration (NASA) grants GO9-20083X, GO0-21110X, and GO1-22087X. I.A., S.A.C., and V.R. are partially supported by grant PIP 1220200102169CO, Argentine Research Council (CONICET). A.G.-P. acknowledges support from the CONACyT program for their PhD studies. V.C. acknowledges support from the Fulbright—García Robles scholarship. This work was partially supported by CONACyT (Consejo Nacional de Ciencia y Tecnología) research grant 280789.

This research has made use of the NASA/IPAC Extragalactic Database (NED), which is operated by the Jet Propulsion Laboratory, California Institute of Technology, under contract with the National Aeronautics and Space Administration. This research has made use of the SIMBAD database, operated at CDS, Strasbourg, France (Wenger et al. 2000).

This research has made use of the CIRADA cutout service at URL cutouts.cirada.ca, operated by the Canadian Initiative for Radio Astronomy Data Analysis (CIRADA). CIRADA is funded by a grant from the Canada Foundation for Innovation 2017 Innovation Fund (Project 35999), as well as by the Provinces of Ontario, British Columbia, Alberta, Manitoba, and Quebec, in collaboration with the National Research Council of Canada, the US National Radio Astronomy Observatory, and Australia’s Commonwealth Scientific and Industrial Research Organisation. The National Radio Astronomy Observatory is a facility of the National Science Foundation operated under cooperative agreement by Associated Universities, Inc. Part of this work is based on the NVSS (NRAO VLA Sky Survey): The National Radio Astronomy Observatory is operated by Associated Universities, Inc., under contract with the National Science Foundation and on the VLA low-frequency Sky Survey (VLSS). We thank the staff of the GMRT that made these observations possible. GMRT is run by the National Centre for Radio Astrophysics of the Tata Institute of Fundamental Research. The Molonglo Observatory site manager, Duncan Campbell-Wilson, and the staff, Jeff Webb, Michael White, and John Barry, are responsible for the smooth operation of Molonglo Observatory Synthesis Telescope (MOST) and the day-to-day observing program of SUMSS. The SUMSS survey is dedicated to Michael Large, whose expertise and vision made the project possible. MOST is operated by the School of Physics with the support of the Australian Research Council and the Science Foundation for Physics within the University of Sydney. This scientific work makes use of the Murchison Radio-

⁴⁷ <https://www.sarao.ac.za>

astronomy Observatory, operated by CSIRO. We acknowledge the Wajarri Yamatji people as the traditional owners of the Observatory site. Support for the MWA comes from the US National Science Foundation (grants AST-0457585, PHY-0835713, CAREER-0847753, and AST-0908884), the Australian Research Council (LIEF grants LE0775621 and LE0882938), the US Air Force Office of Scientific Research (grant FA9550-0510247), and the Centre for All-sky Astrophysics (an Australian Research Council Centre of Excellence funded by grant CE110001020). Support is also provided by the Smithsonian Astrophysical Observatory, the MIT School of Science, the Raman Research Institute, the Australian National University, and the Victoria University of Wellington (via grant MED-E1799 from the New Zealand Ministry of Economic Development and an IBM Shared University Research Grant). The Australian Federal government provides additional support via the Commonwealth Scientific and Industrial Research Organisation (CSIRO), National Collaborative Research Infrastructure Strategy, Education Investment Fund, and the Australia India Strategic Research Fund, and Astronomy Australia Limited, under contract to Curtin University. This work was supported by resources provided by the Pawsey Supercomputing Centre with funding from the Australian Government and the Government of Western Australia. We acknowledge the iVEC Petabyte Data Store, the Initiative in Innovative Computing, and the CUDA Center for Excellence sponsored by NVIDIA at Harvard University, and the International Centre for Radio Astronomy Research (ICRAR), a Joint Venture of Curtin University, and The University of Western Australia, funded by the Western Australian State government.

This publication makes use of data products from the Wide-field Infrared Survey Explorer, which is a joint project of the University of California, Los Angeles, and the Jet Propulsion Laboratory/California Institute of Technology, funded by the National Aeronautics and Space Administration.

This project used public archival data from the Dark Energy Survey (DES). Funding for the DES Projects has been provided by the U.S. Department of Energy, the U.S. National Science Foundation, the Ministry of Science and Education of Spain, the Science and Technology Facilities Council of the United Kingdom, the Higher Education Funding Council for England, the National Center for Supercomputing Applications at the University of Illinois at Urbana-Champaign, the Kavli Institute of Cosmological Physics at the University of Chicago, the Center for Cosmology and Astro-Particle Physics at The Ohio State University, the Mitchell Institute for Fundamental Physics and Astronomy at Texas A&M University, Financiadora de Estudos e Projetos, Fundação Carlos Chagas Filho de Amparo à Pesquisa do Estado do Rio de Janeiro, Conselho Nacional de Desenvolvimento Científico e Tecnológico and the Ministério da Ciência, Tecnologia e Inovação, the Deutsche Forschungsgemeinschaft, and the Collaborating Institutions in the Dark Energy Survey. The Collaborating Institutions are Argonne National Laboratory, the University of California at Santa Cruz, the University of Cambridge, Centro de Investigaciones Energéticas, Medioambientales y Tecnológicas-Madrid, the University of Chicago, University College London, the DES-Brazil Consortium, the University of Edinburgh, the Eidgenössische Technische Hochschule (ETH) Zürich, Fermi National Accelerator Laboratory, the University of Illinois at Urbana-Champaign, the Institut de Ciències de l'Espai (IEEC/CSIC), the Institut de Física d'Altes Energies, Lawrence Berkeley National Laboratory, the Ludwig-Maximilians Universität

München and the associated Excellence Cluster Universe, the University of Michigan, the National Optical Astronomy Observatory, the University of Nottingham, The Ohio State University, the OzDES Membership Consortium, the University of Pennsylvania, the University of Portsmouth, SLAC National Accelerator Laboratory, Stanford University, the University of Sussex, and Texas A&M University. Based in part on observations at Cerro Tololo Inter-American Observatory, National Optical Astronomy Observatory, which is operated by the Association of Universities for Research in Astronomy (AURA) under a cooperative agreement with the National Science Foundation. The Pan-STARRS1 Surveys (PS1) have been made possible through contributions of the Institute for Astronomy, the University of Hawaii, the Pan-STARRS Project Office, the Max-Planck Society and its participating institutes, the Max Planck Institute for Astronomy, Heidelberg and the Max Planck Institute for Extraterrestrial Physics, Garching, Johns Hopkins University, Durham University, the University of Edinburgh, Queen's University Belfast, the Harvard-Smithsonian Center for Astrophysics, the Las Cumbres Observatory Global Telescope Network Incorporated, the National Central University of Taiwan, the Space Telescope Science Institute, the National Aeronautics and Space Administration under grant No. NNX08AR22G issued through the Planetary Science Division of the NASA Science Mission Directorate, the National Science Foundation under grant No. AST-1238877, the University of Maryland, and Eotvos Lorand University (ELTE). Based on photographic data obtained using the UK Schmidt Telescope. The UK Schmidt Telescope was operated by the Royal Observatory Edinburgh, with funding from the UK Science and Engineering Research Council, until 1988 June, and thereafter by the Anglo-Australian Observatory. Original plate material is copyright (c) of the Royal Observatory Edinburgh and the Anglo-Australian Observatory. The plates were processed into the present compressed digital form with their permission. The Digitized Sky Survey was produced at the Space Telescope Science Institute under US Government grant NAG W-2166. We acknowledge the efforts of the staff of the Anglo-Australian Observatory, who have undertaken the observations and developed the 6dF instrument.

SAOImageDS9 development has been made possible by funding from the Chandra X-ray Science Center (CXC), the High Energy Astrophysics Science Archive Center (HEASARC), and the JWST Mission office at Space Telescope Science Institute (Joye & Mandel 2003). This research has made use of data obtained from the High-Energy Astrophysics Science Archive Research Center (HEASARC) provided by NASA's Goddard Space Flight Center. We acknowledge the use of NASA's SkyView facility (<http://skyview.gsfc.nasa.gov>) located at NASA Goddard Space Flight Center. This data set or service is made available by the Infrared Science Archive (IRSA) at IPAC, which is operated by the California Institute of Technology under contract with the National Aeronautics and Space Administration. TOPCAT and STILTS astronomical software (Taylor 2005) were used for the preparation and manipulation of the tabular data and the images. The analysis is partially based on the OCCAM computing facility hosted by C3S⁴⁸ at UniTO (Aldinucci et al. 2017).

⁴⁸ <http://c3s.unito.it/>

Appendix A

Notes on Individual Sources

Here we provide additional information, in addition to that retrievable from the main table. This list will then be updated in all forthcoming publications. Radio sources not listed below are those for which relevant information was not found in the literature. For the FR I and FR II radio classification of radio galaxies we mainly considered the information reported in the literature, as well as the radio morphology observed in high-resolution radio maps when available, adopting the same criteria of Capetti et al. (2017a, 2017b). In several sources we also reported additional names provided in the literature, but full information about radio cross-identifications can be retrieved in Appendix B.

G4Jy 4: Hunstead et al. (1978) reported the results of optical spectroscopic observations, collected with the 3.9 m Anglo-Australian Telescope, for 22 QSOs and emission-line galaxies associated with southern radio sources detected with Molonglo telescope at 408 MHz, and having flux densities above 0.95 Jy. The first source in their sample is 0000–117, a QSO at $z=1.465$, having the optical position reported therein (00:03:22.12, $-17:27:14.1$ in J2000), which is a $3''.5$ angular separation from the location of the counterpart assigned in our analysis with G4Jy 4. Despite the one-side radio structure of G4Jy 4, typical of core-dominated QSOs, the source identified by Hunstead et al. (1978) appears to be more consistent with the relatively brighter object located in the southeastern direction with respect to that coincident with the radio core of G4Jy 4, thus having a z estimate labeled with a question mark. It could also be associated with the radio source PKS 0000–17, but the lack of optical information prevented us from claiming this association.

G4Jy 9: is a nearby radio source at $z=0.2912$ (Jones et al. 2009) and correspondent to PKS 0003–56. This source also belongs to the MS4 radio catalog (Burgess & Hunstead 2006a, 2006b) and has a radio counterpart at 20 GHz (aka AT20G J000558–562828; Murphy et al. 2010), optically identified as a normal galaxy (Mahony et al. 2011) in agreement with the optical image reported in our analysis.

G4Jy 12: is also known as PKS 0003–83 and with a photometric redshift estimate of $z=0.32$ (Burgess & Hunstead 2006b). It is a classical double source with unresolved components. The association provided by our analysis is consistent with that performed by Jones & McAdam (1992), reporting an optical magnitude of 19.0 mag and a nearby fainter companion galaxy of 20.0 mag.

G4Jy 20: (aka PKS 0008–44) has a photometric redshift estimate of $z=1.0$ reported in the MS4 optical identification analysis (Burgess & Hunstead 2006b). In this case the lack of high-resolution radio maps prevented us from claiming that the optical counterpart is the one assigned in the MS4 catalog.

G4Jy 26: is a celestial object belonging to several catalogs of southern radio sources and thus known also as PKS 0012–38 and PMN J0015–3804 (Griffith & Wright 1993; Gregory et al. 1994). It has a tentative photometric redshift estimate reported in the literature of $z=0.57$ (Burgess & Hunstead 2006b), but having an $IDF=3.0$ if the optical counterpart associated in the MS4 sample is the correct one.

G4Jy 33: is also known as 3C 8, PKS 0016–12, and MRC 0016–129. This source belongs to the original 3C catalog (Edge et al. 1959) but not to its revised version (Spinrad et al. 1985). This radio source, classified as a high-redshift

radio galaxy, lies in a galaxy-rich large-scale environment (Wylezalek et al. 2013), and it has a redshift estimate of $z=1.589$ (Best et al. 1999).

G4Jy 43: is a classical lobe-dominated radio source, associated with PKS 0020–25 since its large-scale radio structure resembles that visible at 4.8 GHz (Kapahi et al. 1998) and its optical identification (McCarthy et al. 1996) corresponds to the WISE source associated in the G4Jy being a radio galaxy at redshift $z=0.35$.

G4Jy 45: is associated with PKS 0021–29 (aka AT20G J002430–292853), optically identified as a nearby QSO at $z=0.40645$ (Ho & Minjin 2009), having mid-IR colors similar to those of flat-spectrum radio quasars (FSRQs; see, e.g., D’Abrusco et al. 2012, 2019).

G4Jy 48: is associated with PKS 0023–26, having both an [O III] and a bolometric luminosity typical of type 2 QSOs (Dicken et al. 2009), with a first redshift estimate of $z=0.32162$ (Holt et al. 2008) more recently refined at $z=0.32188$ (Santoro et al. 2020). It is also a young radio source, showing two relatively symmetric lobes (Tzioumis et al. 2002; Morganti et al. 2021), hosted by an early-type galaxy (Ramos Almeida et al. 2011). G4Jy 48 was also observed during the X-ray survey of the 2 Jy sample (see Wall & Peacock 1985), showing an X-ray spectrum with a dominant jet component and a low intrinsic absorption (Mingo et al. 2014). Morganti et al. (2021) recently observed this radio source using ALMA and discovered a very extended distribution of molecular gas revealing that, already on galaxy scales, the impact of the AGN is not limited to outflows. Given its high star formation rate, G4Jy 48 lies in the region occupied by the star-forming galaxies on the $SFR-M_*$ plane (see, e.g., Bernhard et al. 2021).

G4Jy 64: has mid-IR colors of an FSRQ (D’Abrusco et al. 2014), and being at $z=0.518$ (Baker et al. 1999), this radio source is also known as PKS 0032–20 and has a radio counterpart at 20 GHz (i.e., AT20G J003508–200359).

G4Jy 70: is identified with the QSO (aka PKS 0035–39) at $z=0.59313$ (Thompson et al. 1990; Jones et al. 2009), having a radio counterpart also listed in the MRC and in the MS4 catalogs (see Large et al. 1981; Burgess & Hunstead 2006a, respectively), as well as in the AT20G sample (aka AT20G J003826–385948; Murphy et al. 2010).

G4Jy 77: is an extended radio source located at $\sim 6'$ from the X-ray position of the cool-core galaxy cluster A85 (see, e.g., Durret et al. 2005; Ichinohe et al. 2015, for details about its X-ray emission). At the redshift of the galaxy cluster (i.e., $z=0.0557$; Abell 1958; Abell et al. 1989; Pislari et al. 1997; Oegerle & Hill 2001) the kiloparsec scale is ~ 1.1 kpc arcsec $^{-1}$; thus, the distance between G4Jy 77 and A85 is ~ 360 kpc. It is a well-known radio phoenix (Kempner et al. 2004), an example of fossil plasma present in galaxy clusters owing to past AGN activity, with a very steep radio spectrum (Bagchi et al. 1998; Slee et al. 2001; Rahaman et al. 2022).

G4Jy 78: is associated with PKS 0039–44, a radio galaxy that belongs to the 2 Jy sample (Wall & Peacock 1985) at $z=0.346$ (Tadhunter et al. 1993; di Serego Alighieri et al. 1994).

G4Jy 85: belongs to the 2 Jy sample (aka PKS J0043–42; see, e.g., Wall & Peacock 1985; Morganti et al. 1997) and is an LERG (Hine & Longair 1979) at $z=0.0526$ (Whiteoak 1972; Tadhunter et al. 1993) with a very extended radio structure (Morganti et al. 1999) and a classical FR II radio morphology.

It appears to be located at the center of a group/cluster of galaxies being also surrounded by a diffuse halo (Ramos Almeida et al. 2011). It also shows the presence of a bridge detected at infrared and optical frequencies related to the interaction with a nearby companion galaxy (see also Inskip et al. 2010). Both hot spots are detected in the soft X-rays, together with a relative faint extended emission of the ICM (Mingo et al. 2017).

G4Jy 86: is the nearby star-forming galaxy NGC 253 (aka Sculptor Galaxy; see, e.g., Hoopes et al. 1996) with $z=0.00081$ (Springob et al. 2005). More details about this association are reported in the G4Jy catalog.

G4Jy 90: associated with PKS 0048–44, has only a photometric redshift estimate of $z=0.67$ (Burgess & Hunstead 2006b), not spectroscopically confirmed.

G4Jy 93: (aka PKS 0049–43) is a radio source with a tentative photometric redshift estimate of $z=0.39$ (Burgess & Hunstead 2006b) also listed in the catalog of γ -ray blazar candidates (D’Abrusco et al. 2014, 2019) with mid-IR colors similar to FSRQs.

G4Jy 108: is a radio galaxy with a typical FR II radio structure at $z=1.019$ (Best et al. 1999), also associated with PKS 0056–17.

G4Jy 113: is a “retired” radio source (López-Cobá et al. 2020) with $z=0.0564$ and located in the galaxy cluster A133 (Owen et al. 1995). McDonald et al. (2010) observed the presence of a thin H α filament toward the northeast, extending ~ 25 kpc, cospatial with an X-ray filament, and not consistent with a buoyant radio bubble. Radio and X-ray observations of the radio relic revealed that the relic lobe is energized by the central cD galaxy associated with G4Jy 113, rather than by a shock generated in the radio relic (Fujita et al. 2002).

G4Jy 120: is a lobe-dominated radio source. The SUMSS radio position marks the location of G4Jy 120 at an angular separation of $\sim 17''$ from PKS 0103–45, a value too large to claim this association.

G4Jy 122: is a classical double radio galaxy at $z=0.4$ (Tadhunter et al. 1993), optically classified as a narrow-line radio galaxy (see also Ramos Almeida et al. 2011) and showing a prominent Fe K α emission line in its XMM-Newton observation (Mingo et al. 2014). This radio source is known as PKS 0105–16, and it is listed in the original 3C catalog as 3C 32 (Edge et al. 1959) but not in the 3CR revised version (Spinrad et al. 1985). Archival optical images seem to indicate that the host galaxy of G4Jy 122 appears to be connected with an early-type galaxy of similar brightness located at ~ 70 kpc in the northwestern direction (Ramos Almeida et al. 2011).

G4Jy 129: is potentially associated with the radio source PKS 0110–69 (aka AT20G J011143-690016; Murphy et al. 2010) owing to the proximity to the intensity peak of the SUMSS radio map at 843 MHz.

G4Jy 133: according to our analysis, it is labeled with an IDF=3.0; however, if follow-up observations confirm its WISE association reported in the G4Jy, the radio source could be associated with PKS 0114–47 (White et al. 2020b), a giant radio galaxy (Jones & McAdam 1992) with $z=0.146$ (Jones et al. 2009).

G4Jy 136: (aka PKS 0114–21) is a compact steep-spectrum (CSS) radio source with two hot spots embedded in a dense gaseous environment (Mantovani et al. 1994) with $z=1.4153$ (De Breuck et al. 2010; Seymour et al. 2007), with mid-IR emission dominated by a stellar continuum and several rest-

frame optical emission lines detected in its spectrum (Nesvadba et al. 2017).

G4Jy 143: is associated with 3C 38 (aka PKS 0117–15), again not listed in the revised release 3CR (Spinrad et al. 1985), and it is classified as a radio galaxy at $z=0.565$ (Tadhunter et al. 1993), having a clear FR II morphology and showing high ionization emission lines detected in the optical spectrum. There is a nearby optical source, potentially a companion galaxy; however, due to the lack of spectroscopic information, we cannot claim that this is the case of a galaxy pair.

G4Jy 145: is a QSO also at mid-IR frequencies (D’Abrusco et al. 2019), originally located at $z=0.837$ (Hunstead et al. 1978). More recent ultraviolet observations give a redshift measurement of $z=0.834$ (Monroe et al. 2016).

G4Jy 157: belongs to the sample of Best et al. (1999) and is classified as a radio galaxy at $z=0.372$ showing a typical FR II radio morphology.

G4Jy 162: has a clear optical counterpart, while the lack of a mid-IR associated source is mainly due to the artifacts present in the WISE image created by a nearby bright star located in the southwestern direction. In the literature G4Jy 162 is classified as a radio galaxy with $z=2.34665$ (Best et al. 1999; Nesvadba et al. 2017), being the most distant source listed in the G4Jy-3CRE sample to date. G4Jy 162 also shows a fairly regular emission-line region morphology, albeit with an increasing [O III] surface brightness toward the northern side, and roughly aligned with the radio axis on the northwestern side (Nesvadba et al. 2017).

G4Jy 168: is a classical double-lobed radio source associated with PKS 0129–073 (aka MRC 0129–073 and PMN J0131–0703). There are three sources detected in the optical image that could be its potential counterpart, but in the WISE image only the brightest one is detected. This prevents us from labeling this source with an IDF different from 3.0.

G4Jy 171: is the nearby lenticular galaxy NGC 612 (Ekers et al. 1978) located at $z=0.02977$ (see, e.g., Burbidge & Burbidge 1972; Menzies et al. 1989; da Costa et al. 1991), associated with the powerful radio source PKS 0131–36 and showing a wide double radio structure, with the axis perpendicular to the disk of the galaxy. G4Jy 171 also shows an unusual absorption in its optical spectrum, mainly due to its host galaxy structure with gas and dust in its disk (Tadhunter et al. 1993).

G4Jy 192: is a double radio galaxy with a redshift $z=0.41$, evaluated comparing our finding chart with that reported in the literature (McCarthy et al. 1996). Three nearby companion optical galaxies appear to lie close to the host galaxy of G4Jy 192.

G4Jy 208: (aka PKS 0155–10) is a radio QSO at $z=0.61847$ (Burbidge 1968; Best et al. 1999; Jones et al. 2009).

G4Jy 213: is a radio source at $z=0.67680$ (Croom et al. 2004; Jones et al. 2004) with a mid-IR counterpart showing WISE colors similar to those of FSRQs (D’Abrusco et al. 2014) and also tentatively classified as a QSO on the basis of its optical properties (di Serego Alighieri et al. 1994).

G4Jy 217: was optically identified by Jauncey et al. (1978) and is aka PKS 0202–76. It was classified as a QSO at $z=0.38939$ (see also Jauncey et al. 1978; Danziger & Goss 1983; Ho & Minjin 2009).

G4Jy 219: is classified as a radio galaxy with a photometric redshift estimate of $z=0.45$ belonging to the MS4 sample

(Burgess & Hunstead 2006b). In our analysis we used the radio map at 14.9 GHz to clearly identify the optical counterpart.

G4Jy 227: comparing the VLASS observation and the optical finding chart used in our analysis to those available in the literature at a nominal frequency of 5 GHz (Reid et al. 1999), we confirmed the location of the host galaxy. *G4Jy 227* shows mid-IR colors typical of FSRQs (D’Abrusco et al. 2019) but does not have spectroscopic information.

G4Jy 238: also known as 3C 62, is an HERG (Hine & Longair 1979) with a classical FR II radio morphology with $z = 0.13784$ (Tadhunter et al. 1993) and also a hard X-ray counterpart (see, e.g., Koss et al. 2017; Kosiba et al. 2022).

G4Jy 241: shows a flat radio spectrum since it was selected as part of the Combined Radio All-Sky Targeted Eight GHz Survey (aka CRATES J021645.12–474908.9; Healey et al. 2007). According to the literature, this is a giant radio galaxy (~ 1 Mpc size; Christiansen et al. 1977) hosted in an elliptical galaxy at $z = 0.06427$ that is harbored in a galaxy-rich large-scale environment (Danziger & Goss 1983; Zirbel 1997; Jones et al. 2009) and located in the direction of the AS 239 galaxy cluster (Robertson & Roach 1990) that lies at a similar distance, being at $z = 0.0635$ (Abell 1958; Abell et al. 1989).

G4Jy 247: with no associated counterparts in the MRC, PKSCAT, and PMN samples, has a counterpart at 20 GHz (AT20G J021902–362607; Murphy et al. 2010), and it also appears to be hosted in an elliptical galaxy (see also Mahony et al. 2011) clearly visible in both the mid-IR and the optical images with $z = 0.48881$ (Jones et al. 2009).

G4Jy 249: is associated with PKS 0219–706 (aka MRC 0219–706 and PMN J0220–7022). This source was tentatively associated with an elliptical galaxy having a photometric redshift estimate of $z = 0.4$ belonging to the MS4 sample (Burgess & Hunstead 2006b), but according to our analysis, it has an IDF = 3.0 since there are too many sources close to radio intensity peak that prevent us from claiming the location of the host galaxy.

G4Jy 257: as the previous source *G4Jy 249*, is a radio galaxy with several counterparts at radio frequencies and a photometric redshift estimate of $z = 1.27$ belonging to the MS4 sample (Burgess & Hunstead 2006b).

G4Jy 260: is a lobe-dominated radio QSO with $z = 0.23224$ (Best et al. 1999; Jones et al. 2009), with mid-IR colors similar to those of γ -ray-emitting QSOs (D’Abrusco et al. 2019), and with a hard X-ray counterpart (Cusumano et al. 2010; Baumgartner et al. 2013; Koss et al. 2017).

G4Jy 280: is also associated with PKS 0235–19 and is classified as a broad-line radio galaxy with a classical FR II radio structure (Ramos Almeida et al. 2011) at $z = 0.62$ (Tadhunter et al. 1993; Best et al. 1999), with mid-IR colors of γ -ray blazars (D’Abrusco et al. 2014, 2019). Despite the fact that the radio core is not detected in the high-resolution JVLA radio map at 5 GHz (Reid et al. 1999), its radio morphology confirms our assigned optical counterparts and association.

G4Jy 290: has only a photometric redshift estimate of $z = 0.72$ (Burgess & Hunstead 2006b) but no clear optical identification.

G4Jy 293: is also associated with the MS4 radio galaxy MRC 0245–558 with a photometric redshift estimate of $z = 0.82$ (Burgess & Hunstead 2006b); however, the presence of several nearby companions, coupled with the lack of spectroscopic information, prevents us from positively assigning an optical counterpart.

G4Jy 301: is a QSO located at $z = 1.002$ (Murdoch et al. 1984) with mid-IR colors similar to those of γ -ray-detected FSRQs (D’Abrusco et al. 2019).

G4Jy 304: is a CSS radio galaxy located at $z = 0.56288$ (Tadhunter et al. 1993; Holt et al. 2008) belonging to the 2 Jy sample (Wall & Peacock 1985; Morganti et al. 1993) and also known as PKS 0252–71.

G4Jy 312: is associated with PKS 0254–23 and is classified as a radio galaxy located at $z = 0.509$ (McCarthy et al. 1996), showing a classical FR II radio morphology (see also Kapahi et al. 1998; Best et al. 1999).

G4Jy 326: is a typical FR II radio galaxy with $z = 0.268$ (McCarthy et al. 1996).

G4Jy 335: is a high-redshift radio galaxy at $z = 1.769$ (Best et al. 1999).

G4Jy 347: is a 2.5 Mpc giant radio galaxy (aka MRC 0319–454, PMN J0321–4510, and MSH 03–43; see, e.g., Burgess & Hunstead 2006b; Malarecki et al. 2015, for a recent analysis) located within a galaxy filament of the Horologium–Reticulum supercluster (Fleenor et al. 2005). The host galaxy (Bryant & Hunstead 2000) is located close to the northeastern radio lobe, the only part of its radio structure reported in our finding chart, and it is associated with the optical source ESO 248–G10 having a weak counterpart at 20 GHz (Saripalli et al. 1994). The redshift of the host galaxy is $z = 0.0622$ (Safouris et al. 2009), and its radio structure on the northeastern side goes through an environment having higher galaxy density than the southern radio structure, indicating the presence of a surrounding group of galaxies. There are also several galaxy clusters in its vicinity (Fleenor et al. 2006), namely S0345, A3111, A3112, and APMCC369 at $z = 0.071, 0.078, 0.075,$ and $0.075,$ respectively.

G4Jy 350: is a large radio galaxy with the southeastern radio lobe located at the same position of PKS 0352–88 (aka MRC 0352–884 and SUMSS J032359–881618), at $\sim 25''$ from the *G4Jy* position, as marked in the finding chart. A recent MeerKat observation revealed that the position of the mid-IR counterpart is consistent with that of WISE J032259.32–881600.4 (Sejake et al. 2023).

G4Jy 373: is a radio galaxy with a typical FR II radio structure with $z = 0.1126$ (Carter & Malin 1983) behind the Fornax Cluster at an angular separation of $\sim 5'$ from NGC 1399 (aka PKS 0336–35), the Fornax brightest cluster galaxy (BCG; see, e.g., Carter & Malin 1983; Killeen et al. 1988; Hilker et al. 1999).

G4Jy 381: is an FR II radio galaxy with a redshift estimate of $z = 0.0535$ (Scarpa et al. 1996; Drinkwater et al. 2001), in the foreground of the galaxy cluster A3165 (Abell 1958; Abell et al. 1989; Robertson & Roach 1990) but not related to it.

G4Jy 386: is also known as PKS 0349–27 and PMN J0351–2744 and was already detected as extended at 408 MHz (Schilizzi 1975; Schilizzi & McAdam 1975), as well as at higher frequencies (Reid et al. 1999). It was then optically identified with the same counterpart associated in both the *G4Jy* at mid-IR frequencies and in our analysis with being (Bolton et al. 1965) classified as a radio galaxy at $z = 0.6569$ (Searle & Bolton 1968; Jones et al. 2009). This radio source shows extended emission in the optical band with remarkable features, including an extended narrow-line region and bridges connecting *G4Jy 386* to two companion galaxies (Inskip et al. 2010; Ramos Almeida et al. 2013). These bridges are interpreted as being due to tidal interaction with neighbor

galaxies and/or mergers (Danziger et al. 1984; Tadhunter et al. 1989). X-ray emission was also detected between the lobes and, with an offset of a few arcseconds, on the location of the northern hot spot (Mingo et al. 2017).

G4Jy 387: is a lobe-dominated QSO at $z = 0.3245$ (Lanzetta et al. 1995; Marziani et al. 1996), also known as 3C 95 and PMN J0351–1429, inhabiting a galaxy-rich large-scale environment (see, e.g., Hutchings et al. 1996).

G4Jy 392: is a QSO (aka 3C 94) showing a double radio structure and with $z = 0.96354$ (Lynds 1967; Best et al. 1999; Ahn et al. 2012), recently included in the list of giant radio quasars having the size of the extended radio emission larger than 0.7 Mpc (Kuźmicz & Jamroz 2021).

G4Jy 404: is a radio galaxy at $z = 0.584$ (Best et al. 1999).

G4Jy 411: is a well-known γ -ray-emitting blazar (see, e.g., Acero et al. 2015, and references therein) known to emit also in the hard X-rays (see, e.g., Cusumano et al. 2010; Koss et al. 2017), belonging to the class of FSRQs (aka BZQ J0405–1308 as listed in the Roma-BZCAT; Massaro et al. 2009, 2015c), at $z = 0.57055$ (Lynds 1967; Marziani et al. 1996).

G4Jy 415: is one of the most luminous QSO at $z < 1$ (see, e.g., Punsly et al. 2016), optically identified by Hunstead (1971) with a measured $z = 0.5731$ (Kinman & Burbidge 1967; Bechtold et al. 2002; Decarli et al. 2010; Johnson et al. 2018). *G4Jy 415* (aka PKS 0405–12) shows X-ray emission arising from the northern hot spot (Sambruna et al. 2004), thus being included in the XJET database (Massaro et al. 2011), and it is also listed in the Roma-BZCAT (Massaro et al. 2015c), classified as a blazar of uncertain type (i.e., BZU J0407–1211). Recent MUSE observations revealed the presence of six spatially extended line-emitting nebulae in the galaxy group where it is harbored, suggesting a connection between large-scale gas streams and the nuclear activity (Johnson et al. 2018). It also shows the detection of a narrow filament extending toward the QSO consistent with a cool intragroup medium filament similar to those occurring in cool-core galaxy clusters (see, e.g., McDonald et al. 2010).

G4Jy 416: was originally identified with an optical counterpart by Hunstead (1971) and then classified as a gigahertz-peaked spectrum (GPS) radio source (see, e.g., O’Dea et al. 1991; Callingham et al. 2017). It has a redshift measurement of $z = 0.962$ (Labiano et al. 2007) and is also known as PKS 0408–65 (Bolton et al. 1979).

G4Jy 417: does not have an optical counterpart in the DSS image we retrieved from the archive, but it was identified with the same mid-IR counterpart listed in the *G4Jy* catalog in the literature (Hunstead 1971; Alvarez et al. 1993). However, we did not report any optical position and/or magnitude, and we assigned it an IDF = 4.1. *G4Jy 417* (aka PKS 0409–752) also belongs to the MS4 catalog, and it is classified as a narrow-line radio galaxy with a typical FR II radio morphology at $z = 0.694$ (Alvarez et al. 1993; Tadhunter et al. 1993; di Serego Alighieri et al. 1994). It is harbored in a galaxy-rich environment (Ramos Almeida et al. 2011) and shows evidence for a young stellar population (Holt et al. 2007) and a far-infrared excess (Dicken et al. 2009).

G4Jy 427: has the same optical counterpart associated in the MS4 catalog (Burgess & Hunstead 2006b), where a photometric redshift estimate of $z = 0.42$ is also reported. In the optical image used in our analysis we found a relatively brighter star in the southwestern direction and several nearby

companion galaxies of similar intensity, suggesting that *G4Jy 427* could lie in a galaxy-rich environment.

G4Jy 436: is also known as PKS 0413–21, a core-dominated quasar at $z = 0.808$ (Wilkes 1986; Best et al. 1999) showing mid-IR colors similar to those of γ -ray blazars (D’Abrusco et al. 2014, 2019) and having a radio jet detected in the X-rays (Marshall et al. 2005; Massaro et al. 2011).

G4Jy 446: is optically identified with a galaxy (Savage et al. 1976) and has a photometric redshift estimate obtained thanks to the MS4 analysis that places the radio source at $z = 0.81$ (Burgess & Hunstead 2006b). In our analysis we could not clearly identify the radio core position and its optical counterpart. The mid-IR counterpart was not found in the *G4Jy* catalog (White et al. 2020b). *G4Jy 436* also shows a CSS radio core (Randall et al. 2011).

G4Jy 453: is a giant radio source already known since the MRC release (Jones & McAdam 1992), but the lack of a high-resolution image prevented us from verifying the position of the host galaxy and whether the redshift estimate reported in the literature is correct (Kuźmicz & Jamroz 2021).

G4Jy 462: is one of the dumbbell FR I radio galaxies in the southern hemisphere (Ekers 1969; McAdam et al. 1988; Morganti et al. 1993), also known as IC 2082 and PKS 0427–53, with a twin tail (Carter et al. 1981; Lilly & Prestage 1987), and lying in the nearby galaxy cluster AS 463. It has a redshift measurement of $z = 0.03931$ (see, e.g., Raimann et al. 2005), showing weak emission lines in its optical spectrum. It also belongs to both the samples of local radio galaxies detected at 20 GHz (Sadler et al. 2014). We adopted here the same optical identification provided in the literature (see also Jones & McAdam 1992; Burgess & Hunstead 2006b; White et al. 2020b). However, the lack of high-resolution radio maps prevented us from classifying this radio source as a wide-angle tail (WAT) radio galaxy (Burns 1981; Owen & Rudnick 1976; O’Donoghue et al. 1990, 1993; Sakelliou & Merrifield 2000; Missaglia et al. 2019).

G4Jy 492: is an FR II radio galaxy at $z = 0.147$ (Tadhunter et al. 1993; di Serego Alighieri et al. 1994; Best et al. 1999) with several nearby companion galaxies (Ramos Almeida et al. 2013) and surrounding diffuse X-ray emission. *G4Jy 492*, also belonging to the 2 Jy sample (see, e.g., Wall & Peacock 1985; Morganti et al. 1993), has been recently observed in the X-rays, and both its radio core and the northern hot spot were detected (Mingo et al. 2017). It was also detected in the hard X-ray band (see, e.g., Cusumano et al. 2010; Oh et al. 2018).

G4Jy 506: was associated with the same optical counterpart in the literature (Bolton et al. 1968; Hunstead 1971). It shows a classical FR II radio structure. It is listed in the MS4 catalog with a photometric redshift estimate of $z = 0.22$ (Burgess & Hunstead 2006b).

G4Jy 507: is also known as NGC 1692 and is a radio galaxy at $z = 0.035364$ (Allison et al. 2014), optically identified in the literature (Bolton et al. 1965; Burbidge & Burbidge 1972; Wills et al. 1973; McCarthy et al. 1996; Best et al. 1999). According to the optical image used in our analysis, its entire radio structure lies within the brightness profiles of its host galaxy, and it has two nearby companion galaxies, probably harbored in a galaxy-rich environment (Miller et al. 1999).

G4Jy 510: is a nearby QSO at $z = 0.533$ (Wright et al. 1979; Henriksen et al. 1991; Bechtold et al. 2002) showing Mg II absorption system (Tytler et al. 1987) and giant optical nebulae surrounding it (Helton et al. 2021). It shows a lobe-dominated

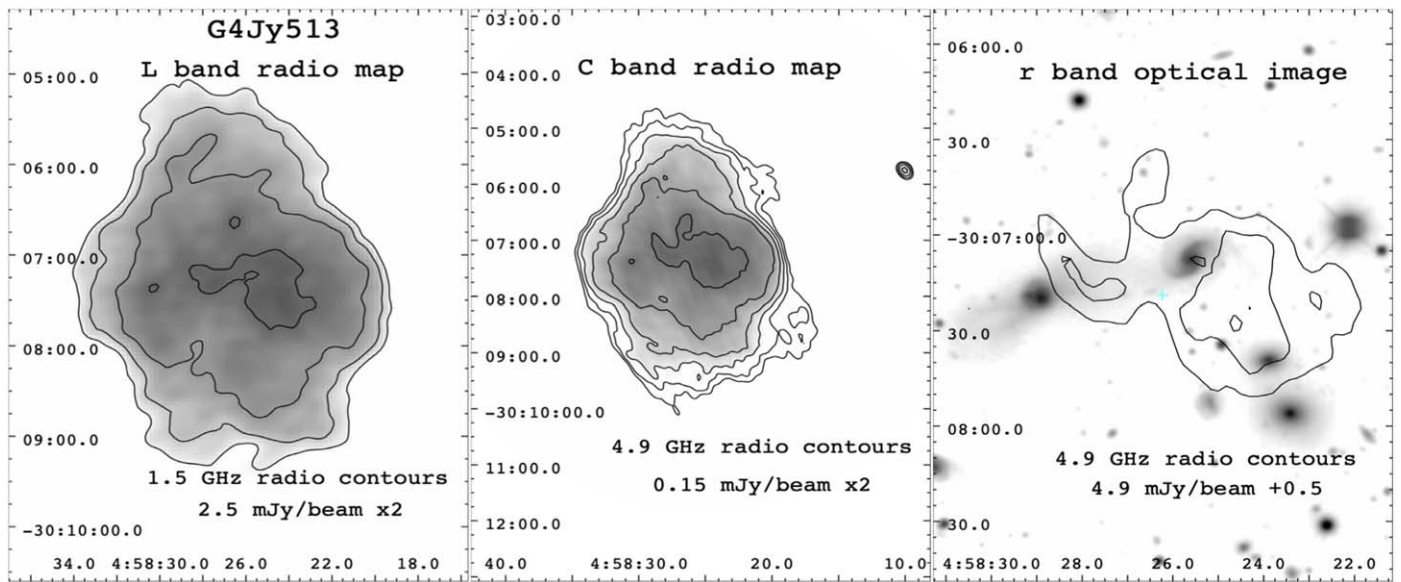


Figure 9. Left and middle panels: radio maps of G4Jy 513 at 1.4 and 4.9 GHz, respectively, retrieved from the NVAS. The frequency of each radio map from which radio contours were drawn is reported together with the intensity of the first level and the binning factor indicating how they increase. Right panel: the r -band optical image collected from one of the surveys used in our analysis, with three levels of radio contours drawn from the radio map at 4.9 mJy starting at 4.9 mJy and increasing by 0.5 mJy. No clear detection of the radio core and of a potential optical counterpart is reported for this radio source showing diffuse radio emission.

radio structure (Reid et al. 1999) also listed in the CRATES catalog (Healey et al. 2007).

G4Jy 513: is not optically identified, but there is an optical interacting pair of galaxies within the highest radio contour drawn in our finding chart. We found two archival radio maps of G4Jy 513, as reported in Figure 9 in comparison with the archival r -band optical image, showing diffuse radio emission at both 1.4 and 4.9 GHz but lacking a clear detection of its radio core. In this case the nearby radio source known as PKS 0456–301 could be potentially associated with G4Jy 513, thus suggesting the position of its optical counterpart as shown in the finding chart. G4Jy 513 appears to also be associated with the galaxy cluster A3297 (see, e.g., Robertson & Roach 1990, and references therein), even if spectroscopic confirmation is needed.

G4Jy 517: is a giant radio galaxy (Saripalli et al. 1986; Subrahmanya & Hunstead 1986; Ishwara-Chandra & Saikia 1999; Kuźmicz et al. 2018; aka 0503–286 and MSH 05–22) with a size of ~ 1 Mpc, located at $z = 0.0381$ (Menzies et al. 1989; Fouque et al. 1990; da Costa et al. 1991; Jones et al. 2009). We adopted the same association listed in the literature (Saripalli et al. 1986; White et al. 2020a), where 6dF J0505492–283519 is the host galaxy of the radio core, and inhabiting a small group (Subrahmanyan et al. 2008) with a galaxy overdensity and a filamentary large-scale radio structure indicating a relatively low density ICM environment.

G4Jy 518: is an FSRQ, also listed in the Roma-BZCAT (Massaro et al. 2015c) as BZQ J0506–6109 with $z = 1.093$ (Wright et al. 1977; Bechtold et al. 2002). It also belongs to the MS4 catalog (Burgess & Hunstead 2006a) labeled as MRC 0506–612 (Large et al. 1981), and it is a γ -ray-emitting blazar (see, e.g., Acero et al. 2015; D’Abrusco et al. 2019).

G4Jy 524: is a radio galaxy (aka MRC 0508–187 and TXS 0508–187) with a lobe-dominated radio structure. The optical image shows the presence of several nearby companion galaxies. G4Jy 524 is also listed in a sample of ultra-steep-spectrum (USS) radio sources (De Breuck et al. 2000).

G4Jy 530: shows a large double-lobed radio morphology. The lack of a mid-IR association and the resolution of radio maps used in our analysis did not permit us to locate the host galaxy in the optical image. However, we tentatively associated this radio source with the narrow-line radio galaxy PKS 0511–48 (05:12:47.22, $-48:24:16.4$ in J2000) lying in the center of the radio structure and having a redshift estimate of $z = 0.30638$ (Eracleous & Halpern 2003, 2004).

G4Jy 531: is listed in the MS4 sample (aka MRC 0511–305; Burgess & Hunstead 2006a) and is classified as an asymmetric giant radio galaxy (Malarecki et al. 2013) at $z = 0.05764$ (Jones et al. 2009).

G4Jy 538: is a compact radio galaxy (McCarthy et al. 1996) also known as PKS 0519–20, with $z = 1.086$ (Best et al. 1999) and a peaked spectrum determined thanks to the GLEAM observations (Callingham et al. 2017).

G4Jy 540: is a well-known γ -ray-emitting blazar (aka PKS 0521–36; Bolton et al. 1965; Hunstead 1971; Danziger et al. 1979; Acero et al. 2015) at $z = 0.05655$ (Sbarufatti et al. 2006), listed as BZU J0522–3627 in the Roma-BZCAT (Massaro et al. 2015c), with an X-ray-emitting jet also detected by Chandra (Birkinshaw et al. 2002; Massaro et al. 2011).

G4Jy 563: is optically identified with a galaxy (Hunstead et al. 1971; Bolton & Savage 1977) being also listed in the MS4 sample (Burgess & Hunstead 2006a), with a photometric redshift estimate of $z = 0.184$ (Burgess & Hunstead 2006b).

G4Jy 580: has a mid-IR counterpart associated in the G4Jy that is the same as listed in the MS4 sample (Burgess & Hunstead 2006a, 2006b) as discussed in White et al. (2020b). However, the presence of several optical sources around the radio intensity peak, marked in the finding chart, coupled with relatively poor angular resolution of the radio map available, prevented us from claiming a firm identification.

G4Jy 590: could be associated with PKS 0601–34 (06:03:11.64, $-34:26:45.1$ s in J2000) since, as reported in our finding chart, its position could be “confused” with that of the relatively brighter southern hot spot. In the MS4 sample it is

classified as a radio galaxy having a photometric $z=0.58$ (Burgess & Hunstead 2006b).

G4Jy 605: is a double-lobed radio galaxy optically identified in the literature (Bolton et al. 1965; Burbidge & Burbidge 1972), and it has a close companion galaxy (i.e., being classifiable as a galaxy pair) clearly visible in the optical image.

G4Jy 607: is a radio galaxy at $z=0.051$ (Tritton 1972; Wills et al. 2004) having a flat radio spectrum (Healey et al. 2007).

G4Jy 611: is an LERG hosted in a dumbbell galaxy (Frank et al. 2013; Ramos Almeida et al. 2013; Ineson et al. 2015) located at the center of the A3391 galaxy cluster (Abell 1958; Abell et al. 1989) at $z=0.054$ (Danziger & Goss 1983; Landt et al. 2002) showing a classical WAT radio structure (Morganti et al. 1999). Its optical images show signatures of galaxy interactions with nearby companions (Ramos Almeida et al. 2011), while in the X-rays the ICM emission decreases in intensity in the region occupied by the northern radio lobe, tentatively indicating the possible presence of an X-ray cavity (Mingo et al. 2017).

G4Jy 613: is the BCG of the galaxy cluster A3395 (Abell 1958; Abell et al. 1989; Brown & Burns 1991) with $z=0.051976$ (Cava et al. 2009), being also detected in the X-rays (see, e.g., Sun 2009).

G4Jy 614: lies close to the galaxy cluster A3392 (Abell 1958; Abell et al. 1989; Quintana & Ramirez 1995; Ebeling et al. 1996), originally detected in the X-rays by Trussoni et al. (1999) and then confirmed by Ramos Almeida et al. (2013), Ineson et al. (2015), and Mingo et al. (2017). The radio source is optically classified as an LERG, and it has a redshift estimate of $z=0.054855$ (Tadhunter et al. 1993; Wills et al. 2004; Jones et al. 2009). There are also several companion galaxies clearly detected in the optical image used to carry out our analysis. It is listed in both the MS4 sample (Burgess & Hunstead 2006a) and the CRATES catalog (Healey et al. 2007), as well as in the 2 Jy one (see, e.g., Wall & Peacock 1985; Morganti et al. 1993; Mingo et al. 2014).

G4Jy 618: is the γ -ray FSRQ known as BZQ J0635–7516 (Massaro et al. 2015c) with $z=0.653$ (Hunstead et al. 1978; Bechtold et al. 2002; Danforth et al. 2016) and with a relatively compact radio core (Jauncey et al. 1989; Morganti et al. 1993).

G4Jy 619: is a radio galaxy at $z=0.055198$ (Storchi-Bergmann et al. 1996; Jones et al. 2009) also detected in the hard X-rays (Cusumano et al. 2010; Oh et al. 2018). It is listed in the literature as a giant radio galaxy (Danziger et al. 1978; Kronberg et al. 2004; Kuźmicz & Jamrozy 2021), and at larger scales it shows a classical FR II radio morphology.

G4Jy 639: is also known as PKS 0700–47, and it is listed in the MS4 sample classified as a radio galaxy and having a photometric redshift estimate of $z=0.86$ (Burgess & Hunstead 2006b).

G4Jy 642: lies in a crowded optical field and, as for the previous radio source, is listed in the MS4 sample (aka MRC 0704–427; Burgess & Hunstead 2006b) with a photometric redshift estimate of $z=1.33$.

G4Jy 644: can be considered a giant radio galaxy even if its extension is below the 1 Mpc threshold (Ishwara-Chandra & Saikia 1999; Malarecki et al. 2015; Proctor 2016; Kuźmicz & Jamrozy 2021). It is also a double–double radio galaxy candidate, where the inner radio structure is misaligned with respect to the outer one (Jones & McAdam 1992; Bruni et al. 2020). *G4Jy 644* emits in the hard X-rays (aka PBC J0709.2

–3601; Cusumano et al. 2010; Koss et al. 2017; Bruni et al. 2021), and it lies at $z=0.11$ (Parisi et al. 2014).

G4Jy 651: is a radio galaxy with $z=0.031358$ (Jones et al. 2009; Allison et al. 2014), and its radio morphology on larger scales than those visible in our finding chart reveals a WAT structure.

G4Jy 653: is a radio source (aka PKS 0719–55) inhabiting a moderately rich environment (Zirbel 1996) and being listed in the MS4 sample with a photometric redshift estimate of $z=0.22531$ (Burgess & Hunstead 2006b).

G4Jy 672: is an FSRQ, showing an ultraluminous accretion disk and a high kinetic luminosity jet (Punsly & Tingay 2005). It is listed in the Roma-BZCAT (Massaro et al. 2009; aka BZQ J0743–6726), as well as in the CRATES catalog (Healey et al. 2007), and it lies at $z=1.512$ (Bergeron & Kunth 1984; di Serego Alighieri et al. 1994; Bechtold et al. 2002; Jones et al. 2009).

G4Jy 680: was optically identified by Schilizzi (1975), and it is a radio galaxy with $z=0.0699$ (Danziger & Goss 1983). *G4Jy 680* appears as an FR I radio source, but at larger scales and at lower frequencies (e.g., 74 MHz and 150 MHz) with respect to those we used to build radio contours over the optical image, its radio structure appears more extended.

G4Jy 685: is known as 3C 195 and PKS 0806–10, an FR II radio galaxy at $z=0.10898$ (Tadhunter et al. 1993; Jones et al. 2009) listed in the 2 Jy sample (Wall & Peacock 1985; Morganti et al. 1993). The detection of extended X-ray emission around the radio core (Ineson et al. 2015; Mingo et al. 2017), coupled with optical signatures of galaxy interaction (Inskip et al. 2010; Ramos Almeida et al. 2011), clearly indicates that *G4Jy 685* is harbored in a galaxy-rich large-scale environment. The southern radio hot spot is also detected in the X-rays (Mingo et al. 2017).

G4Jy 706: is a lobe-dominated radio quasar at $z=0.822$ (Stickel et al. 1993) with mid-IR colors similar to γ -ray blazars (D’Abrusco et al. 2014).

G4Jy 718: belongs to the MS4 sample (aka MRC 0842–835) with a photometric redshift estimate of $z=0.82$ (Burgess & Hunstead 2006b). The lack of optical detection in the finding chart at the location of the mid-IR associated source prevented us from assigning this source an IDF = 1.0.

G4Jy 721: is the FR II radio galaxy 3C 206, not listed in the revised 3CR catalog (Spinrad et al. 1985), with $z=0.19787$ (Ho & Minjin 2009), and harbored in a galaxy cluster (Yee & Green 1983; Ellingson et al. 1987, 1989; Yates et al. 1989). It is also detected in the hard X-rays (see, e.g., Ajello et al. 2008a, 2008b; Oh et al. 2018; Kang et al. 2020).

G4Jy 723: is a radio quasar at $z=0.521$ (Browne & Savage 1977; Hunstead et al. 1978) listed in the 2 Jy sample (see, e.g., Morganti et al. 1993; Burgess & Hunstead 2006a), with mid-IR colors of γ -ray blazars (D’Abrusco et al. 2019).

G4Jy 730: is a high-redshift radio galaxy (aka MRC 0850–206; Large et al. 1981; De Breuck et al. 2000), with an FR II radio morphology, with $z=1.337$ (Best et al. 1999), for which the presence of a bright star in the northeastern direction prevented the detection of its mid-IR counterpart.

G4Jy 734: is a high-redshift radio galaxy at $z=1.665$ optically identified in the literature (Best et al. 1999; De Breuck et al. 2000) appearing to inhabit a large-scale environment with high galaxy density (Wylezalek et al. 2013). The lack of an optical detection in our finding chart prevented us from assigning this source an IDF = 1.0.

G4Jy 747: is an FR II radio galaxy, optically classified as a narrow-line radio galaxy (NLRG; Ramos Almeida et al. 2011), at $z = 0.305$ (Tadhunter et al. 1993), and listed in the 2 Jy sample (Wall & Peacock 1985; Morganti et al. 1997) with mid-IR colors of γ -ray blazars (D’Abrusco et al. 2019). *G4Jy 747* lies in a relatively crowded field with several nearby companion galaxies and appears as a double system, including the radio galaxy nucleus and a faint component a few kiloparsecs in the southwestern direction (Ramos Almeida et al. 2011). Its morphological classification is the same as that from the near-infrared investigation presented by Inskip et al. (2010).

G4Jy 796: is a giant, double-lobed, radio galaxy (aka MRC 0947–249; Ishwara-Chandra et al. 2001) for which diffuse X-ray emission has been detected, arising from its extended radio structure (Laskar et al. 2010). A redshift estimate of $z = 0.854$ is reported in the literature (McCarthy et al. 1996; Kapahi et al. 1998) but unconfirmed.

G4Jy 818: is a candidate double–double radio galaxy (aka MRC 1002–215) with an unconfirmed redshift estimate of $z = 0.59$ reported in the literature (McCarthy et al. 1996). Despite the presence of nearby galaxies on the western side, the host galaxy was not detected in our optical image.

G4Jy 835: is a CSS radio source (Prestage & Peacock 1983) with $z = 1.346$ (di Serego Alighieri et al. 1994).

G4Jy 836: is an FR II radio galaxy listed in the MS4 sample with a photometric redshift estimate of $z = 0.7$ (Burgess & Hunstead 2006b). The presence of several optical sources prevented us from associating the radio core with its optical counterpart.

G4Jy 837: is an extremely powerful (i.e., with a luminosity higher than all 3C radio sources at the same redshift with the exception of 3C 196) FR II radio galaxy (Punsly & Tingay 2006) at $z = 1.28$ (Murdoch et al. 1984; Stickel et al. 1993; Decarli et al. 2010) with mid-IR colors of γ -ray blazars (D’Abrusco et al. 2019).

G4Jy 854: is listed in the MS4 catalog as a radio galaxy with a photometric redshift estimate $z = 0.5$ (Burgess & Hunstead 2006b). It has an ultrasteepest radio spectrum (De Breuck et al. 2000). Both the mid-IR and the optical counterparts are not detected according to our analysis.

G4Jy 876: is a lobe-dominated radio QSO for which the high-resolution radio map used in our investigation allowed us to precisely locate the position of its host galaxy, being also coincident with that at other radio frequencies (Bolton et al. 1979; Large et al. 1981; Griffith & Wright 1993). *G4Jy 876* seems to be associated with 3C 246 (Edge et al. 1959) with $z = 0.345296$ (Kinman & Burbidge 1967; Veron-Cetty et al. 1988; Lanzetta et al. 1993; Jones et al. 2009; Shi et al. 2014), and it resides in a galaxy-rich large-scale environment (Hintzen et al. 1983; Ellingson 1988; Ellingson et al. 1991; Hutchings et al. 1996).

G4Jy 894: is a radio galaxy with an unconfirmed redshift estimate of $z = 0.59$ reported in the literature (McCarthy et al. 1996; Best et al. 1999).

G4Jy 917: is an unusual radio galaxy showing a circularly bent tail. It lies at $z = 0.033753$ (see, e.g., Burbidge & Burbidge 1972; Tritton 1972; Sandage 1978; Allison et al. 2014), and it is harbored in the galaxy cluster AS 665 (Abell 1958; Abell et al. 1989).

G4Jy 926: is a classical lobe-dominated radio source being associated with the nearby object PKS 1131–19. We could not

detect any counterpart in the optical image used to draw our finding chart at this location. However, according to Wills et al. (1974), there is an optical source showing Ca H and K broad and shallow absorption lines, but the finding chart they refer to, given by Moseley et al. (1970), seems to point to a different target at more than $20''$ angular separation in the eastern direction from the radio position.

G4Jy 927: is a lobe-dominated QSO (aka PKS 1131–17) at $z = 1.618$ (Best et al. 1999).

G4Jy 933: is listed in the sample of Parkes half-Jansky flat-spectrum radio sources (Drinkwater et al. 1997), being a QSO with a radio jet extending up to 60 kpc in the northwest direction detected in the optical band (Uchiyama et al. 2007), as well as in the X-rays (Sambruna et al. 2002), and with $z = 0.55646$ (Tadhunter et al. 1993; Drinkwater et al. 1997; Jones et al. 2009). A shorter tidal tail pointing to the west of the QSO is also detected in the optical band (Ramos Almeida et al. 2011). *G4Jy 933* is also classified as a blazar of uncertain type in the Roma-BZCAT (aka BZU J1139–1350; Massaro et al. 2015c).

G4Jy 934: is an FR II radio galaxy listed in the MS4 sample with a photometric redshift estimate of $z = 0.67$ (Burgess & Hunstead 2006b). The mid-IR associated source listed in the *G4Jy* catalog is the one marked in the finding chart and in agreement with the MS4 identification (Burgess & Hunstead 2006a), which is based on the possible radio core detection proposed by Duncan & Sproats (1992) as reported in White et al. (2020b). The MRC 1136–320 radio source position is also cospatial with the associated mid-IR counterpart. The lack of any optical spectroscopic information prevented us from associating it with its optical counterpart, also because the closest source to the radio centroid is the brightest one, as visible in our finding chart.

G4Jy 937: is the well-known Spiderweb Galaxy (see, e.g., Pentericci et al. 1997, 1998, 2002; Carilli et al. 2002; Miley et al. 2006) with $z = 2.1585$ (see, e.g., Kuiper et al. 2011).

G4Jy 939: is the BCG located at the center of a galaxy cluster (Chapman et al. 2000), photometrically identified using the red sequence.

G4Jy 952: is an FR II radio galaxy listed in the MS4 sample with a photometric redshift estimate of $z = 1.35$ (Burgess & Hunstead 2006b) having a mid-IR counterpart associated in the *G4Jy* catalog but lacking an optical correspondence.

G4Jy 957: is a radio galaxy with $z = 0.117$ (Danziger & Goss 1983) with several nearby optical and mid-IR sources.

G4Jy 965: is a core-dominated QSO at $z = 0.258$ (Jauncey et al. 1978) with a CSS radio core (Morganti et al. 1997; Reid et al. 1999).

G4Jy 977: is a USS radio source (De Breuck et al. 2000; Broderick et al. 2007) for which optical follow-up observations provided a redshift estimate of $z = 0.12$ (Bryant et al. 2009); however, the lack of the optical counterpart in our finding chart did not allow us to confirm this association.

G4Jy 987: is a candidate hybrid morphology radio source (HyMoR: having an FR I radio morphology on one side and FR II on the other side of the radio core; Gopal-Krishna & Wiita 2000; Cheung et al. 2009), but in our finding chart we only focused on the northern side to highlight the host galaxy position. It lies at $z = 0.0874$ (Danziger & Goss 1983; Best et al. 1999).

G4Jy 1009: is a lobe-dominated QSO at $z=0.355209$ (Wright et al. 1979; Eracleous & Halpern 2003; Jones et al. 2009).

G4Jy 1034: is the famous WAT hosted in the dumbbell massive group of interacting elliptical galaxies NGC 4782 and NGC 4783 (aka 3C 278; Borne & Hoessel 1984; Borne et al. 1988; de Souza & Quintana 1990; Madejsky et al. 1991; Colina & Borne 1995) at $z=0.015464$ (Fairall et al. 1992; Quintana et al. 1996).

G4Jy 1035: is a radio galaxy at $z=0.057353$ (Melnick & Quintana 1981; Kaldare et al. 2003) located in the central region of the Shapley supercluster in the double system AS 3528 and A3528A, with the BCG lying ~ 4 kpc away from the the X-ray center, and having a tailed radio morphology coupled with steep radio spectra, mainly due to a dense ICM of a premerging environment (Slee et al. 1994; Quintana et al. 1995; Reid et al. 1998; Lopes et al. 2018).

G4Jy 1038: is one of the most famous γ -ray-emitting QSO/blazars since it is well known as 3C 279 (see, e.g., Knight et al. 1971; Whitney et al. 1971) with $z=0.5362$ (see, e.g., Marziani et al. 1996).

G4Jy 1052: is an NLRG with a CSS radio core (aka 1306–09) showing an inverted radio spectrum (Mhaskey et al. 2020). In the optical band G4Jy 1052 shows a secondary nucleus being also harbored in a group of galaxies, and it is undergoing interactions with other nearby sources hosted therein (Inskip et al. 2010; Ramos Almeida et al. 2011, 2013), and with $z=0.46685$ (Tadhunter et al. 1993; Holt et al. 2008).

G4Jy 1071: is a lobe-dominated QSO at $z=0.528$ (Burbidge & Kinman 1966; Best et al. 1999) with mid-IR colors of γ -ray blazars (D’Abrusco et al. 2019) and an Mg II absorption system (Aldcroft et al. 1994).

G4Jy 1080: is the radio galaxy IC 4296 (see, e.g., Younis et al. 1985; Killeen et al. 1986; Killeen & Bicknell 1988; Smith et al. 2000; Wegner et al. 2003; Grossová et al. 2019; Condon et al. 2021; Grossová et al. 2022, and references therein), the BCG of the A3565 galaxy cluster (Abell 1958; Abell et al. 1989), a radio galaxy with $z=0.0125$ (see, e.g., Sandage 1978; Efstathiou et al. 1980).

G4Jy 1083: is a QSO with a WAT radio morphology (Hintzen 1984) with $z=0.625$ (Burbidge & Kinman 1966) and showing mid-IR colors of γ -ray blazars (D’Abrusco et al. 2014, 2019).

G4Jy 1093: is a radio galaxy at $z=0.384$ (Best et al. 1999).

G4Jy 1129: is a radio galaxy at $z=1.094$ (Best et al. 1999).

G4Jy 1135: is a radio galaxy (aka PKS 1413–36) with a classical FR II morphology at large scales and with $z=0.07470$ (Simpson et al. 1993), also emitting in the hard X-rays (Oh et al. 2018), and listed in the MS4 sample (Burgess & Hunstead 2006a).

G4Jy 1136: is an FR II radio galaxy (aka PMN J1416–2146) at $z=1.116$ (Best et al. 2000) for which the lack of an optical counterpart detected in our finding chart did not allow us to assign an IDF = 1.0.

G4Jy 1145: is a radio galaxy showing an FR II radio structure, lying at $z=0.1195$ (Burbidge 1967; Grandi & Osterbrock 1978; Hunstead et al. 1978; Eracleous & Halpern 2004), and also emitting in the hard X-rays (Oh et al. 2018; Kosiba et al. 2022).

G4Jy 1148: is known as MRC 1416–493 (Large et al. 1981) and PKS 1416–49 in the MS4 sample (Burgess &

Hunstead 2006a), classified as a radio galaxy with an intermediate FR I/II radio morphology at $z=0.09142$ (Simpson et al. 1993; Jones et al. 2009), and harbored in a non-cool-core galaxy cluster (Worrall & Birkinshaw 2017) visible in the X-rays. G4Jy 1148 also shows an X-ray cavity spatially associated with the northeastern radio lobe and an X-ray excess associated with the southwestern lobe, probably due to inverse Compton emission.

G4Jy 1152: is a lobe-dominated QSO at $z=0.985$ (Goncalves et al. 1998) with mid-IR colors of γ -ray blazars (D’Abrusco et al. 2019).

G4Jy 1157: is a lobe-dominated QSO (aka PKS 1421–38) for which the original spectroscopic observation identified only a single emission line; assuming that this is due to Mg II, it yields a source redshift $z=0.41$ (Tritton 1971), in agreement with subsequent analyses that refined the measurement of $z=0.4068$ (Veron-Cetty et al. 1988; Eracleous & Halpern 2003).

G4Jy 1158: is the FSRQ PKS B1421–490 (aka PMN J1424–4913) with a one-sided jet and a unique knot detected in both the optical band and the X-rays (Gelbord et al. 2005). Marshall et al. (2011) reported a note claiming that there is an optical spectrum with a redshift estimate of $z=0.662$, but we could not retrieve this information from the literature and thus marked it as uncertain.

G4Jy 1161: is listed in the equatorial sample of powerful radio sources (Best et al. 1999) as a radio galaxy at $z=1.632$; however, the lack of detection in the optical image we used in our analysis prevented us from confirming this association.

G4Jy 1166: is a lobe-dominated QSO with $z=0.8295$ (Bechtold et al. 2002; Jones et al. 2009).

G4Jy 1209: is a radio lobe-dominated QSO with $z=0.942$ (Schmidt 1966).

G4Jy 1225: is an FSRQ listed in the Roma-BZCAT (aka BZQ J1510–0543; Massaro et al. 2015c) with mid-IR colors of γ -ray blazars. In Peterson & Bolton (1972) there is a reported redshift measurement of $z=1.191$, while the most recent optical spectrum places it at $z=0.36$ (Torrealba et al. 2012); thus, we labeled it as uncertain in our analysis.

G4Jy 1262: is a radio galaxy listed in the MS4 sample (aka PMN J1530–4231) with a photometric redshift estimate of $z=0.5$ (Burgess & Hunstead 2006b).

G4Jy 1276: is a radio galaxy listed in the MS4 sample (aka PKS 1540–73) with a photometric redshift estimate of $z=0.68$ (Burgess & Hunstead 2006b).

G4Jy 1279: is listed in the literature as a double–double giant radio galaxy (Ishwara-Chandra & Saikia 1999; Saripalli et al. 2003; Proctor 2016) with $z=0.1082$ (Simpson et al. 1993) with recurrent activity (Machalski et al. 2010; Kuźmicz et al. 2017), and a radio structure interpreted as due to the interaction of restarted jets with preexisting relic cocoons (Safouris et al. 2008).

G4Jy 1284: is an HERG with $z=0.483$ (Tadhunter et al. 1993; Hernán-Caballero et al. 2016), and showing a double nucleus with a fainter companion ~ 9 kpc to the south of the radio core (Inskip et al. 2010; Ramos Almeida et al. 2011).

G4Jy 1301: is an FR II radio galaxy at $z=2.043$ (Best et al. 1999; Venemans et al. 2007).

G4Jy 1302: is a radio galaxy at $z=0.482$ (Best et al. 1999), with an FR II radio structure. We adopted the same association proposed in the literature (Best et al. 1999) and thus different

from the mid-IR counterpart listed in the G4Jy catalog (White et al. 2020b).

G4Jy 1303: is an FR II radio galaxy at $z = 0.109$ (Best et al. 1999).

G4Jy 1330: is a radio galaxy (aka PKS 1621–11) at $z = 0.375$ (Best et al. 1999) having a bright star in the northeastern direction visible in the mid-IR image that prevented us from assigning the mid-IR counterpart.

G4Jy 1336: is a QSO with a compact radio structure with $z = 1.124$ (Jauncey et al. 1984) and having mid-IR colors similar to γ -ray blazars (D’Abrusco et al. 2019). It is also listed in the MS4 sample (aka PKS 1622–310; Burgess & Hunstead 2006a).

G4Jy 1343: is a nearby radio galaxy with an FR II morphology at $z = 0.166$ (Best et al. 1999).

G4Jy 1360: is an LERG at $z = 0.0427$ (Simpson et al. 1993) in agreement with previous estimates present in the literature (Burbidge & Burbidge 1972; Whiteoak 1972), but not with the value of 0.024 reported in Danziger & Goss (1983). It shows an FR II radio morphology in a high-resolution map (Morganti et al. 1993).

G4Jy 1365: is a QSO with $z = 0.799$ having the same associated optical counterpart as in Best et al. (1999) but lacking a mid-IR detection, probably due to the presence of a nearby bright source visible in our finding chart.

G4Jy 1370: is an FR II LERG at $z = 0.236$ (Best et al. 1999).

G4Jy 1423: is an FR II radio galaxy located at $z = 0.09846$ (Tadhunter et al. 1993) associated in our analysis thanks to the optical identification reported in the literature (Jauncey et al. 1989; Morganti et al. 1993) being listed in the 2Jy sample (Wall & Peacock 1985).

G4Jy 1432: is a hard X-ray radio source (Baumgartner et al. 2013; Oh et al. 2018) listed in the MS4 sample with a photometric redshift estimate of $z = 0.41$ (Burgess & Hunstead 2006b).

G4Jy 1453: is a radio galaxy listed in the MS4 sample (aka PKS 1754–59 and AT20G J175906–594702) at the photometric redshift $z = 0.8$ (Burgess & Hunstead 2006b) and optically identified in the literature (Hunstead 1971). The lack of a high-resolution radio map prevented us from confirming the host galaxy association.

G4Jy 1472: is the rare case of a powerful radio-loud AGN in a disk-dominated galaxy with radio luminosity similar to powerful FR II radio galaxies (Morganti et al. 2011). *G4Jy 1472* (aka PKS 1814–63 and PMN J1819–6345) is classified as a CSS radio source (see, e.g., Morganti et al. 1997, and references therein) with $z = 0.06412$ (Thompson et al. 1990; Tadhunter et al. 1993; Holt et al. 2008; Morganti et al. 2011), a similar redshift estimate to that reported by Danziger & Goss (1979) and Grandi (1983). It is also a hard X-ray source (Maselli et al. 2010) listed in the Roma-BZCAT (aka BZU J1819–6345; Massaro et al. 2015c).

G4Jy 1504: is classified as a WAT (aka PKS 1839–48) given the radio structure shown in Morganti et al. (1993) and Mingo et al. (2017) but classified, more recently, as a head–tail radio galaxy by White et al. (2020b). The host galaxy identification adopted here is the same as found in the literature and corresponding to an early-type galaxy at $z = 0.1108$ (Simpson et al. 1993; Jones et al. 2009; White et al. 2020b) lacking strong optical emission lines (Tadhunter et al. 1993). *G4Jy 1504* is interacting with the two nearby companion

galaxies, and it shows an apparent secondary nucleus located at ~ 6 kpc in the southeastern direction (Ramos Almeida et al. 2011). It also shows a bright arc-like shell of ~ 7 kpc in size, potentially due to gravitational lensing, in the northwestern direction (Ramos Almeida et al. 2011, 2013). The ICM emission around *G4Jy 1504* is clearly detected in the soft X-rays (Mingo et al. 2017), and the radio source is also associated with a Fermi γ -ray object (Abdollahi et al. 2020).

G4Jy 1513: is a radio galaxy (aka PKS 1859–23) at $z = 1.430$ (Best et al. 2000), and it resides in a region with several nearby companion galaxies. However, the lack of spectroscopic information about the nearby sources, coupled with the lack of the counterpart associated with the radio emission at both mid-IR and optical frequencies, did not allow us to confirm this association.

G4Jy 1518: also belongs to the equatorial sample of Best et al. (1999), where it is classified as a radio galaxy at $z = 0.226$, as well as in the MRC (MRC 1912–269; Large et al. 1981).

G4Jy 1532: is a radio galaxy (aka MRC 1920–077 and TXS 1920–077) listed in the sample of Best et al. (1999) with the optical counterpart correspondent to our association, but lacking a mid-IR correspondence. It has a redshift estimate of $z = 0.648$.

G4Jy 1555: is a double-lobed radio galaxy (see also Jones & McAdam 1992) with $z = 0.07507$ (aka 6dF J1933250–394021; Scarpa et al. 1996; Jones et al. 2009), harbored in the AS 820 galaxy cluster (Abell 1958; Abell et al. 1989; Quintana & Ramirez 1995).

G4Jy 1558: is a broad-line radio galaxy (BLRG; aka PKS 1932–464), with a relatively broad and strong H α emission line, with $z = 0.2307$ (Tadhunter et al. 1993; Villar-Martín et al. 1998; Hernán-Caballero et al. 2016), and with a FR II radio morphology (Morganti et al. 1993). *G4Jy 1558* shows a complex gas distribution resulting from the interaction with a nearby companion galaxy, and there is a knotty extended emission-line nebula extending beyond the radio structure and the ionization cones, one of the largest ever detected around a radio galaxy at any redshift (Villar-Martín et al. 2005). The origin of the nebula is due to the presence of a star-forming halo associated with the debris of the merger that triggered the activity. *G4Jy 1558* has sufficient luminosity at mid-to-far-IR wavelengths to be classified as a luminous infrared galaxy (Inskip et al. 2007). The star formation structure can extend on the scale of a galaxy group, beyond the old stellar halo of the host galaxy (Villar-Martín et al. 2005). The gas in the emission-line nebula is predominantly ionized by a mixture of AGN photoionization and emission from young stars (Inskip et al. 2007; Tadhunter et al. 2011). *G4Jy 1558* is a member of an interacting galaxy group that includes a highly disturbed starburst galaxy at a similar redshift, located at ~ 100 kpc in the northeastern direction (Inskip et al. 2007), and connected with *G4Jy 1558* by a series of arc-like irregular features up to ~ 70 kpc distance from the galaxy center (Ramos Almeida et al. 2011, 2013).

G4Jy 1562: is a radio galaxy listed in the MS4 sample with a photometric redshift estimate of $z = 1.92$ (Burgess & Hunstead 2006b).

G4Jy 1565: is a QSO at $z = 0.452$ (Tadhunter et al. 1993; Best et al. 1999; Hernán-Caballero et al. 2016) with mid-IR color of γ -ray blazars (Massaro et al. 2012a; D’Abrusco et al.

2014) and belonging to the 2Jy catalog (aka PKS 1938–15; see, e.g., Morganti et al. 1993, and references therein).

G4Jy 1569: is a double-lobed radio galaxy belonging to the MS4 sample with a photometric redshift estimate of $z = 0.18$ (Burgess & Hunstead 2006b) and showing an ultrasteep radio spectrum (De Breuck et al. 2000). The radio source, aka MRC 1940–406, appears to be associated with the galaxy cluster A3646 (see, e.g., Abell et al. 1989; Robertson & Roach 1990), even if this information requires optical spectroscopic observation to be confirmed.

G4Jy 1587: is also known as 3C 404 (Edge et al. 1959; Bennett 1962), with a counterpart at 20 GHz (aka AT20G J195611–073655; Murphy et al. 2010) being classified as a radio galaxy at $z = 1.338$ (Best et al. 2000). However, the lack of mid-IR and optical counterparts in the images used in our analysis did not allow us to confirm the association found in the literature.

G4Jy 1590: is an LERG with $z = 0.0581$ (Simpson et al. 1993) with an FR I radio morphology (Morganti et al. 1993) harbored in a rich galaxy cluster at $z = 0.05845$ (Stein 1996; Ramos Almeida et al. 2011; Ineson et al. 2015), having the ICM clearly detected in the X-rays (Mingo et al. 2017).

G4Jy 1605: is the galaxy cluster relic of A3367 (Abell 1958; Abell et al. 1989) at $z = 0.055$ (see, e.g., Johnston-Hollitt et al. 2008; Owers et al. 2009, and references therein) located in the northwestern direction from the head–tail radio galaxy at its center, namely G4Jy 1606, not belonging to our G4Jy-3CRE catalog (see White et al. 2020b, for additional details).

G4Jy 1613: is an X-shaped radio source (aka PKS 2013–557) with $z = 0.060629$ with an optical spectrum showing the following emission lines: [O II] $\lambda 3727$, [Ne III] $\lambda 3868$, [O III] $\lambda \lambda 4959, 5007$ (Tritton 1972; Jones et al. 2009). It is a restarted giant radio galaxy (Malarecki et al. 2015; Kuźmicz et al. 2018), belonging to the sample selected as hard X-ray emitters (Cusumano et al. 2010; Oh et al. 2018; Ursini et al. 2018; Bruni et al. 2019, 2020), and its X-shaped structure could be a signature of jet reorientation (Saripalli 2007). Recent MeerKAT spectropolarimetric observations revealed a double boomerang radio structure at 1.28 GHz, mainly due to hydrodynamical backflows from the straight radio jets deflected by the large and oblique hot-gas halo of its host galaxy (Cotton et al. 2020). The radio source is also embedded in relatively faint cocoons with uniform brightness temperature and sharp edges owing to subsonic expansion into the ambient intragroup medium (Cotton et al. 2020). The source is also listed in the MS4 and CRATES catalogs (see Burgess & Hunstead 2006a; Healey et al. 2007, respectively).

G4Jy 1618: is an extended radio source (Jones & McAdam 1992) located at $z = 0.352$ (Buchanan et al. 2006) listed in both the MS4 sample (Burgess & Hunstead 2006a) and the catalogs of γ -ray blazar candidates (D’Abrusco et al. 2014, 2019).

G4Jy 1626: is a lobe-dominated QSO at $z = 1.5$ (Best et al. 1999). We did not detect its optical counterpart in the image collected from the surveys used in our analysis; thus, in the finding chart we also report the radio position (i.e., 20:28:07.75, –15:21:21.7 in J2000).

G4Jy 1635: with $z = 0.13149$ (aka 6dF J2033166–225317; Hunstead et al. 1978; Jones et al. 2009), is a radio galaxy living in a small group (Allington-Smith et al. 1993).

G4Jy 1643: is an FR I radio galaxy at $z = 0.0406$ (Tritton 1972; Whiteoak 1972) belonging to the galaxy cluster AS 894 (Abell 1958; Green et al. 1988; Abell et al. 1989).

G4Jy 1646: is a USS radio source located at $z = 1.464$ (De Breuck et al. 2001; aka MP J2045–6018), but lacking an optical counterpart in our finding chart, thus being labeled with a question mark.

G4Jy 1664: is a radio galaxy lying at $z = 0.15662$ (aka 6dF J2056043–195635; Stickel & Kuehr 1994; Jones et al. 2009) originally derived from stellar absorption features. It shows a GPS radio core (O’Dea et al. 1991).

G4Jy 1671: (aka NGC 6998 and PMN J2101–2802) is a winged radio galaxy in the low radio frequency images, showing a one-sided jet feeding the southern lobe. It lies at $z = 0.039444$ (Tritton 1972; Tadhunter et al. 1993; Jones et al. 2009), and it belongs to the galaxy cluster A3733 (Abell 1958; Abell et al. 1989; Stein 1996; Katgert et al. 1998; Smith et al. 2000; Kaya et al. 2019).

G4Jy 1677 and G4Jy 1678: (aka NGC 7016 and NGC 7018) both belong to the galaxy cluster A3744 (Abell 1958; Abell et al. 1989; Postman & Lauer 1995; da Costa et al. 1998; Katgert et al. 1998) and lie at $z = 0.036845$ and $z = 0.03881$, respectively (Garilli et al. 1993; Tadhunter et al. 1993; Smith et al. 2000). More details about these interacting galaxies are given in the literature (see, e.g., Worrall & Birkinshaw 2014, and references therein), while the optical image with a larger field of view retrieved from the Pan-STARRS archive and with radio contours overlaid is shown in Figure 10.

G4Jy 1684: is a QSO with a steep radio spectrum (Baker et al. 1995) with $z = 0.602$ (Baker et al. 1999).

G4Jy 1686: is a lobe-dominated QSO at $z = 0.97779$ (Searle & Bolton 1968; Aldcroft et al. 1994; Jones et al. 2009) also listed in the MS4 sample and in the catalogs of γ -ray blazar candidates (Burgess & Hunstead 2006a; D’Abrusco et al. 2019, respectively).

G4Jy 1692: is an FR II radio galaxy at $z = 0.882$ (Best et al. 1999).

G4Jy 1698: (aka PKS 2128–20) is a QSO at $z = 1.615$ (Best et al. 1999) with a nearby companion galaxy with no emission lines in its optical spectrum. G4Jy 1698 does not show evidence for any net overdensity of red galaxies on small (~ 150 kpc) and/or large scales up to Mpc (Best et al. 2003).

G4Jy 1708: is a lobe-dominated QSO (MacDonald & Miley 1971; Morganti et al. 1993) with $z = 0.20047$ (Baldwin 1975; Ho & Minjin 2009) in the direction of the galaxy cluster A2361 (Abell 1958; Abell et al. 1989; Bahcall 1969; McLure & Dunlop 2001) and detected in the hard X-rays (Baumgartner et al. 2013; Koss et al. 2017) with extended soft X-ray emission (Mingo et al. 2017). Optical images reveal a disturbed morphology with a shell on the western side embedded in an amorphous halo and a faint tidal tail pointing to the southeastern direction (Ramos Almeida et al. 2011).

G4Jy 1709: (aka PKS 2135–20) is a BLRG at $z = 0.63634$ (Tadhunter et al. 1993; Holt et al. 2008; Hernán-Caballero et al. 2016) with a CSS radio core (Morganti et al. 1993). It shows a broad fan on the northern side, interpreted as due to a past interaction, and in agreement with the detection of a young stellar population in the nuclear region (Holt et al. 2007) and a far-infrared excess (Dicken et al. 2009), being also extremely luminous at mid-IR frequencies (Ramos Almeida et al. 2011).

G4Jy 1747: is a radio QSO at $z = 0.668$ (Dunlop et al. 1989).

G4Jy 1748 and G4Jy 1749: the former one is a lobe-dominated QSO (aka PKS 2152–69; Tadhunter et al. 1987; Jones & McAdam 1992; Morganti et al. 1993) with $z = 0.0281$

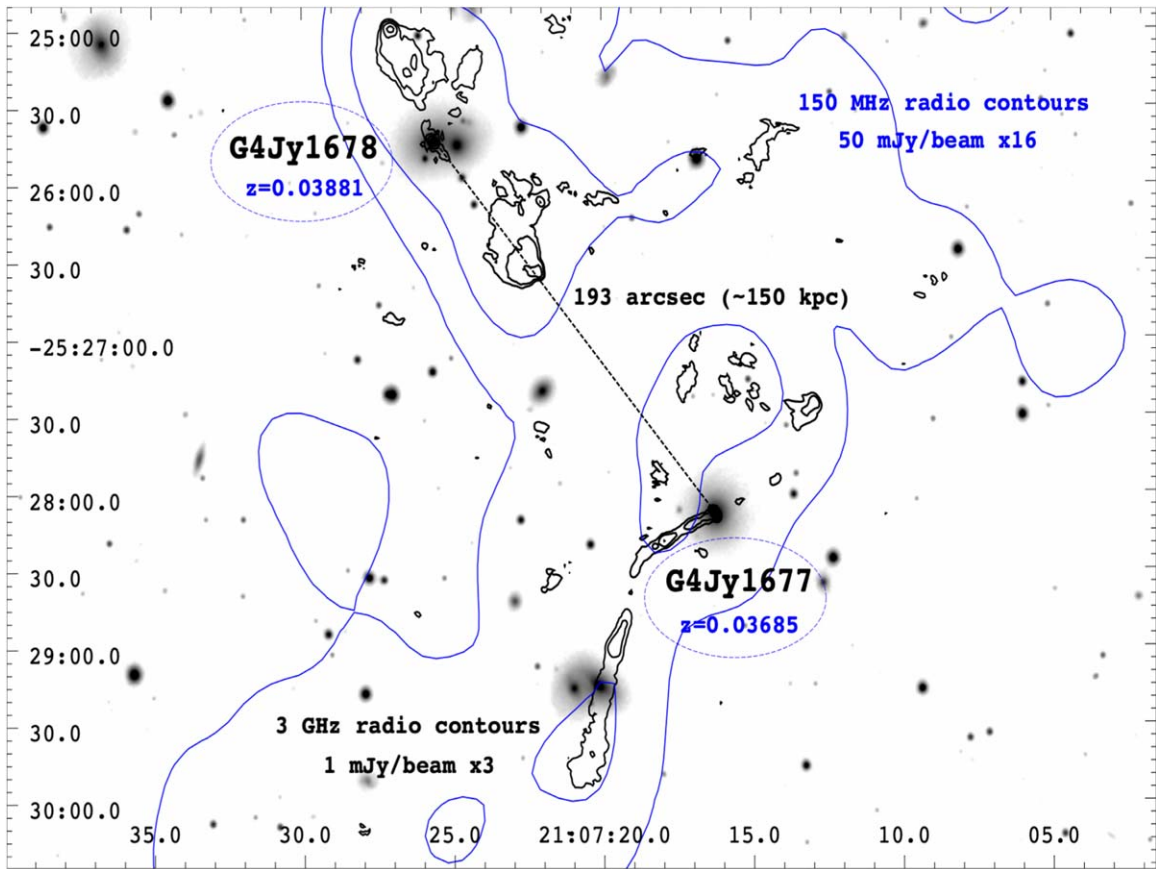


Figure 10. The two radio galaxies G4Jy 1677 and G4Jy 1678 (aka NGC 7016 and NGC 7018) harbored in the galaxy cluster A374 and lying at an angular separation of $\sim 190''$ (i.e., corresponding to ~ 150 kpc at the galaxy cluster redshift). Radio contours from the TGSS and the VLASS archival images at 150 MHz and 3 GHz are overlaid, in blue and black, respectively, on the optical image in r band available in the Pan-STARRS database.

(Marenbach & Appenzeller 1982; Tadhunter et al. 1993) and showing a wide range of features associated with radio galaxy/gas interactions typical of sources where radio mode feedback processes are occurring (Worrall et al. 2012). High-resolution radio observations reveal a radio component at $\sim 10''$ in the northeastern direction from the core, close to an optical highly ionized cloud. At larger scale, G4Jy 1748 shows an FR II morphology with the northern lobe having a “relaxed” structure, while the southern lobe shows an edge-brightened, arc-like structure (Fosbury et al. 1998). The X-ray surface brightness has two depressions spatially associated with the radio lobes, thus suggesting the presence of X-ray cavities inflated with radio plasma (Young et al. 2005). Both radio lobes have their hot spot detected in the X-rays (see also Ly et al. 2005; Massaro et al. 2011). G4Jy 1748 has also been detected in both the hard X-ray and the γ -ray bands (see, e.g., Cusumano et al. 2010; Baumgartner et al. 2013; Abdollahi et al. 2020, respectively). On the other hand, at an angular separation of $\sim 3'6$ from G4Jy 1748, in the eastern direction, there is the nearby radio source G4Jy 1749 as shown in Figure 11. In this case the lack of spectroscopic information on G4Jy 1749 prevents us from claiming that they belong to the same galaxy cluster as for G4Jy 1677 and G4Jy 1678.

G4Jy 1757: is a QSO (aka PKS 2203–18) with $z = 0.61850$ in a group of four QSOs (Morton & Tritton 1982; Stickel et al. 1989), also classified as FSRQ in the Roma-BZCAT (aka BZQ J2206–1835; Drinkwater et al. 1997; Massaro et al. 2009) and in the catalogs of γ -ray blazar candidates (D’Abrusco et al. 2014).

G4Jy 1767: is an FR II radio galaxy (aka 3C 444) with $z = 0.153$ (Lazareff 1975; Dunlop et al. 1989; Tadhunter et al. 1993) and is the BCG of the galaxy cluster A3847 (Abell 1958; Heckman et al. 1986; Abell et al. 1989; Ramos Almeida et al. 2013; Ineson et al. 2015). It is embedded in a relatively dense ICM with clear X-ray cavities spatially associated with its radio lobes, driven by shocks (Croston et al. 2011; Mingo et al. 2017; Vagshette et al. 2017).

G4Jy 1781: is a QSO (aka PKS 2226–41) at $z = 0.446$ (Hewitt & Burbidge 1989).

G4Jy 1786: is a WAT with a bent radio jet (Loken et al. 1995) in the northeastern direction, with $z = 0.0742$. G4Jy 1786 is the BCG of the galaxy cluster A2462 (Dalton et al. 1994; Owen et al. 1995; Quintana & Ramirez 1995) and also close to A3897 (Katgert et al. 1998), with the ICM clearly detected in the soft X-rays (Sun 2009).

G4Jy 1795: (aka PKS 2250–41) is an FR II radio galaxy hosted by an elliptical galaxy at a redshift of $z = 0.308$ (Tadhunter et al. 1993; Inskip et al. 2008) also listed in the MS4 and in the 2 Jy samples (Burgess & Hunstead 2006a; Morganti et al. 1993, respectively). It has an emission-line region showing clear evidence of jet–cloud interactions (Tadhunter et al. 1994; Clark et al. 1997; Villar-Martín et al. 1999; Tilak et al. 2005), shaped as an arc around the western radio lobe with shock signatures (Inskip et al. 2008), probably due to star formation triggered by a faint companion. Recent ALMA observations revealed molecular gas with the broadest velocity profiles in the central, subkiloparsec region due to a direct interaction of the jet with dense clouds and outflowing

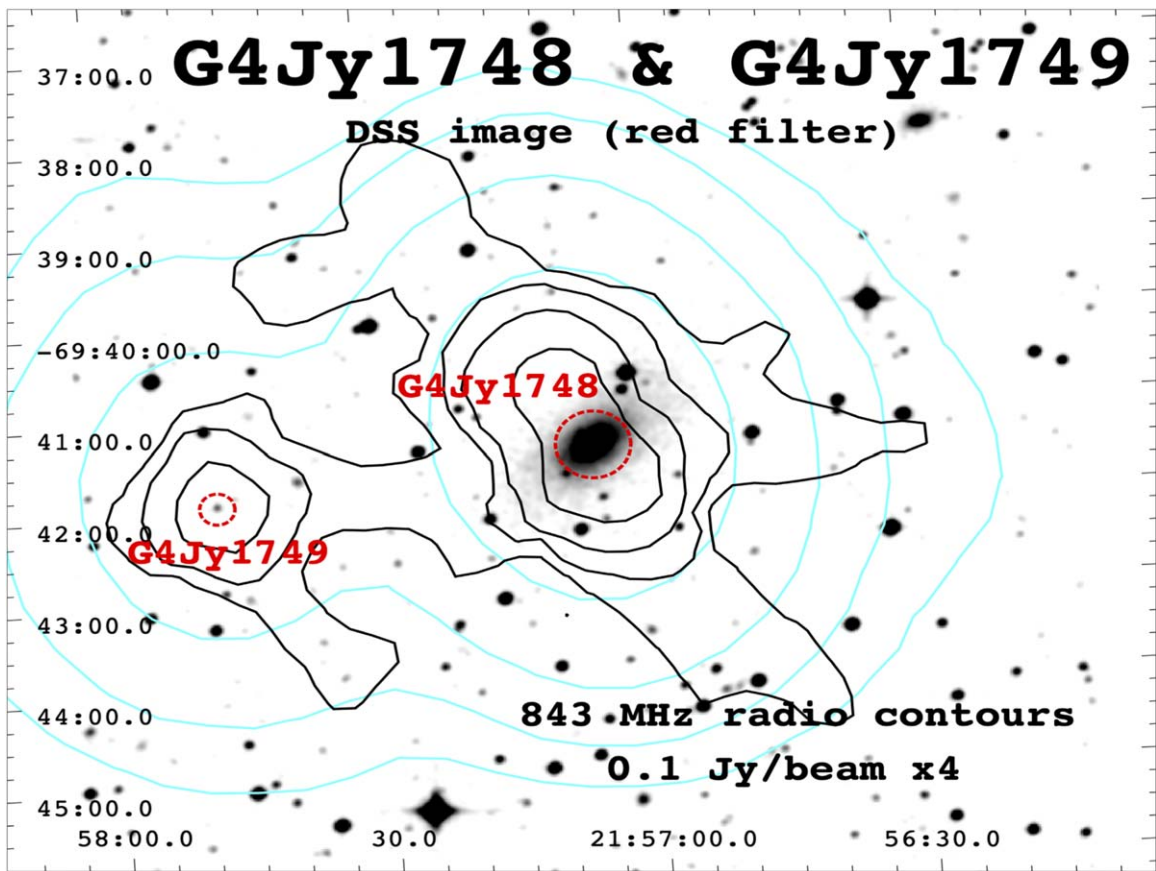


Figure 11. The DSS optical image, in the red filter, of the field including the two radio sources G4Jy 1748 and G4Jy 1749, the former one harbored in a galaxy cluster at $z = 0.0281$ and lying at an angular separation of $\sim 3''6$ (i.e., corresponding to ~ 120 kpc at its redshift) from G4Jy 1749. Radio contours from the SUMSS at 843 MHz are overlaid in black, while those obtained from the GLEAM radio maps between 171 and 230 MHz are reported in cyan; the former ones start at a level of 0.1 Jy beam^{-1} , while the latter ones start at 0.4 Jy beam^{-1} , and both increase by a factor of 4.

molecular gas. On larger, kiloparsec scales, the molecular gas appears to avoid the radio lobes, affected by the expanding cocoon around the radio source, likely dispersing and heating preexisting molecular clouds (Morganti et al. 2021).

G4Jy 1822: is a radio galaxy at $z = 1.414$ (Best et al. 1999).

G4Jy 1824: This radio source, aka PKS J2322–5445 and MRC 2319–550, appears to lie in the direction of the galaxy cluster A1115 (see, e.g., Abell et al. 1989; Robertson & Roach 1990). Optical spectroscopic observations are necessary to confirm this claim.

G4Jy 1829: is a young radio source with molecular gas “hugging” its radio lobes (Morganti et al. 2021). It lies at $z = 0.082991$ (Schmidt 1965; Costero & Osterbrock 1977; Owen et al. 1995; Jones et al. 2009; Fernández-Ontiveros et al. 2016) in the central region of the massive cooling flow galaxy cluster A2597 (Abell 1958; Abell et al. 1989; Crawford et al. 1989). At radio frequencies it shows straight and symmetric jets emerging from both sides and an inverted spectrum of its radio core (Taylor et al. 1999), all confined by the ambient X-ray gas having the southern lobe deflected from its original southwestern direction to the south (Pollack et al. 2005). Both ionized gas and cold molecular gas components wrap around the radio jet and the X-ray cavities (Tremblay et al. 2016), and the cospatial and comoving warm ionized and cold molecular components are consistent with a scenario of chaotic cold accretion, precipitation, and stimulated feedback (Tremblay et al. 2018). A ghost cavity at 330 MHz was also detected (Kokotanekov et al. 2017).

G4Jy 1840: is radio source with $z = 0.907$ (di Serego Alighieri et al. 1994) and listed also in the MS4 sample (Burgess & Hunstead 2006a).

G4Jy 1848: is a USS radio galaxy with $z = 0.644$ (De Breuck et al. 2006).

G4Jy 1854: is a lobe-dominated radio QSO having a steep radio spectrum and emission line in its optical spectrum that, if interpreted as Mg II, suggests a redshift estimate of $z = 1.39$ (Thompson et al. 1990).

G4Jy 1858: is the FRI BCG (aka PKS 2354–35) of the galaxy cluster A4059 (Abell 1958; Abell et al. 1989; Green et al. 1990) with $z = 0.049021$ (Green et al. 1988; da Costa et al. 1989, 1998; Jones et al. 2009). The radio galaxy is classified as “quiescent” since it lacks any signature, in $H\alpha$ emission, of recent major events that could have disturbed the gas (Hamer et al. 2016) and also shows a thick filament of ionized gas, with low velocity dispersion, toward the eastern side with LINER-like line ratios (Pagotto et al. 2021). The galaxy cluster shows a relatively strong cooling flow (Schwartz et al. 1991), and there is evidence that radio emission is inflating X-ray cavities located in the ICM (Heinz et al. 2002; Dunn & Fabian 2006), which could be ghosts of a previous burst of G4Jy 1854 due to the lack of any shock-heated ICM (Choi et al. 2004). There is also a central asymmetric ridge of X-ray emission extending for ~ 30 kpc in the southwestern direction from the galaxy cluster center (see, e.g., Choi et al. 2004, and references therein), colder and denser than the surrounding ICM, with supersolar metallicity and significant

ICM asymmetry, possibly due to a starburst/stripping event (Reynolds et al. 2008).

G4Jy 1863: is a narrow-line hard-X-ray-selected giant radio galaxy (Cusumano et al. 2010; Malarecki et al. 2015; Oh et al. 2018; Ursini et al. 2018; Bruni et al. 2020) with $z = 0.0959$ (Tritton 1972; Danziger & Goss 1983) and with several signatures of a past merger/interaction in its optical spectrum, as irregular shells and two faint arcs (Ramos Almeida et al. 2011). *G4Jy 1863* lies in the direction of the galaxy cluster A4067 (Abell 1958; Abell et al. 1989; Teague et al. 1990).

Appendix B Radio Cross-identifications

Here we present a comparison between the *G4Jy-3CRE* catalog and several radio surveys carried out mainly in the Southern Hemisphere. All results of these crossmatches are also reported in Table 5. The first comparison was carried out with the latest release (i.e., v1.01) of the Parkes radio catalog (PKSCAT90;⁴⁹ Bolton et al. 1979) listing radio and optical data for ~ 8000 radio sources and covering essentially all the sky south of decl. $+27^\circ$ but largely excluding the Galactic plane and the Magellanic Cloud regions as for the *G4Jy*. The original catalog included observations performed at frequencies of 408 and 2700 MHz.

Then, we compared the *G4Jy-3CRE* sample with the MRC (Large et al. 1981). The MRC is one of the largest homogeneous catalogs of radio sources observed at 408 MHz, containing $\sim 12,000$ discrete sources with flux densities greater than 0.7 Jy in the decl. range between $+18.5^\circ$ and -85° (in B1950 equinox) and excluding regions within 3° of the Galactic equator.

We also used the Texas Survey of 66,841 discrete radio sources (TXS; Douglas et al. 1996) detected in the decl. range between -35.5° and $+71.5^\circ$ (in B1950 equinox), which was performed at 365 MHz. The survey lists accurate positions with positional uncertainty of the order of arcseconds and flux densities of a few percent. TXS is 90% complete at 0.4 Jy and 80% complete at 0.25 Jy, being nearly free from spurious sources, and has a low level of lobe-shift incidence.

In addition, the Australia Telescope 20 GHz Survey (AT20G; Murphy et al. 2010) was also compared with the *G4Jy-3CRE* sample. AT20G is a blind radio survey carried out at 20 GHz with the Australia Telescope Compact Array (ATCA) from 2004 to 2008 and covers the whole sky south of decl. 0° . The latest release of the AT20G source catalog lists 5890 sources above a 20 GHz flux density limit of 40 mJy. All AT20G sources have total intensity and polarization measured at 20 GHz, and most sources south of decl. -15° also have near-simultaneous flux density measurements at 5 and 8 GHz with a completeness level of 91% above 100 mJy beam⁻¹.

Then, we crossmatched the *G4Jy-3CRE* sample with the Parkes-MIT-NRAO catalog (PMN; Griffith & Wright 1993; Wright et al. 1994) in several regions of the sky: Southern, Zenith, Tropical, and Equatorial surveys. These surveys were made using the Parkes 64 m radio telescope at a frequency of 4850 Hz with the NRAO multibeam receiver mounted at the prime focus. These surveys had a spatial resolution of $\sim 4''.2$. This survey covers 2.50 sr, listing 23,277 radio sources to a flux limit ranging as a function of decl. between ~ 20 mJy at the southern survey limit and ~ 50 mJy at the northern limit.

We found that 237 sources out of those 264 included in the *G4Jy-3CRE* catalog have a radio counterpart in PKSCAT90. In particular, 171 of them have $IDF = 1.0$, and this optical identification was augmented by a literature search for *G4Jy 538*, *G4Jy 939*, *G4Jy 1401*, and *G4Jy 1854* (see, e.g., Bolton et al. 1965; Bolton & Ekers 1966a, 1966b; Bolton et al. 1968; Hunstead et al. 1971; Peterson et al. 1973, 1976; White et al. 1987). Then, 249 out of 264 show a radio counterpart in the MRC catalog being detected at 408 MHz; in particular, 84 are also selected in the equatorial sample of Best et al. (1999), while 125 were selected to create the MS4 catalog, both built using MRC observations. There are also 235 *G4Jy-3CRE* radio sources with a counterpart listed in the PMN catalog, but only 126 and 118 in the TXS and AT20G catalogs, respectively.

In the following tables, we report the *G4Jy* name together with those available in several radio catalogs based on surveys carried out at different frequencies and mainly covering the Southern Hemisphere, namely TXS, MRC, PKS, and PMN catalogs. These cross-identifications can be used to retrieve observations out of different databases. These associations were mainly based on the NED and SIMBAD databases. The last two columns are dedicated to common names and to highlighting those objects that are associated with Abell galaxy clusters as found in our literature search (see Appendix A).

This search for radio counterparts, as well as that on information regarding classifications and redshifts, was also augmented by the results achieved for the 2 Jy catalog⁵⁰ (see, e.g., Wall & Peacock 1985), a southern sample of radio galaxies defined as having flux densities above 2 Jy at 2.7 GHz, decl. below $+10^\circ$, and redshifts up to 0.7, as well as its full subsample (see, e.g., Tadhunter et al. 1993; Morganti et al. 1997), for which a large suite of multifrequency observations is already available (see, e.g., Morganti et al. 1993, 1999; Tadhunter et al. 2002; Ramos Almeida et al. 2011; Mingo et al. 2014). However, crossmatching the *G4Jy-3CRE* sample with the 2 Jy catalog, we found that only 45 out of 264 radio sources are also listed therein.

⁴⁹ <https://heasarc.gsfc.nasa.gov/W3Browse/all/pkscat90.html>

⁵⁰ https://2jy.extragalactic.info/The_2Jy_Sample.html

Table 5
Radio Cross-identifications

G4Jy Name	TXS Name	MRC Name	PKS Name	PMN Name	Common Name	Abell Cluster
4	0000–177	0000–177	J0003–1727	J0003–1727
9	...	0003–567	J0005–5628	J0005–5628
12	...	0003–833	J0006–8306	J0006–8305
20	...	0007–446	J0010–4422	J0010–4422
26	...	0012–383	J0015–3804	J0015–3804
27	...	0013–634	J0016–6310	J0016–6310
33	0016–129	0016–129	J0018–1242	J0018–1242	3C8	...
43	0020–253	0020–253	J0023–2502	J0023–2502
45	0022–297	0022–297	J0024–2928	J0024–2928
48	0023–263	0023–263	J0025–2602	J0025–2602

(This table is available in its entirety in machine-readable form.)

Appendix C Crossmatching GLEAM and WISE Surveys: A Statistical Test

Assuming those radio sources for which (i) the optical counterpart is coincident with the mid-IR one (i.e., $IDF = 1.0$) plus those (ii) lacking an optical counterpart but having a mid-IR one associated with their radio core (i.e., $IDF = 4.1$) as correct mid-IR associations, we count 203 out of 264 objects, $\sim 77\%$ of the whole G4Jy-3CRE sample. This fraction can be compared with the expected number of spurious associations that can arise when matching the G4Jy catalog with the AllWISE potential counterparts. We computed the chance probability of associations between mid-IR sources and those listed in the full G4Jy catalog since this was originally used to assign counterparts, although the G4Jy-3CRE sample was extracted out of it later.

We adopted here the same procedure described in Massaro et al. (2012a, 2014b) and D’Abrusco et al. (2013, 2014) to compute the probability of having spurious associations between those sources listed in the G4Jy catalog, using their brightness-weighted radio centroids as positions, and their AllWISE potential counterparts. Here we report just a brief overview of the method used. All crossmatches computed in the following analysis are based on their positions reported in the catalogs.

We started counting the total number of mid-IR counterparts $N(R)$ within circular regions of radius R in the range between $0''$ and $10''$, for each G4Jy source. Next, we generated 1000 mock catalogs, based on the distribution of the mid-IR sources around the brightness-weighted radio centroid reported in the G4Jy catalog, and shifted it by a random value uniformly distributed between $10''$ and $20''$ in a random direction of the sky. The shifts used to create the mock catalogs were chosen to be not too distant from the original position reported in the G4Jy to guarantee that fake catalogs have the same sky distribution as the original G4Jy. This allowed us to crossmatch mock sources with real G4Jy objects taking into account the local density distribution of mid-IR sources (see Massaro et al. 2014b, for additional information). The total number of G4Jy sources in all mock catalogs is also preserved.

For each mock realization of the G4Jy catalog, we counted the number of fake associations with the AllWISE catalog occurring at angular separations R smaller than $10''$. Then, we computed the mean number $\lambda(R)$ of these fake associations, averaged over the 1000 mock catalogs, verifying that $\lambda(R)$ has

a Poissonian distribution. Increasing the radius by $\Delta R = 0''1$, we also calculated the difference $\Delta \lambda(R)$ between the number of mock sources within a radius of $R + \Delta(R)$ and those within R , defined as $\Delta \lambda(R) = \lambda(R + \Delta R) - \lambda(R)$.

Finally, in Figure 12 we show the comparison between $\Delta N(R)$ (i.e., the difference between the number of real matches within a radius of $R + \Delta(R)$ and those within R) and $\Delta \lambda(R)$. For angular separations larger than $R_{\text{assoc}} = 5''4$ the $\Delta \lambda(R)$ curve begins to match that of $\Delta N(R)$. Thus, we choose $5''4$ as the maximum angular separation at which we could consider the mid-IR source a reliable counterpart of the G4Jy radio object. An association between a G4Jy source and its potential mid-IR counterpart, occurring at angular separation above $5''4$, has almost the same probability of being either correct or random. Positional uncertainties of the NVSS and SUMSS radio surveys typically range between $1''$ and $5''$ and between $2''$ and $10''$, respectively (see, e.g., Vollmer et al. 2005, and references therein for a recent analysis). These were the radio surveys used in the G4Jy analysis to compute brightness-weighted radio centroids and associate radio sources with their mid-IR counterparts. Thus, our statistical result is also in agreement with previous analyses.

As shown in Figure 12, the chance probability of spurious associations $p(R_{\text{assoc}})$ was computed as the ratio between the number of real associations $N(R_{\text{assoc}})$ and the average of those found in the mock realizations $\lambda(R_{\text{assoc}})$, corresponding to a value of $\sim 26\%$ (see also Massaro et al. 2011; D’Abrusco et al. 2013, for additional details on $p(R_{\text{assoc}})$). Thus, the choice of R_{assoc} is based on the comparison between differential distributions of real and average mock matches, while $p(R_{\text{assoc}})$ is based on their cumulative ones. Adopting the same statistical procedure used here to search for mid-IR counterparts of blazars listed in the Roma-BZCAT (Massaro et al. 2009, 2015c), we found $p(R_{\text{assoc}})$ below 1% at a radius of $\sim 3''$ (see also Massaro et al. 2013a, 2014a; D’Abrusco et al. 2019; de Menezes et al. 2020). This was mainly due to the blazar nature (i) being core-dominated radio sources, thus mostly point-like objects at GHz frequencies, and (ii) having more precise positions reported in the comparison catalog, as well as a combination of these two effects.

The probability of having spurious associations (i.e., $\sim 26\%$) is certainly in good agreement with our refined analysis on optical counterparts, for which the number of incorrect associations is expected to be $\sim 23\%$. Then, angular separations θ_{ow} between the mid-IR counterpart, assigned in the G4Jy catalog, and the optical one with $IDF = 1.0$ are all below $4''8$,

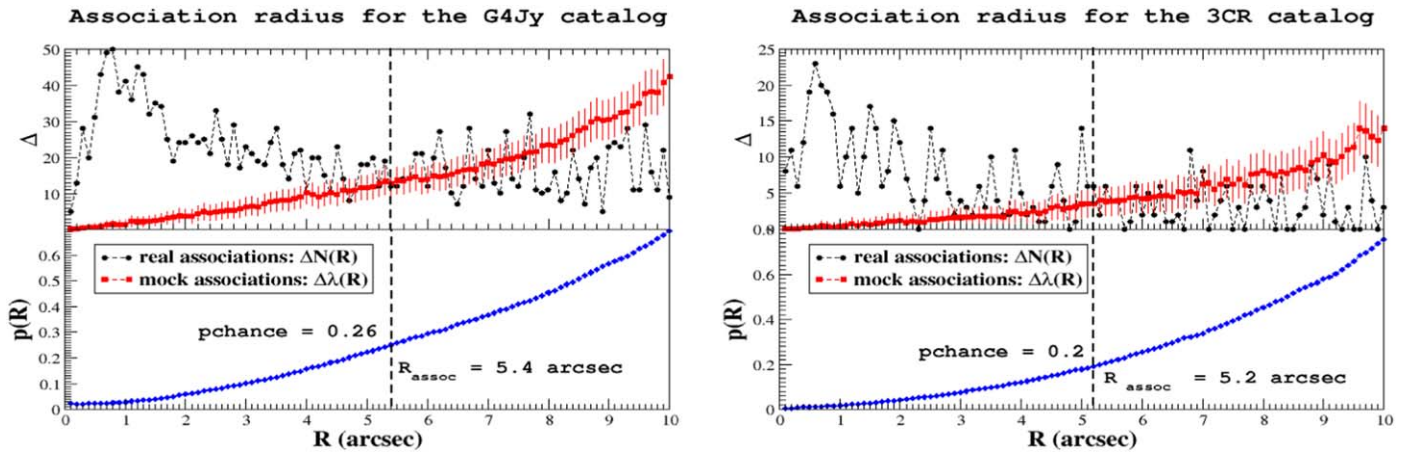


Figure 12. The values of $\Delta \lambda(R)$ (red squares) and $\Delta N(R)$ (black circles) as a function of the angular separation R . Our choice of R_{assoc} is marked by the vertical dashed line. It occurs when $\Delta \lambda(R) \simeq \Delta N(R)$. Uncertainties on the average $\lambda(R)$ values obtained by the crossmatches with mock catalogs were computed from their distributions at each R . The correspondent chance probability of having spurious associations at $R = R_{\text{assoc}}$ is then reported in the lower panel. Left panels correspond to the G4Jy catalog, used to extract the G4Jy-3CRE sample, while, for comparison, in the right panels we show the results of the same procedure applied to the 3CR sample. In the latter case we used NVSS coordinates similar to those adopted in the G4Jy catalog to estimate the brightness-weighted radio centroids at declinations above $-39^\circ 5'$. Considering that in the Southern Hemisphere the source sky density (i.e., number of sources per square degree) of mid-IR potential counterparts is $\sim 10\%$ larger than that correspondent to the 3CR, results on these two different catalogs are in agreement.

with only one exception having $5''6$, as shown in Figure 7, thus consistent with being correct. In Figure 12 we also report the same plots but computed for the 3CR catalog (Spinrad et al. 1985). In this case the value of the association radius is $5''2$, estimated according to the same method previously described. This was computed using the NVSS coordinates of the 3CR radio sources that have a similar precision to those used in the G4Jy catalog to determine the brightness-weighted radio centroids. This association radius corresponds to a chance probability of spurious associations of $\sim 19\%$. However, the source sky density (i.e., number of sources per square degree) of mid-IR potential counterparts around 3CR sources is $\sim 10\%$ smaller than the one measured for the G4Jy-3CRE catalog; thus, taking this into account, the chance probability computed for the G4Jy-3CRE catalog is also in agreement with the expectations based on the 3CR catalog.

In the G4Jy-3CRE catalog 225 out of 264 sources have a mid-IR counterpart assigned by the original G4Jy catalog (White et al. 2020a, 2020b), and 136 out of 225 sources lie below the threshold of $5''4$ angular separation between the brightness-weighted radio centroid and the position of the assigned mid-IR counterpart. A similar situation occurs when comparing the brightness-weighted radio centroid with the optical position of the counterpart assigned thanks to our optical analysis. We have been able to find 211 optical counterparts out of 264 examined sources, and only 109 have angular separation between radio and optical position below $5''4$, in agreement with the expectations of the statistical analysis. The main reason underlying the relatively high probability of getting spurious associations is the use of a brightness-weighted radio centroid since, as previously stated, it does not always provide a reliable position of the host galaxy for sources having an extended radio morphology that is unresolved in radio maps used to compute it and/or for those that are clearly asymmetric. This motivated our analysis based on higher-resolution radio images, thus allowing us to determine the precise location of the host galaxies for the G4Jy-3CRE catalog presented here. An extreme example on how the radio centroid can provide misleading information about the position of the host galaxy is shown in Figure 13,

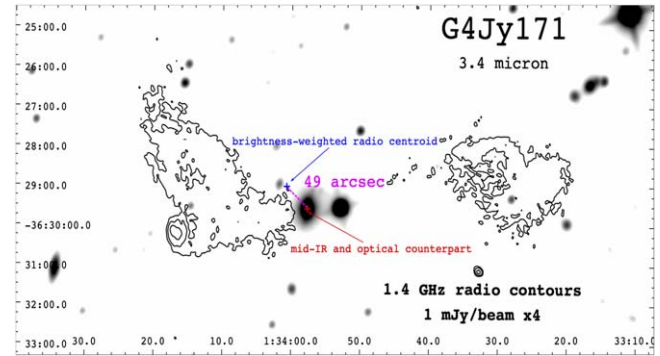














Figure 13. Same as the left panel of Figure 3, but for G4Jy 171. The blue plus sign marks the position of the brightness-weighted radio centroid, while the red one marks that of the mid-IR and optical counterpart, associated with the radio core. The location of the radio core was identified thanks to the NVSS archival radio map at 1.4 GHz used also to draw radio contours overlaid to the mid-IR image. The radio core is not clearly detected in archival images of the TGSS, NVSS, and SUMSS. The angular separation between the two plus signs is $\sim 49''$.

where the high-resolution radio map at 1.4 GHz available in the NVSS archive allowed us to confirm the position of the host galaxy, being the same as that assigned at mid-IR frequencies in the G4Jy catalog, but lying at $\sim 49''$ angular separation from the location of the brightness-weighted radio centroid. Diffuse radio emission arising from lobes could bias the location of the brightness-weighted radio centroid as shown in the case of G4Jy 171 (Figure 13).

ORCID iDs

- F. Massaro <https://orcid.org/0000-0002-1704-9850>
 S. V. White <https://orcid.org/0000-0002-2340-8303>
 A. García-Pérez <https://orcid.org/0000-0002-9896-6430>
 A. Jimenez-Gallardo <https://orcid.org/0000-0003-4413-7722>
 A. Capetti <https://orcid.org/0000-0003-3684-4275>
 C. C. Cheung <https://orcid.org/0000-0002-4377-0174>
 W. R. Forman <https://orcid.org/0000-0002-9478-1682>

C. Mazzucchelli  <https://orcid.org/0000-0002-5941-5214>
 A. Paggi  <https://orcid.org/0000-0002-5646-2410>
 N. P. H. Nesvadba  <https://orcid.org/0000-0001-5783-6544>
 I. Andruchow  <https://orcid.org/0000-0003-1562-5188>
 S. Cellone  <https://orcid.org/0000-0002-3866-2726>
 H. A. Peña-Herazo  <https://orcid.org/0000-0003-0032-9538>
 R. Grossová  <https://orcid.org/0000-0003-3471-7459>
 B. Balmaverde  <https://orcid.org/0000-0002-0690-0638>
 E. Sani  <https://orcid.org/0000-0002-3140-4070>
 V. Chavushyan  <https://orcid.org/0000-0002-2558-0967>
 R. P. Kraft  <https://orcid.org/0000-0002-0765-0511>
 V. Reynaldi  <https://orcid.org/0000-0002-6472-6711>

References

- Abbott, T. M. C., Abdalla, F. B., Allam, S., et al. 2018, *ApJS*, 239, 18
 Abdullahi, S., Acero, F., Ackermann, M., et al. 2020, *ApJS*, 247, 33
 Abell, G. O. 1958, *ApJS*, 3, 211
 Abell, G. O., Corwin, H. G., Jr., & Olowin, O. P. 1989, *ApJS*, 70, 1
 Acero, F., Ackermann, M., Ajello, M., et al. 2015, *ApJS*, 218, 23
 Ahn, C. P., Alexandroff, R., Allende Prieto, C., et al. 2012, *ApJS*, 203, 21
 Ajello, M., Greiner, J., Kanbach, G., et al. 2008a, *ApJ*, 678, 102
 Ajello, M., Rau, A., Greiner, J., et al. 2008b, *ApJ*, 673, 96
 Aldcroft, T. L., Bechtold, J., & Elvis, M. 1994, *ApJS*, 93, 1
 Aldinucci, M., Bagnasco, S., Lusso, S., et al. 2017, *JPhCS*, 898, 082039
 Alexander, D. M., & Hickox, R. C. 2012, *NewAR*, 56, 93
 Allington-Smith, J. R., Ellis, R. S., Zirbel, E. L., & Oemler, A., Jr. 1993, *ApJ*, 404, 521
 Allison, J. R., Sadler, E. M., & Meekin, A. M. 2014, *MNRAS*, 440, 696
 Alvarez, H., Aparici, J., May, J., & Navarrete, M. 1993, *A&A*, 271, 435
 Álvarez Crespo, N., Masetti, N., Ricci, F., et al. 2016, *AJ*, 151, 32
 Bacon, R., Accardo, M., Adjali, L., et al. 2010, *Proc. SPIE*, 7735, 773508
 Bagchi, J., Pislar, V., & Lima Neto, G. B. 1998, *MNRAS*, 296, L23
 Bahcall, J. N. 1969, *ApJL*, 158, 87
 Baker, J. C., Hunstead, R. W., & Brinkmann, W. 1995, *MNRAS*, 277, 553
 Baker, J. C., Hunstead, R. W., Kapahi, V. K., & Subrahmanya, C. R. 1999, *ApJS*, 122, 29
 Baldi, R. D., Capetti, A., Buttiglione, S., et al. 2013, *A&A*, 560, A81
 Baldi, R. D., Chiaberge, M., Capetti, A., et al. 2010, *ApJ*, 725, 2426
 Baldwin, A. J. 1975, *ApJ*, 201, 26
 Balmaverde, B., Capetti, A., Baldi, R. D., et al. 2022, *A&A*, 662, A23
 Balmaverde, B., Capetti, A., Grandi, P., et al. 2012, *A&A*, 545, A143
 Balmaverde, B., Capetti, A., Marconi, A., & Venturi, G. 2018, *A&A*, 612, A19
 Balmaverde, B., Capetti, A., Marconi, A., et al. 2018, *A&A*, 619, A83
 Balmaverde, B., Capetti, A., Marconi, A., et al. 2019, *A&A*, 632, A124
 Balmaverde, B., Capetti, A., Marconi, A., et al. 2021, *A&A*, 645, A12
 Baum, S. A., Heckman, T. M., Bridle, A., et al. 1988, *ApJS*, 68, 643
 Baumgartner, W. H., Tueller, J., Markwardt, C. B., et al. 2013, *ApJS*, 207, 19
 Bechtold, J., Dobrzycki, A., Wilden, B., et al. 2002, *ApJS*, 140, 143
 Begelman, M. C., Blandford, R. D., & Rees, M. J. 1984, *RvMP*, 56, 255
 Bergeron, J., & Kunth, D. 1984, *MNRAS*, 207, 263
 Bennett, A. S. 1962, *MmRAS*, 68, 163
 Bennett, C. L., Larson, D., Weiland, J. L., & Hinshaw, G. 2014, *ApJ*, 794, 135
 Bernhard, E., Tadhunter, C., Mullaney, J. R., et al. 2021, *MNRAS*, 503, 2598
 Best, P. N., Lehnert, M. D., Miley, G. K., & Röttgering, H. J. A. 2003, *MNRAS*, 343, 1
 Best, P. N., Röttgering, H. J. A., & Lehnert, M. D. 1999, *MNRAS*, 310, 223
 Best, P. N., Röttgering, H. J. A., & Lehnert, M. D. 2000, *MNRAS*, 315, 21
 Birkinshaw, M., Worrall, D. M., & Hardcastle, M. J. 2002, *MNRAS*, 335, 142
 Blanton, E. L., Randall, S. W., Clarke, T. E., et al. 2011, *ApJ*, 737, 99
 Böhringer, H., Voges, W., Fabian, A. C., Edge, A. C., & Neumann, D. M. 1993, *MNRAS*, 264L, 25
 Bolton, J. G., Clarke, M. E., & Ekers, R. D. 1965, *AuJPh*, 18, 627
 Bolton, J. G., & Ekers, J. 1966a, *AuJPh*, 19, 559
 Bolton, J. G., & Ekers, J. 1966b, *AuJPh*, 19, 713
 Bolton, J. G., & Savage, A. 1977, *AuJPA*, 41, 25
 Bolton, J. G., Savage, A., & Wright, A. E. 1979, *AuJPA*, 46, 1
 Bolton, J. G., Shimmins, A. J., & Merkleijn, J. 1968, *AuJPh*, 21, 81
 Borne, K. D., Balcells, M., & Hoessel, J. G. 1988, *ApJ*, 333, 567
 Borne, K. D., & Hoessel, J. G. 1984, *BAAS*, 16, 881
 Broderick, J. W., Bryant, J. J., Hunstead, R. W., Sadler, E. M., & Murphy, T. 2007, *MNRAS*, 381, 341
 Browne, L. W. A., & Savage, A. 1977, *MNRAS*, 179, 65
 Brown, D. L., & Burns, J. O. 1991, *AJ*, 102, 1917
 Bruni, G., Brienza, M., Panessa, F., et al. 2021, *MNRAS*, 503, 4681
 Bruni, G., Panessa, F., Bassani, L., et al. 2019, *ApJ*, 875, 88
 Bruni, G., Panessa, F., Bassani, L., et al. 2020, *MNRAS*, 494, 902
 Bryant, J. J., & Hunstead, R. W. 2000, *ApJ*, 545, 216
 Bryant, J. J., Johnston, H. M., Broderick, J. W., et al. 2009, *MNRAS*, 395, 1099
 Buchanan, C. L., McGregor, P. J., Bicknell, G. V., & Dopita, M. A. 2006, *AJ*, 132, 27
 Burbidge, E. M. 1967, *ApJ*, 149L, 51
 Burbidge, E. M. 1968, *ApJ*, 154L, 109
 Burbidge, E. M., & Burbidge, G. R. 1972, *ApJ*, 172, 37
 Burgess, A. M., & Hunstead, R. W. 2006a, *AJ*, 131, 100
 Burgess, A. M., & Hunstead, R. W. 2006b, *AJ*, 131, 114
 Burbidge, E. M., & Kinman, T. D. 1966, *ApJ*, 145, 654
 Burns, J. O. 1981, *MNRAS*, 195, 523
 Buttiglione, S., Capetti, A., Celotti, A., et al. 2009, *A&A*, 495, 1033
 Buttiglione, S., Capetti, A., Celotti, A., et al. 2010, *A&A*, 509, A6
 Buttiglione, S., Capetti, A., Celotti, A., et al. 2011, *A&A*, 525, A28
 Callingham, J. R., Ekers, R. D., Gaensler, B. M., et al. 2017, *ApJ*, 836, 174
 Capetti, A., Buttiglione, S., Axon, D. J., et al. 2011, *A&A*, 527, L2
 Capetti, A., Massaro, F., & Baldi, R. D. 2017a, *A&A*, 598, A49
 Capetti, A., Massaro, F., & Baldi, R. D. 2017b, *A&A*, 601, A81
 Carilli, C. L., Harris, D. E., Pentericci, L., et al. 2002, *ApJ*, 567, 781
 Carter, D., Efstathiou, G., Ellis, R. S., Inglis, I., & Godwin, J. 1981, *MNRAS*, 195, 15
 Carter, D., & Malin, D. F. 1983, *MNRAS*, 203, 49
 Cava, A., Bettoni, D., Poggianti, B. M., et al. 2009, *A&A*, 495, 707
 Chapman, S. C., McCarthy, P. J., & Persson, S. E. 2000, *AJ*, 120, 1612
 Cheung, C. C., Healey, S. E., Landt, H., Kleijn, G. V., & Jordán, A. 2009, *ApJS*, 181, 548
 Chiaberge, M., Capetti, A., & Celotti, A. 2000, *A&A*, 355, 873
 Chiaberge, M., Gilli, R., Lotz, J. M., & Norman, C. 2015, *ApJ*, 806, 147
 Choi, Y.-Y., Reynolds, C. S., Heinz, S., et al. 2004, *ApJ*, 606, 185
 Christiansen, W. N., Frater, R. H., Watkinson, A., et al. 1977, *MNRAS*, 181, 183
 Churazov, E., Brügggen, M., Kaiser, C. R., Böhringer, H., & Forman, W. 2001, *ApJ*, 554, 261
 Churazov, E., Forman, W., Jones, C., & Böhringer, H. 2000, *A&A*, 356, 788
 Clark, N. E., Tadhunter, C. N., Morganti, R., et al. 1997, *MNRAS*, 286, 558
 Clarke, M. E. 1964, *MNRAS*, 127, 405
 Colina, L., & Borne, K. D. 1995, *ApJL*, 454, L101
 Cohen, A. S., Lane, W. M., Cotton, W. D., et al. 2007, *AJ*, 134, 1245
 Condon, J. J., Cotton, W. D., Greisen, E. W., et al. 1998, *AJ*, 115, 1693
 Condon, J. J., Cotton, W. D., White, S. V., et al. 2021, *ApJ*, 917, 18
 Costero, R., & Osterbrock, D. E. 1977, *ApJ*, 211, 675
 Cotton, W. D., Thorat, K., Condon, J. J., et al. 2020, *MNRAS*, 495, 1271
 Crawford, C. S., Arnaud, K. A., Fabian, A. C., & Johnstone, R. M. 1989, *MNRAS*, 236, 277
 Croom, S. M., Smith, R. J., Boyle, B. J., et al. 2004, *MNRAS*, 349, 1397
 Croston, J. H., Hardcastle, M. J., Mingo, B., et al. 2011, *ApJ*, 734L, 28
 Cusumano, G., La Parola, V., Segreto, A., et al. 2010, *A&A*, 524, A64
 Cutri, R. M., Wright, E. L., Conrow, T., et al. 2012, Explanatory Supplement to the WISE All-Sky Data Release Products
 Cutri, R. M., Wright, E. L., Conrow, T., et al. 2013, Explanatory Supplement to the AllWISE Data Release Products, 1
 D'Abrusco, R., Álvarez Crespo, N., Massaro, F., et al. 2019, *ApJS*, 242, 4
 D'Abrusco, R., Massaro, F., Ajello, M., et al. 2012, *ApJ*, 748, 68
 D'Abrusco, R., Massaro, F., Paggi, A., et al. 2013, *ApJS*, 206, 12
 D'Abrusco, R., Massaro, F., Paggi, A., et al. 2014, *ApJS*, 215, 15
 da Costa, L. N., Pellegrini, P. S., Davis, M., et al. 1991, *ApJS*, 75, 935
 da Costa, L. N., Pellegrini, P. S., Willmer, C., et al. 1989, *AJ*, 97, 315
 da Costa, L. N., Willmer, C. N. A., Pellegrini, P. S., et al. 1998, *AJ*, 116, 1
 Dalton, G. B., Efstathiou, G., Maddox, S. J., & Sutherland, W. J. 1994, *MNRAS*, 269, 151
 Danforth, C. W., Keeney, B. A., Tilton, E. M., et al. 2016, *ApJ*, 817, 111
 Danziger, I. J., Fosbury, R. A. E., Goss, W. M., Bland, J., & Boksenberg, A. 1984, *MNRAS*, 208, 589
 Danziger, I. J., Fosbury, R. A. E., Goss, W. M., & Ekers, R. D. 1979, *MNRAS*, 188, 415
 Danziger, I. J., & Goss, W. M. 1979, *MNRAS*, 186, 93
 Danziger, I. J., & Goss, W. M. 1983, *MNRAS*, 202, 703
 Danziger, I. J., Goss, W. M., & Frater, R. H. 1978, *MNRAS*, 184, 341
 Dasadia, S., Sun, M., Morandi, A., et al. 2016, *MNRAS*, 458, 681
 De Breuck, C., Klammer, I., Johnston, H., et al. 2006, *MNRAS*, 366, 58
 De Breuck, C., Seymour, N., Stern, D., et al. 2010, *ApJ*, 725, 36

- De Breuck, C., van Breugel, W., Röttgering, H., et al. 2001, *AJ*, **121**, 1241
- De Breuck, C., van Breugel, W., Röttgering, H. J. A., & Miley, G. 2000, *A&AS*, **143**, 303
- Decarli, R., Falomo, R., Treves, A., et al. 2010, *MNRAS*, **402**, 2441
- de Koff, S., Baum, S. A., Sparks, W. B., et al. 1996, *ApJS*, **107**, 621
- de Menezes, R., D'Abrusco, R., Massaro, F., Gasparrini, D., & Nemmen, R. 2020, *ApJS*, **248**, 23
- de Souza, R., & Quintana, H. 1990, *AJ*, **99**, 1065
- Dicken, D., Tadhunter, C., Axon, D., et al. 2009, *ApJ*, **694**, 268
- Dicken, D., Tadhunter, C., Morganti, R., et al. 2014, *ApJ*, **788**, 98
- di Serego Alighieri, S., Danziger, I. J., Morganti, R., & Tadhunter, C. N. 1994, *MNRAS*, **269**, 998
- Djorgovski, S., Spinrad, H., McCarthy, P., et al. 1988, *AJ*, **96**, 836
- Douglas, J. N., Bash, F. N., Bozyan, F., Torrence, C. W., & Wolfe, C. 1996, *AJ*, **111**, 1945
- Drinkwater, M. J., Gregg, M. D., Holman, B. A., & Brown, M. J. I. 2001, *MNRAS*, **326**, 1076
- Drinkwater, M. J., Webster, R. L., Francis, P. J., Condon, J. J., & Ellison, S. L. 1997, *MNRAS*, **284**, 85
- Duncan, R. A., & Sproats, L. N. 1992, *PASA*, **10**, 16
- Dunlop, J. S., Peacock, J. A., Savage, A., et al. 1989, *MNRAS*, **238**, 1171
- Dunn, R. J. H., & Fabian, A. C. 2006, *MNRAS*, **373**, 959
- Durret, F., Lima Neto, G. B., & Forman, W. 2005, *A&A*, **432**, 809
- Ebeling, H., Voges, W., Bohringer, H., et al. 1996, *MNRAS*, **281**, 799
- Edge, D. O., Shakeshaft, J. R., McAdam, W. B., Baldwin, J. E., & Archer, S. 1959, *MmRAS*, **68**, 37
- Efstathiou, G., Ellis, R. S., & Carter, D. 1980, *MNRAS*, **193**, 931
- Ekers, R. D. 1969, *AuJPA*, **6**, 3
- Ekers, R. D., Goss, W. M., Kotanyi, C. G., & Skellern, D. J. 1978, *A&A*, **69**, L21
- Ellingson, E. 1988, *BAAS*, **20**, 1025
- Ellingson, E., Green, R. F., & Yee, H. K. C. 1987, *BAAS*, **19**, 685
- Ellingson, E., Green, R. F., & Yee, H. K. C. 1991, *ApJ*, **378**, 476
- Ellingson, E., Yee, H. K. C., Green, R. F., & Kinman, T. D. 1989, *AJ*, **97**, 1539
- Eracleous, M., & Halpern, J. P. 2003, *ApJ*, **599**, 886
- Eracleous, M., & Halpern, J. P. 2004, *ApJS*, **150**, 181
- Evans, D. A., Worrall, D. M., Hardcastle, M. J., et al. 2006, *ApJ*, **642**, 96
- Fabian, A. C. 2012, *ARA&A*, **50**, 455
- Fairall, A. P., Willmer, C. N. A., Calderon, J. H., et al. 1992, *AJ*, **103**, 11
- Fanaroff, B. L., & Riley, J. M. 1974, *MNRAS*, **167**, P31
- Fernández-Ontiveros, J. A., Spinoglio, L., Pereira-Santaella, M., et al. 2016, *ApJS*, **226**, 19
- Fleenor, M. C., Rose, J. A., Christiansen, W. A., et al. 2005, *AJ*, **130**, 957
- Fleenor, M. C., Rose, J. A., Christiansen, W. A., et al. 2006, *AJ*, **131**, 1280
- Flewelling, H. A., Magnier, E. A., Chambers, K. C., et al. 2020, *ApJS*, **251**, 7
- Fouque, P., Bottinelli, L., Durand, N., Gougenheim, L., & Paturel, G. 1990, *A&AS*, **86**, 473
- Fosbury, R. A. E., Morganti, R., Wilson, W., et al. 1998, *MNRAS*, **296**, 701
- Frank, K. A., Peterson, J. R., Andersson, K., Fabian, A. C., & Sanders, J. S. 2013, *ApJ*, **764**, 46
- Fujita, Y., Sarazin, C. L., Kempner, J. C., et al. 2002, *ApJ*, **575**, 764
- Gairilli, B., Maccagni, D., & Tarengchi, M. 1993, *A&AS*, **100**, 33
- Gelbord, J. M., Marshall, H. L., Worrall, D. M., et al. 2005, *ApJ*, **632**, 75
- Giovannini, G., Taylor, G. B., Feretti, L., et al. 2005, *ApJ*, **618**, 635
- Goncalves, A. C., Veron, P., & Veron-Cetty, M.-P. 1998, *A&AS*, **127**, 107
- Gopal-Krishna, & Wiita, P. J. 2000, *A&A*, **363**, 507
- Grandi, S. A. 1983, *MNRAS*, **204**, 691
- Grandi, S. A., & Osterbrock, D. E. 1978, *ApJ*, **220**, 783
- Green, M. R., Godwin, J. G., & Peach, J. V. 1988, *MNRAS*, **234**, 1051
- Green, M. R., Godwin, J. G., & Peach, J. V. 1990, *MNRAS*, **243**, 159
- Gregory, P. C., Vavasour, J. D., Scott, W. K., & Condon, J. J. 1994, *ApJS*, **90**, 173
- Griffith, M. R., & Wright, A. E. 1993, *AJ*, **105**, 1666
- Grossová, R., Werner, N., Massaro, F., et al. 2022, *ApJS*, **258**, 30
- Grossová, R., Werner, N., Rajpurohit, K., et al. 2019, *MNRAS*, **488**, 1917
- Hamer, S. L., Edge, A. C., Swinbank, A. M., et al. 2016, *MNRAS*, **460**, 1758
- Hardcastle, M. J., Evans, D. A., & Croston, J. H. 2006, *MNRAS*, **370**, 1893
- Hardcastle, M. J., Massaro, F., & Harris, D. E. 2010, *MNRAS*, **401**, 2697
- Hardcastle, M. J., Massaro, F., Harris, D. E., et al. 2012, *MNRAS*, **424**, 1774
- Hardcastle, M. J., & Worrall, D. M. 2000, *MNRAS*, **314**, 359
- Harvanek, M., Ellingson, E., Stocke, J. T., et al. 2001, *AJ*, **122**, 2874
- Healey, S. E., Romani, R. W., Taylor, G. B., et al. 2007, *ApJS*, **171**, 61
- Heckman, T. M., Smith, E. P., Baum, S. A., et al. 1986, *ApJ*, **311**, 526
- Heinz, S., Choi, Y.-Y., Reynolds, C. S., & Begelman, M. C. 2002, *ApJL*, **569**, L79
- Helton, J. M., Johnson, S. D., Greene, J. E., & Chen, H.-W. 2021, *MNRAS*, **505**, 5497
- Henriksen, M., Harms, R., Burbidge, M., et al. 1991, *BAAS*, **23**, 1423
- Hernán-Caballero, A., Spoon, H. W. W., Leboutteiller, V., Rupke, D. S. N., & Barry, D. P. 2016, *MNRAS*, **455**, 1796
- Hewitt, A., & Burbidge, G. 1989, *ApJS*, **69**, 1
- Hilbert, B., Chiaberge, M., Kotyla, J. P., et al. 2016, *ApJS*, **225**, 12
- Hilker, M., Infante, L., Vieira, G., Kissler-Patig, M., & Richtler, T. 1999, *A&AS*, **134**, 75
- Hiltner, P. R., & Roeser, H. J. 1991, *A&A*, **244**, 37
- Hine, R. G., & Longair, M. S. 1979, *MNRAS*, **188**, 111
- Hintzen, P. 1984, *ApJS*, **55**, 533
- Hintzen, P., Ulvestad, J., & Owen, F. 1983, *AJ*, **88**, 709
- Ho, L. C., & Minjin, K. 2009, *ApJS*, **184**, 398
- Holt, J., Tadhunter, C. N., González Delgado, R. M., et al. 2007, *MNRAS*, **381**, 611
- Holt, J., Tadhunter, C. N., & Morganti, R. 2008, *MNRAS*, **387**, 639
- Hoopes, C. G., Walterbos, R. A. M., & Greenwalt, B. E. 1996, *AJ*, **112**, 1429
- Hunstead, R. W. 1971, *MNRAS*, **152**, 277
- Hunstead, R. W., Lasker, B. M., Mintz, B., & Smith, M. G. 1971, *AuJPh*, **24**, 601
- Hunstead, R. W., Murdoch, H. S., & Shobbrook, R. R. 1978, *MNRAS*, **185**, 149
- Hurley-Walker, N., Callingham, J. R., Hancock, P. J., et al. 2017, *MNRAS*, **464**, 1146
- Hutchings, J. B., Gower, A. C., Ryneveld, S., & Dewey, A. 1996, *AJ*, **111**, 2167
- Ichinohe, Y., Werner, N., Simionescu, A., et al. 2015, *MNRAS*, **448**, 2971
- Ineson, J., Croston, J. H., Hardcastle, M. J., et al. 2015, *MNRAS*, **453**, 2682
- Inskip, K. J., Tadhunter, C. N., Dicken, D., et al. 2007, *MNRAS*, **382**, 95
- Inskip, K. J., Tadhunter, C. N., Morganti, R., et al. 2010, *MNRAS*, **407**, 1739
- Inskip, K. J., Villar-Martín, M., Tadhunter, C. N., et al. 2008, *MNRAS*, **386**, 1797
- Intema, H. T., Jagannathan, P., Mooley, K. P., et al. 2017, *A&A*, **598**, A78
- Ishwara-Chandra, C. H., & Saikia, D. J. 1999, *MNRAS*, **309**, 100
- Ishwara-Chandra, C. H., Saikia, D. J., McCarthy, P. J., & van Breugel, W. J. M. 2001, *MNRAS*, **323**, 460
- Ivezić, Ž., Kahn, S. M., Tyson, J. A., et al. 2019, *ApJ*, **873**, 111
- Jauncey, D. L., Batty, M. J., Wright, A. E., Peterson, B. A., & Savage, A. 1984, *ApJ*, **286**, 498
- Jauncey, D. L., Savage, A., Morabito, D. D., et al. 1989, *AJ*, **98**, 54
- Jauncey, D. L., Wright, A. E., Peterson, B. A., & Condon, J. J. 1978, *ApJ*, **219**, L1
- Jimenez-Gallardo, A., Massaro, F., Paggi, A., et al. 2021, *ApJS*, **252**, 31
- Jimenez-Gallardo, A., Massaro, F., Prieto, M. A., et al. 2020, *ApJS*, **250**, 7
- Jimenez-Gallardo, A., Sani, E., Ricci, F., et al. 2022, *ApJ*, **941**, 114
- Johnson, S. D., Chen, H.-W., Straka, L. A., Schaye, J., & Cantalupo, S. 2018, *ApJL*, **869**, L1
- Johnston-Hollitt, M., Hunstead, R. W., & Corbett, E. 2008, *A&A*, **479**, 1
- Jones, D. H., Read, M. A., Saunders, W., et al. 2009, *MNRAS*, **399**, 683
- Jones, D. H., Saunders, W., Colless, M., et al. 2004, *MNRAS*, **355**, 747
- Jones, P. A., & McAdam, W. B. 1992, *ApJS*, **80**, 137
- Joye, W. A., & Mandel, E. 2003, in *ASP Conf. Ser. 295, Astronomical Data Analysis Software and Systems XII*, ed. H. E. Payne et al. (San Francisco, CA: ASP), 489
- Kaldare, R., Colless, M., Raychaudhury, S., & Peterson, B. A. 2003, *MNRAS*, **339**, 652
- Kang, J., Wang, J., & Kang, W. 2020, *ApJ*, **901**, 111
- Kapahi, V. K., Athreya, R. M., van Breugel, W., McCarthy, P. J., & Subrahmanya, C. R. 1998, *ApJS*, **118**, 275
- Katgert, P., Mazure, A., den Hartog, R., et al. 1998, *A&AS*, **129**, 399
- Kaya, H. I., Caglar, T., & Sert, H. 2019, *MNRAS*, **485**, 4550
- Kempner, J. C., Blanton, E. L., Clarke, T. E., et al. 2004, *Proc. of The Riddle of Cooling Flows in Galaxies and Clusters of Galaxies*, ed. T. Reiprich, J. Kempner, & N. Soker, 335
- Killeen, N. E. B., & Bicknell, G. V. 1988, *ApJ*, **324**, 198
- Killeen, N. E. B., Bicknell, G. V., & Carter, D. 1986, *ApJ*, **309**, 45
- Killeen, N. E. B., Bicknell, G. V., & Ekers, R. D. 1988, *A&A*, **80**, 180
- Kinman, T. D., & Burbidge, E. M. 1967, *ApJ*, **148**, L59
- Knight, C. A., Robertson, D. S., Rogers, A. E. E., et al. 1971, *Sci*, **172**, 52
- Kokotanekov, G., Wise, M., Heald, G. H., et al. 2017, *A&A*, **605**, A48
- Kosiba, M., Peña-Herazo, H. A., Massaro, F., et al. 2022, *A&A*, in press
- Koss, M., Trakhtenbrot, B., Ricci, C., et al. 2017, *ApJ*, **850**, 74
- Kotyla, J. P., Chiaberge, M., Baum, S., et al. 2016, *ApJ*, **826**, 46
- Kristian, J., Sandage, A., & Katem, B. 1978, *ApJ*, **219**, 803
- Kronberg, P. P., Colgate, S. A., Li, H., & Dufton, Q. W. 2004, *ApJL*, **604**, L77

- Kuiper, E., Hatch, N. A., Miley, G. K., et al. 2011, *MNRAS*, **415**, 2245
- Kuraszkiewicz, J., Wilkes, B. J., Atanas, A., et al. 2021, *ApJ*, **913**, 134
- Kuźmicz, A., & Jamroz, M. 2021, *ApJS*, **253**, 25
- Kuźmicz, A., Jamroz, M., Bronarska, K., Janda-Boczar, K., & Saikia, D. J. 2018, *ApJS*, **238**, 9
- Kuźmicz, A., Jamroz, M., Kozieł-Wierzbowska, D., & Weźgowiec, M. 2017, *MNRAS*, **471**, 3806
- Labiano, A., Barthel, P. D., O’Dea, C. P., et al. 2007, *A&A*, **463**, 97
- Lacy, M., Baum, S. A., Chandler, C. J., et al. 2020, *PASP*, **132**, 035001
- Laing, R. A., Riley, J. M., & Longair, M. S. 1983, *MNRAS*, **204**, 151
- Landoni, M., Massaro, F., Paggi, A., et al. 2015, *AJ*, **149**, 163
- Landt, H., Padovani, P., & Giommi, P. 2002, *MNRAS*, **336**, 945
- Lanzetta, K. M., Bowen, D. V., Tytler, D., & Webb, J. K. 1995, *ApJ*, **442**, 538
- Lanzetta, K. M., Turnshek, D. A., & Sandoval, J. 1993, *ApJS*, **84**, 109
- Large, M. L., Mills, B. Y., Little, A. G., Crawford, D. F., & Sutton, J. M. 1981, *MNRAS*, **194**, 693
- Laskar, T., Fabian, A. C., Blundell, K. M., & Erlund, M. C. 2010, *MNRAS*, **401**, 1500
- Law-Green, J. D. B., Leahy, J. P., Alexander, P., et al. 1995, *MNRAS*, **274**, 939
- Lazareff, B. 1975, *A&A*, **42**, 25
- Leahy, J. P. 1993, in *Jets in Extragalactic Radio Sources*, ed. H.-J. Röser & K. Meisenheimer (Berlin: Springer), 1
- Lehnert, M. D., Miley, G. K., Sparks, W. B., et al. 1999, *ApJS*, **123**, 351
- Lilly, S. J., & Prestage, R. M. 1987, *MNRAS*, **225**, 531
- Loken, C., Roettiger, K., Burns, J. O., & Norman, M. 1995, *ApJ*, **445**, 80
- Longair, M. S., Best, P. N., & Röttgering, H. J. A. 1995, *MNRAS*, **275**, L47
- Longair, M. S., & Lilly, S. J. 1984, *JApA*, **5**, 349
- Lopes, P. A. A., Trevisan, M., & Laganá, T. F. 2018, *MNRAS*, **478**, 5473
- López-Cobá, C., Sánchez, S. F., Anderson, J. P., et al. 2020, *AJ*, **159**, 167
- Ly, C., De Young, D., & Bechtold, J. 2005, *ApJ*, **618**, 609
- Lynds, C. R. 1967, *ApJ*, **147**, 837
- MacDonald, G. H., & Miley, G. K. 1971, *ApJ*, **164**, 237
- Machalski, J., Jamroz, M., & Konar, C. 2010, *A&A*, **510**, A84
- Madejsky, R., Bender, R., & Mollenhoff, C. 1991, *A&A*, **242**, 58
- Madrid, J. P., Chiaberge, M., Floyd, D., Sparks, W. B., & Macchetto, D. 2006, *ApJS*, **164**, 307
- Madrid, J. P., Donzelli, C. J., & Rodríguez-Ardila, A. 2018, *ApJS*, **238**, 31
- Mahony, E. K., Sadler, E. M., Croom, S. M., et al. 2011, *MNRAS*, **417**, 2651
- Malarecki, J. M., Jones, D. H., Saripalli, L., Staveley-Smith, L., & Subrahmanyan, R. 2015, *MNRAS*, **449**, 955
- Malarecki, J. M., Staveley-Smith, L., Saripalli, L., et al. 2013, *MNRAS*, **432**, 200
- Mantovani, F., Junor, W., Fanti, R., Padrielli, L., & Saikia, D. J. 1994, *A&A*, **292**, 59
- Marenbach, G., & Appenzeller, I. 1982, *A&A*, **108**, 95
- Marshall, H. L., Gelbord, J. M., Schwartz, D. A., et al. 2011, *ApJS*, **193**, 15
- Marshall, H. L., Schwartz, D. A., Lovell, J. E. J., et al. 2005, *ApJS*, **156**, 13
- Martel, A., Sparks, W. B., Macchetto, D., et al. 1998, *AJ*, **115**, 1348
- Martel, A. R., Baum, S. A., Sparks, W. B., et al. 1999, *ApJS*, **122**, 81
- Marziani, P., Sulentic, J. W., Dultzin-Hacyan, D., Calvani, M., & Moles, M. 1996, *ApJS*, **104**, 37
- Masselli, A., Cusumano, G., Massaro, E., et al. 2010, *A&A*, **520**, 47
- Masselli, A., Forman, W. R., Jones, C., Kraft, R. P., & Perri, M. 2022, *ApJS*, **262**, 51
- Masselli, A., Massaro, F., Cusumano, G., et al. 2016, *MNRAS*, **460**, 3829
- Massaro, E., Giommi, P., Leto, C., et al. 2009, *A&A*, **495**, 691
- Massaro, F., Álvarez Crespo, N., D’Abrusco, R., et al. 2016, *Ap&SS*, **361**, 337
- Massaro, F., D’Abrusco, R., Ajello, M., et al. 2011, *ApJL*, **740**, L48
- Massaro, F., D’Abrusco, R., Giroletti, M., et al. 2013a, *ApJS*, **207**, 4
- Massaro, F., D’Abrusco, R., Tosti, G., et al. 2012a, *ApJ*, **750**, 138
- Massaro, F., Giroletti, M., D’Abrusco, R., et al. 2014a, *ApJS*, **213**, 3
- Massaro, F., Harris, D. E., & Cheung, C. C. 2011, *ApJS*, **197**, 24
- Massaro, F., Harris, D. E., Liuzzo, E., et al. 2015a, *ApJS*, **220**, 5
- Massaro, F., Harris, D. E., Tremblay, G. R., et al. 2010, *ApJ*, **714**, 589
- Massaro, F., Harris, D. E., Tremblay, G. R., et al. 2013b, *ApJS*, **206**, 7
- Massaro, F., Landoni, M., D’Abrusco, R., et al. 2015b, *A&A*, **575**, A124
- Massaro, F., Masetti, N., D’Abrusco, R., et al. 2014b, *AJ*, **148**, 66
- Massaro, E., Maselli, A., Leto, C., et al. 2015c, *Ap&SS*, **357**, 75
- Massaro, F., Missaglia, V., Stuardi, C., et al. 2018, *ApJS*, **234**, 7
- Massaro, F., Tremblay, G. R., Harris, D. E., et al. 2012b, *ApJS*, **203**, 31
- Mauch, T., Murphy, T., Buttery, H. J., et al. 2003, *MNRAS*, **342**, 1117
- McAdam, W. B., White, G. L., & Bunton, J. D. 1988, *MNRAS*, **235**, 425
- McCarthy, P. J., Baum, S. A., & Spinrad, H. 1996, *ApJS*, **106**, 281
- McCarthy, P. J., Kapahi, V. K., van Breugel, W., et al. 1996, *ApJS*, **107**, 19
- McCarthy, P. J., Miley, G. K., de Koff, S., et al. 1997, *ApJS*, **112**, 415
- McCarthy, P. J., Spinrad, H., & van Breugel, W. 1995, *ApJS*, **99**, 27
- McDonald, M., Veilleux, S., Rupke, D. S. N., & Mushotzky, R. 2010, *ApJ*, **721**, 1262
- McLure, R. J., & Dunlop, J. S. 2001, *MNRAS*, **321**, 515
- McMullin, J., Diamond, P., McPherson, A., et al. 2020, *Proc. SPIE*, **11445**, 1144512
- McNamara, B. R., & Nulsen, P. E. J. 2007, *ARA&A*, **45**, 117
- McNamara, B. R., & Nulsen, P. E. J. 2012, *NJPh*, **14**, 055023
- Melnick, J., & Quintana, H. 1981, *A&AS*, **44**, 87
- Menzies, J. W., Coulson, I. M., & Sargent, W. L. W. 1989, *AJ*, **97**, 1576
- Mhaskey, M., Paul, S., Gupta, N., Mukherjee, D., & Gopal-Krishna 2020, *A&A*, **643**, 174
- Miley, G. K., Overzier, R. A., Zirm, A. W., et al. 2006, *ApJL*, **650**, L29
- Miller, N. A., Owen, F. N., Burns, J. O., Ledlow, M. J., & Voges, W. 1999, *AJ*, **118**, 1988
- Mingo, B., Hardcastle, M. J., Croston, J. H., et al. 2014, *MNRAS*, **440**, 269
- Mingo, B., Hardcastle, M. J., Ineson, J., et al. 2017, *MNRAS*, **470**, 2762
- Missaglia, V., Madrid, J. P., Schirmer, M., et al. 2023, *ApJS*, **264**, 6
- Missaglia, V., Massaro, F., Capetti, A., et al. 2019, *A&A*, **626**, A8
- Missaglia, V., Massaro, F., Liuzzo, E., et al. 2021, *ApJS*, **255**, 18
- Monroe, T. R., Prochaska, J. X., Tejos, N., et al. 2016, *AJ*, **152**, 25
- Morganti, R. 2017, *FrASS*, **4**, 42
- Morganti, R., Holt, J., Tadhunter, C., et al. 2011, *A&A*, **535**, A97
- Morganti, R., Killeen, N. E. B., & Tadhunter, C. N. 1993, *MNRAS*, **263**, 1023
- Morganti, R., Oosterloo, T. A., Reynolds, J. E., Tadhunter, C. N., & Migenes, V. 1997, *MNRAS*, **284**, 541
- Morganti, R., Oosterloo, T., Tadhunter, C. N., et al. 1999, *A&AS*, **140**, 355
- Morganti, R., Oosterloo, T., Tadhunter, C., Bernhard, E. P., & Raymond Oonk, J. B. 2021, *A&A*, **656**, 55
- Morton, D. C., & Tritton, K. P. 1982, *MNRAS*, **198**, 669
- Moseley, G. F., Brooks, C. C., & Douglas, J. N. 1970, *AJ*, **75**, 1015
- Murdoch, H. S., Hunstead, R. W., & White, G. L. 1984, *PASA*, **5**, 341
- Murphy, T., Sadler, E. M., Ekers, R. D., et al. 2010, *MNRAS*, **402**, 2403
- Nesvadba, N. P. H., De Breuck, C., Lehnert, M. D., Best, P. N., & Collet, C. 2017, *A&A*, **599**, A123
- O’Dea, C. P., Baum, S. A., & Stanghellini, C. 1991, *ApJ*, **380**, 66
- O’Dea, C. P., Daly, R. A., Kharb, P., et al. 2009, *A&A*, **494**, 471
- O’Donoghue, A. A., Eilek, J. A., & Owen, F. N. 1993, *ApJ*, **408**, 428
- O’Donoghue, A. A., Owen, F. N., & Eilek, J. A. 1990, *ApJS*, **72**, 75
- Oegerle, W. R., & Hill, J. M. 2001, *AJ*, **122**, 2858
- Oh, J. B. 1974, *ApJS*, **27**, 21
- Oke, J. B., & Gunn, J. E. 1983, *ApJ*, **266**, 713
- Oh, K., Koss, M., Markwardt, C. B., et al. 2018, *ApJS*, **235**, 4
- Owen, F. N., Ledlow, M. J., & Keel, W. C. 1995, *AJ*, **109**, 14
- Owen, F. N., & Rudnick, L. 1976, *ApJ*, **205**, L1
- Owers, M. S., Couch, W. J., & Nulsen, P. E. J. 2009, *ApJ*, **693**, 901
- Pagotto, I., Krajinović, D., den Brok, M., et al. 2021, *A&A*, **649**, A63
- Parisi, P., Masetti, N., Rojas, A. F., et al. 2014, *A&A*, **561**, A67
- Peña-Herazo, H. A., Amaya-Almazán, R. A., Massaro, F., et al. 2020, *A&A*, **643**, A103
- Peña-Herazo, H. A., Massaro, F., Chavushyan, V., et al. 2022, *A&A*, **659**, A32
- Pentericci, L., Kurk, J. D., Carilli, C. L., et al. 2002, *A&A*, **396**, 109
- Pentericci, L., Röttgering, H. J. A., Miley, G. K., Carilli, C. L., & McCarthy, P. 1997, *A&A*, **326**, 580
- Pentericci, L., Röttgering, H. J. A., Miley, G. K., et al. 1998, *ApJ*, **504**, 139
- Peterson, B. A., & Bolton, J. G. 1972, *ApJ*, **173L**, 19
- Peterson, B. A., Bolton, J. G., & Savage, A. 1976, *ApL*, **17**, 137
- Peterson, B. A., Bolton, J. G., & Shimmins, A. J. 1973, *ApL*, **15**, 109
- Pislar, V., Durret, F., Gerbal, D., Lima Neto, G. B., & Slezak, E. 1997, *A&A*, **322**, 53
- Pollack, L. K., Taylor, G. B., & Allen, S. W. 2005, *MNRAS*, **359**, 1229
- Postman, M., & Lauer, T. R. 1995, *ApJ*, **440**, 28
- Prestage, R. M., & Peacock, J. A. 1983, *MNRAS*, **204**, 355
- Prieto, M. A. 1996, *MNRAS*, **282**, 421
- Privon, G. C., O’Dea, C. P., Baum, S. A., Axon, D. J., & Kharb, P. 2008, *ApJS*, **175**, 423
- Proctor, D. D. 2016, *ApJS*, **224**, 18
- Punsly, B., Marziani, P., Zhang, S., Muzahid, S., & O’Dea, C. P. 2016, *ApJ*, **830**, 104
- Punsly, B., & Tingay, S. J. 2005, *ApJL*, **633**, L89
- Punsly, B., & Tingay, S. J. 2006, *ApJL*, **640**, L21
- Quintana, H., & Ramirez, A. 1995, *ApJS*, **96**, 343
- Quintana, H., Ramirez, A., Melnick, J., Raychaudhury, S., & Slezak, E. 1995, *AJ*, **110**, 463
- Quintana, H., Ramirez, A., & Way, M. J. 1996, *AJ*, **111**, 603

- Rahaman, M., Raja, R., Datta, A., Burns, J. O., & Rapetti, D. 2022, *MNRAS*, **515**, 2245
- Raimann, D., Storchi-Bergmann, T., Quintana, H., Hunstead, R., & Wisotzki, L. 2005, *MNRAS*, **364**, 1239
- Ramos Almeida, C., Bessiere, P. S., Tadhunter, C. N., et al. 2013, *MNRAS*, **436**, 997
- Ramos Almeida, C., Tadhunter, C. N., Inskip, K. J., et al. 2011, *MNRAS*, **410**, 1550
- Randall, K. E., Hopkins, A. M., Norris, R. P., & Edwards, P. G. 2011, *MNRAS*, **416**, 1135
- Reid, A. D., Hunstead, R. W., & Pierre, M. M. 1998, *MNRAS*, **296**, 531
- Reid, R. I., Kronberg, P. P., & Perley, R. A. 1999, *ApJS*, **124**, 285
- Reynolds, C. S., Casper, E. A., & Heinz, S. 2008, *ApJ*, **679**, 1181
- Ricci, F., Lovisari, L., Kraft, R. P., et al. 2018, *ApJ*, **867**, 12
- Ricci, F., Massaro, F., Landoni, M., et al. 2015, *AJ*, **149**, 160
- Robertson, J. G., & Roach, G. J. 1990, *MNRAS*, **247**, 387
- Roger, R. S., Costain, C. H., & Bridle, A. H. 1973, *AJ*, **78**, 1030
- Sadler, E. M., Ekers, R. D., Mahony, E. K., Mauch, T., & Murphy, T. 2014, *MNRAS*, **438**, 796
- Safouris, V., Subrahmanyan, R., Bicknell, G. V., & Saripalli, L. 2008, *MNRAS*, **385**, 2117
- Safouris, V., Subrahmanyan, R., Bicknell, G. V., & Saripalli, L. 2009, *MNRAS*, **393**, 2
- Sakelliou, I., & Merrifield, M. R. 2000, *MNRAS*, **311**, 649
- Sambruna, R. M., Gambill, J. K., Maraschi, L., et al. 2004, *ApJ*, **608**, 698
- Sambruna, R. M., Maraschi, L., Tavecchio, F., et al. 2002, *ApJ*, **571**, 206
- Sandage, A. 1967, *ApJ*, **150**, L145
- Sandage, A. 1978, *AJ*, **83**, 904
- Santoro, F., Tadhunter, C., Baron, D., Morganti, R., & Holt, J. 2020, *A&A*, **644**, 54
- Saripalli, L., Gopal-Krishna, Reich, W., & Kuhr, H. 1986, *A&A*, **170**, 20
- Saripalli, L., Subrahmanyan, R., & Hunstead, R. W. 1994, *MNRAS*, **269**, 37
- Saripalli, L. 2007, in Proc. of Science 052, From Planets to Dark Energy: The Modern Radio Universe (Trieste: SISSA), 130
- Saripalli, L., Subrahmanyan, R., & Udaya Shankar, N. 2003, *ApJ*, **590**, 181
- Saunders, R., Baldwin, J. E., Rawlings, S., Warner, P. J., & Miller, L. 1989, *MNRAS*, **238**, 777
- Savage, A., Bolton, J. G., & Wright, A. E. 1976, *MNRAS*, **175**, 517
- Sbarufatti, B., Falomo, R., Treves, A., & Kotilainen, J. 2006, *A&A*, **457**, 35
- Scarpa, R., Falomo, R., & Pesce, J. E. 1996, *A&AS*, **116**, 295
- Schilizzi, R. T., & McAdam, W. B. 1975, *MmRAS*, **79**, 1
- Schilizzi, R. T. 1975, *MmRAS*, **79**, 75
- Schlafly, E. F., & Finkbeiner, D. P. M. 2011, *ApJ*, **737**, 103
- Schlegel, D. J., Finkbeiner, D. P., & Davis, M. 1998, *ApJ*, **500**, 525
- Schmidt, M. 1965, *ApJ*, **141**, 1
- Schmidt, M. 1966, *ApJ*, **144**, 443
- Schwartz, D. A., Bradt, H. V., Remillard, R. A., & Tuohy, I. R. 1991, *ApJ*, **376**, 424
- Searle, L., & Bolton, J. G. 1968, *ApJ*, **154**, L101
- Sejake, P. K., White, S. V., Heywood, I., Thorat, K., Bester, H. L., et al. 2023, *MNRAS*, **518**, 4290
- Seymour, N., Stern, D., De Breuck, C., et al. 2007, *ApJS*, **171**, 353
- Shi, Y., Rieke, G. H., Ogle, P. M., Su, K. Y. L., & Balog, Z. 2014, *ApJS*, **214**, 23
- Simpson, C., Clements, D. L., Rawlings, S., & Ward, M. 1993, *MNRAS*, **262**, 889
- Simpson, C., Rawlings, S., & Lacy, M. 1999, *MNRAS*, **306**, 828
- Slee, O. B., Roy, A. L., Murgia, M., Andernach, H., & Ehle, M. 2001, *AJ*, **122**, 1172
- Slee, O. B., Roy, A. L., & Savage, A. 1994, *AuJPh*, **47**, 145
- Smith, R. J., Lucey, J. R., Hudson, M. J., Schlegel, D. J., & Davies, R. L. 2000, *MNRAS*, **313**, 469
- Smith, H. E., Spinrad, H., & Smith, E. O. 1976, *PASP*, **88**, 621
- Speranza, G., Balmaverde, B., Capetti, A., et al. 2021, *A&A*, **653**, 150
- Spinrad, H., Marr, J., Aguilar, L., & Djorgovski, S. 1985, *PASP*, **97**, 932
- Springob, C. M., Haynes, M. P., Giovanelli, R., & Kent, B. R. 2005, *ApJS*, **160**, 149
- Stein, P. 1996, *A&AS*, **116**, 203
- Stickel, M., Fried, J. W., & Kuhr, H. 1989, *A&AS*, **80**, 103
- Stickel, M., & Kuehr, H. 1994, *A&AS*, **105**, 67
- Stickel, M., Kuhr, H., & Fried, J. W. 1993, *A&AS*, **97**, 483
- Storchi-Bergmann, T., Wilson, A. S., Mulchaey, J. S., & Binette, L. 1996, *A&A*, **312**, 357
- Stuardi, C., Missaglia, V., Massaro, F., et al. 2018, *ApJS*, **235**, 32
- Subrahmanya, C. R., & Hunstead, R. W. 1986, *A&A*, **170**, 27
- Subrahmanyan, R., Saripalli, L., Safouris, V., & Hunstead, R. W. 2008, *ApJ*, **677**, 63
- Sun, M. 2009, *ApJ*, **704**, 1586
- Tadhunter, C., Dickson, R., Morganti, R., et al. 2002, *MNRAS*, **330**, 977
- Tadhunter, C. N., Fosbury, R. A. E., Binette, L., Danziger, I. J., & Robinson, A. 1987, *Natur*, **325**, 504
- Tadhunter, C. N., Fosbury, R. A. E., & Quinn, P. J. 1989, *MNRAS*, **240**, 225
- Tadhunter, C., Holt, J., González Delgado, R., et al. 2011, *MNRAS*, **412**, 960
- Tadhunter, C. N., Morganti, R., di Serego-Alighieri, S., Fosbury, R. A. E., & Danziger, I. J. 1993, *MNRAS*, **263**, 999
- Tadhunter, C., Shaw, M., Clark, N., & Morganti, R. 1994, *A&A*, **288**, L21
- Taylor, G. B., O'Dea, C. P., Peck, A. B., & Koekemoer, A. M. 1999, *ApJ*, **512**, L27
- Taylor, M. B. 2005, in ASP Conf. Ser. 347, Astronomical Data Analysis Software and Systems XIV, ed. P. Shopbell et al. (San Francisco, CA: ASP), 29
- Teague, S. J., Carter, D., Gray, & Peter, M. 1990, *ApJS*, **72**, 715
- Thompson, D. J., Djorgovski, S., & de Carvalho, R. 1990, *PASP*, **102**, 1235
- Tilak, A., O'Dea, C. P., Tadhunter, C., Wills, K., & Morganti, R. 2005, *AJ*, **130**, 2513
- Tingay, S. J., Goeke, R., Bowman, J. D., et al. 2013, *PASA*, **30**, 7
- Torrealba, J., Chavushyan, V., Cruz-González, I., et al. 2012, *RMxAA*, **48**, 9
- Tremblay, G. R., Chiaberge, M., Sparks, W. B., et al. 2009, *ApJS*, **183**, 278
- Tremblay, G. R., Combes, F., Oonk, J. B. R., et al. 2018, *ApJ*, **865**, 13
- Tremblay, G. R., Oonk, J. B. R., Combes, F., et al. 2016, *Natur*, **534**, 218
- Tritton, K. P. 1971, *MNRAS*, **155**, 1P
- Tritton, K. P. 1972, *MNRAS*, **158**, 277
- Trussoni, E., Vagnetti, F., Massaglia, S., et al. 1999, *A&A*, **348**, 437
- Tytler, D., Boksenberg, A., Sargent, W. L. W., Young, P., & Kunth, D. 1987, *ApJS*, **64**, 667
- Tzioumis, A., King, E., Morganti, R., et al. 2002, *A&A*, **392**, 841
- Uchiyama, Y., Urry, C. M., Coppi, P., Van Deyne, J., & Cheung, C. C. 2007, *ApJ*, **661**, 719
- Urry, P. 1995, *PASP*, **107**, 803
- Ursini, F., Bassani, L., Panessa, F., et al. 2018, *MNRAS*, **481**, 4250
- Vaghshette, N. D., Naik, S., Patil, M. K., & Sonkamble, S. S. 2017, *MNRAS*, **466**, 2054
- Venemans, B. P., Röttgering, H. J. A., Miley, G. K., et al. 2007, *A&A*, **461**, 823
- Veron-Cetty, M. P., Woltjer, L., & Veron, P. 1988, *A&AS*, **76**, 489
- Villar-Martín, M., Tadhunter, C., Morganti, R., et al. 1998, *A&A*, **332**, 479
- Villar-Martín, M., Tadhunter, C., Morganti, R., Axon, D., & Koekemoer, A. 1999, *MNRAS*, **307**, 24
- Villar-Martín, M., Tadhunter, C., Morganti, R., & Holt, J. 2005, *MNRAS*, **359**, L5
- Vollmer, B., Davoust, E., Dubois, P., et al. 2005, *A&A*, **436**, 757
- Wall, J. V., & Peacock, J. A. 1985, *MNRAS*, **216**, 173
- Wayth, R. B., Lenc, E., Bell, M. E., et al. 2015, *PASA*, **32**, e025
- Wegner, G., Bernardi, M., Willmer, C. N. A., et al. 2003, *AJ*, **126**, 2268
- Wenger, M., Ochsenein, F., Egret, D., et al. 2000, *A&AS*, **143**, 9
- Werner, M. W., Murphy, D. W., Livingston, J. H., Gorjian, V., & Jones, D. L. 2012, *ApJ*, **759**, 86
- Worrall, D. M., & Birkinshaw, M. 2014, *ApJ*, **784**, 36
- Worrall, D. M., Birkinshaw, M., Young, A. J., et al. 2012, *MNRAS*, **424**, 1346
- White, G. L., Batty, M. J., Bunton, J. D., Brown, D. R., & Corben, J. B. 1987, *MNRAS*, **227**, 705
- White, S. V., Franzen, T. M. O., Wong, O. I., et al. 2018, arXiv:1810.01226
- White, S. V., Franzen, T. M. O., Riseley, C. J., et al. 2020a, *PASA*, **37**, e017
- White, S. V., Franzen, T. M. O., Riseley, C. J., et al. 2020b, *PASA*, **37**, e018
- Whiteoak, J. B. 1972, *AuJPh*, **25**, 233
- Whitney, A. R., Shapiro, I. I., Rogers, A. E. E., et al. 1971, *Sci*, **173**, 225
- Wilkes, B. J. 1986, *MNRAS*, **218**, 331
- Wilkes, B. J., Kuraszkiewicz, J., Haas, M., et al. 2013, *ApJ*, **773**, 15
- Wills, B. J., Wills, D., & Douglas, J. N. 1973, *AJ*, **78**, 521
- Wills, B. J., Wills, D., & Douglas, J. N. 1974, *ApJ*, **190**, 271
- Wills, D., & Parker, E. A. 1966, *MNRAS*, **131**, 503
- Wills, K. A., Morganti, R., Tadhunter, C. N., Robinson, T. G., & Villar-Martín, M. 2004, *MNRAS*, **347**, 771
- Worrall, D. M., & Birkinshaw, M. 2017, *MNRAS*, **467**, 2903
- Wright, A. E., Griffith, Mark, R., Burke, B. F., & Ekers, R. D. 1994, *ApJS*, **91**, 111
- Wright, A. E., Jauncey, D. L., Peterson, B. A., & Condon, J. J. 1977, *ApJ*, **211**, L115
- Wright, A. E., Peterson, B. A., Jauncey, D. L., & Condon, J. J. 1979, *ApJ*, **229**, 73
- Wright, E. L., Eisenhardt, P. R. M., Mainzer, A. K., et al. 2010, *AJ*, **140**, 1868

Wylezalek, D., Galametz, A., Stern, D., et al. 2013, *ApJ*, 769, 79
Wyndham, J. D. 1966, *ApJ*, 144, 459
Yates, M. G., Miller, L., & Peacock, J. A. 1989, *MNRAS*, 240, 129
Yee, H. K. C., & Green, R. F. 1983, *BAAS*, 15, 957

Young, A. J., Wilson, A. S., Tingay, S. J., & Heinz, S. 2005, *ApJ*, 622, 830
Younis, S., Meaburn, J., & Stewart, P. 1985, *A&A*, 147, 178
Zirbel, E. L. 1996, *ApJ*, 473, 713
Zirbel, E. L. 1997, *ApJ*, 476, 489